

THESIS ON NATURAL AND EXACT SCIENCES B195

**Mechanism of Changes in the Properties of  
Chemically Deposited CdS Thin Films Induced by  
Thermal Annealing**

NATALIA MATICIUC

**TUT**  
PRESS

TALLINN UNIVERSITY OF TECHNOLOGY  
Faculty of Chemical and Materials Technology  
Department of Materials Science  
Laboratory of Thin Film Chemical Technologies

**This dissertation was accepted for the defense of the degree of Doctor of Philosophy in Natural and Exact Sciences on 01.10.2015.**

**Supervisors:** Dr. Jaan Hiie, Senior Research Scientist,  
Department of Materials Science, Tallinn University of Technology

Dr. Tamara Potlog, Associate Professor,  
Faculty of Physics and Engineering, Moldova State University

**Opponents:** Dr. Daniel Lincot, Institute of Research and Development on Photovoltaic Energy (IRDEP), France

Dr. Kaia Ernits, Crystalsol OÜ, Estonia

**Defense of the thesis:** November 25, 2015 at 12.00  
Lecture hall: NRG-226  
Tallinn University of Technology, Ehitajate tee 5, Tallinn

**Declaration:**

*Hereby I declare that this doctoral thesis, my original investigation and achievement, submitted for the doctoral degree at Tallinn University of Technology, has not been previously submitted for any academic degree.*

*/Natalia Maticiuc/*



European Union  
European Social Fund



Investing in your future

Copyright: Natalia Maticiuc, 2015  
ISSN 1406-4723  
ISBN 978-9949-23-851-4 (publication)  
ISBN 978-9949-23-852-1 (PDF)

LOODUS- JA TÄPPISTEADUSED B195

**Keemiliselt sadestatud CdS õhukeste kilede  
omaduste muutumise mehhanism  
termilisel lõõmutamisel**

NATALIA MATICIUC



# TABLE OF CONTENTS

<b>LIST OF PUBLICATIONS.....</b>	<b>7</b>
<b>AUTHOR’S CONTRIBUTION .....</b>	<b>8</b>
<b>LIST OF ABBREVIATIONS .....</b>	<b>9</b>
<b>INTRODUCTION .....</b>	<b>10</b>
<b>1. LITERATURE OVERVIEW .....</b>	<b>12</b>
1.1. The main properties of CdS thin film .....	12
1.2. Reported preparation methods for CdS thin films .....	12
1.2.1. Chemical deposition methods.....	12
1.2.2. Physical deposition methods .....	14
1.3. Properties of CBD CdS film .....	15
1.4. Application of CBD CdS film in CdTe solar cells .....	18
1.5. Summary of the literature overview and aim of the study .....	19
<b>2. EXPERIMENTAL .....</b>	<b>21</b>
2.1. Chemical bath deposition and thermal treatment of CdS thin film .....	21
2.2. Characterization of CBD CdS films .....	22
2.3. Fabrication and characterization of CdS/CdTe solar cells .....	23
<b>3. RESULTS AND DISCUSSION.....</b>	<b>25</b>
3.1. Properties of CBD CdS films annealed in variable conditions of ambient .....	25
3.1.1. Structural properties .....	25
3.1.2. Electrical properties .....	27
3.1.3. Optical band gap .....	28
3.1.4. XRD and Raman analyses .....	29
3.1.5. Elemental analysis .....	33
3.2. Physico-chemistry of the processes in CBD CdS thin films induced by thermal annealing.....	33
3.3. Application of annealed CBD CdS films in CdS/CdTe solar cell .....	38
<b>CONCLUSIONS .....</b>	<b>42</b>
<b>ACKNOWLEDGEMENTS .....</b>	<b>43</b>
<b>ABSTRACT .....</b>	<b>44</b>

<b>KOKKUVÕTE .....</b>	<b>46</b>
<b>REFERENCES .....</b>	<b>48</b>
<b>APPENDIX A .....</b>	<b>55</b>
<b>APPENDIX B .....</b>	<b>95</b>

## LIST OF PUBLICATIONS

The thesis is based on the following publications, which are referred to in the text by the Roman numerals I–V:

- I. **N. Maticiuc**, J. Hiie, V. Mikli, T. Potlog, V. Valdna, Structural and optical properties of cadmium sulfide thin films modified by hydrogen annealing, *Mater. Sci. Semicond. Process.* **26** (2014) 169–174.
- II. **N. Maticiuc**, J. Hiie, T. Potlog, V. Valdna, A. Gavrilov, Influence of annealing in H<sub>2</sub> atmosphere on the electrical properties of thin film CdS, *Mater. Res. Soc. Symp. Proc.* **1324** (2012) 69–73.
- III. **N. Maticiuc**, J. Hiie, Annealing effect on CdS films: transition from glass to ITO, *IOP Conf. Ser.: Mater. Sci. Eng.* **49** (2013) 012061.
- IV. **N. Maticiuc**, M. Kukk, N. Spalatu, T. Potlog, M. Krunkis, V. Valdna, J. Hiie, Comparative study of CdS films annealed in neutral, oxidizing and reducing atmospheres, *Energy Procedia* **44** (2014) 77–84.
- V. **N. Maticiuc**, N. Spalatu, V. Mikli, J. Hiie, Impact of CdS annealing atmosphere on the performance of CdS–CdTe solar cell, *Appl. Surf. Sci.* **350** (2015) 14–18.

Copies of these articles are included in APPENDIX A.

## AUTHOR'S CONTRIBUTION

The contribution by the author to the papers included in the thesis is as follows:

- I. Deposition of CdS thin films by CBD, post-deposition thermal treatment of CdS thin films in H<sub>2</sub> atmosphere, characterization of the film properties (UV-vis spectroscopy, band gap calculation, XRD measurement, crystallographic analysis), major part of writing.
- II. Deposition of CdS thin films by CBD, post-deposition thermal treatment of CdS thin films in H<sub>2</sub> atmosphere, characterization of electrical properties of the films (Van der Paw measurements), minor part of writing.
- III. Deposition of CdS thin films by CBD, post-deposition thermal treatment of CdS thin films in H<sub>2</sub> and N<sub>2</sub> atmosphere, characterization of the film properties (UV-vis spectroscopy, band gap calculation, XRD measurement, crystallographic analysis), major part of writing.
- IV. Deposition of CdS thin films by CBD, post-deposition thermal treatment of CdS thin films in H<sub>2</sub>, N<sub>2</sub> and air atmosphere, characterization of the film properties (UV-vis spectroscopy, band gap calculation, XRD measurement, crystallographic analysis, photoluminescence and Raman spectroscopy), major part of writing.
- V. Deposition of CdS thin films by CBD, post-deposition thermal treatment of CdS thin films in H<sub>2</sub>, N<sub>2</sub> and air atmosphere, characterization of the film properties (UV-vis spectroscopy, band gap calculation, XRD measurement, crystallographic analysis) and of the solar cell parameters (current-voltage and quantum efficiency analysis), major part of writing.

## LIST OF ABBREVIATIONS

AFM	Atomic Force Microscopy
CBD	Chemical Bath Deposition
CIGS	Cu(In, Ga)Se <sub>2</sub>
CSS	Close Spaced Sublimation
CZTS	Cu <sub>2</sub> ZnSnS <sub>4</sub>
EDX	Energy Dispersive X-ray Spectroscopy
E <sub>g</sub>	Optical bandgap
FF	Fill Factor
FTO	Fluorine doped Tin Oxide
ITO	Indium Tin Oxide
J <sub>sc</sub>	Short-circuit current
PL	Photoluminescence
PV	Photovoltaic
PVD	Physical Vapor Deposition
QE	Quantum Efficiency
RF	Radio Frequency
RMS	Root Mean Square
SEM	Scanning Electron Microscopy
TCO	Transparent Conductive Oxide
V <sub>oc</sub>	Open-circuit voltage
XPS	X-ray Photoelectron Spectroscopy
XRD	X-ray Diffraction

# INTRODUCTION

The potential demand in the power generation market requires cheap photovoltaic (PV) modules with efficiencies in excess of 10%. Therefore, research and development efforts shifted gradually from crystalline Si to polycrystalline thin film technologies, such as copper indium gallium diselenide (CIGS), cadmium telluride (CdTe), dye-sensitized, kesterite (CZTS) and Perovskite solar cells due to their low price materials and rapidly escalating efficiencies. During the past twenty years, CdTe and CIGS solar cells have demonstrated long-term stability and competitive performance, and they continue to attract production-scale capital investments. Very recently (February, 2015), First Solar set a world record for CdTe PV research cell conversion efficiency, achieving 21.5% efficiency [1], whereas the Centre for Solar Energy and Hydrogen Research Baden-Württemberg set the world record efficiency for CIGS solar cells at 21.7% in September, 2014 [1]. These achievements place CdTe- and CIGS-based solar cells well above multicrystalline silicon solar cells, which peaked at 20.8% [1]. Another common feature for CdTe and CIGS solar cells is the use of a CdS buffer film, which is shown to drastically influence the performance of both solar cells.

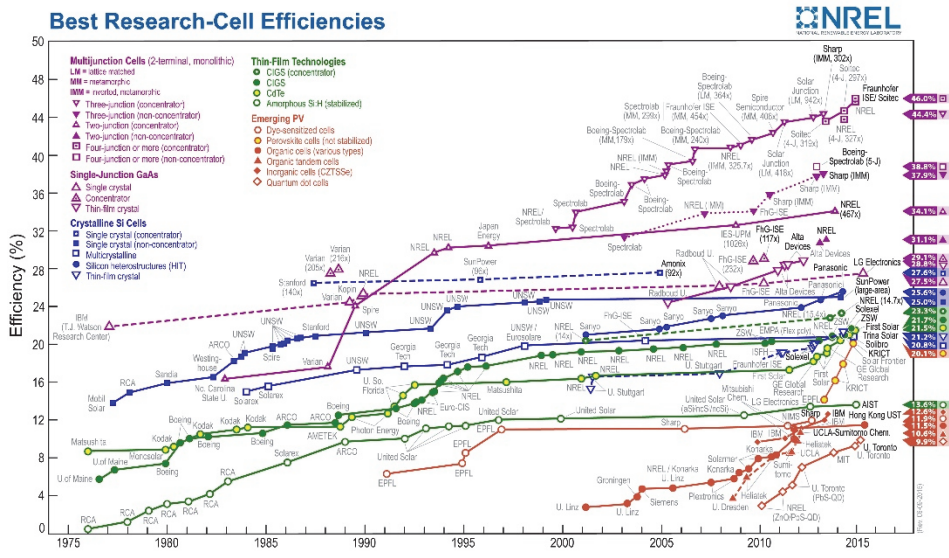


Fig. 1. Best research-cell efficiencies documented in the U.S. Department of Energy's National Renewable Energy Laboratory.

In a CdS/CdTe solar cell, the crystallization and morphology of the absorber are strongly affected not only by the CdCl<sub>2</sub> treatment but also by the CdS deposition method and the structure of the CdS layers on the transparent conductive oxide (TCO) substrates [2]. Additionally, the intermixing of CdS/CdTe is very much dependent on the properties of the CdS layers. CdS pre-treatments, designed to limit intermixing by increasing the grain size, clearly restructure the CdS and sharpens the transmission edge. However, depending on the CdS thickness, it may be detrimental to the open-circuit voltage and fill factor of the CdS/CdTe solar cell [3].

In a CIGS/CdS solar cell, the bulk properties of the CdS buffer create modifications to the CIGS surface: sulfur passivation, the formation of a transition

region (such as  $\text{CdIn}_x\text{Se}_y$ ) [4] and etching effects by the removal of secondary phases, oxides and carbonates [5]. Moreover, with an increased impurity concentration in the CdS layer, the open-circuit voltage of a CIGS solar cell may exhibit a noticeable increase [6].

For an optimal impact on solar cell performance, the CdS layer should be very thin, uniform, adherent and compact. These requirements are mainly fulfilled by chemical bath deposition (CBD), which is a proper technique to produce suitable CdS films with low cost at reduced temperature. However, to fulfill the compactness issue, an adequate post-deposition thermal treatment is required to recrystallize the CdS film by increasing the grain size. As long as CdS is subjected to a thermal processing step during absorber deposition in a CdTe solar cell or TCO deposition in a CIGS solar cell, the post-deposition treatment of the CdS film represents an important step.

The target of this study is the optimization of CdS films for application in CdTe and CIGS solar cells. This improvement of CdS properties is obtained through a post-deposition thermal treatment at variable conditions, including annealing time from 3 to 120 min, annealing temperatures from 200 °C to 450 °C and the presence of different annealing gases, such as hydrogen, nitrogen or air.

The present doctoral thesis is a continuation of the previous studies on the deposition and thermal treatment of CBD CdS films that have been conducted in the Laboratory of Thin Film Chemical Technologies, Department of Materials Science, at Tallinn University of Technology [7, 8, 9]. The aim of this doctoral thesis was to study systematically the effect of post-deposition thermal treatment variables on the optical, structural and electrical properties of CdS films. From an application point of view, we also investigated the influence of an annealed CdS buffer layer on the final performance of CdS/CdTe solar cells. Research regarding CdS/CdTe solar cells with annealed CBD CdS layers was possible through a collaboration with the Department of Physics and Engineering from Moldova State University.

The thesis is divided into three Chapters. Following the introduction, Chapter 1 includes a literature overview describing the main properties of CdS, deposition methods for CdS films, the properties of CBD CdS thin films and solar cells based on a CdTe absorber with CBD CdS as a buffer layer. Chapter 2 briefly describes the preparation, annealing and characterization of CBD CdS thin films, as well as the fabrication and characterization of CdS/CdTe solar cells. Chapter 3 is divided into three sections and includes the results and a discussion of CdS film properties, followed by the application of annealed CBD CdS thin films in practical devices.

# 1. LITERATURE OVERVIEW

## 1.1. The main properties of CdS

CdS is a group II-VI compound semiconductor. This material can be used in the development of several optoelectronic device applications, such as photoconductive detectors, gas sensors, light emitting diodes and particularly in solar cells as a buffer layer due to its suitable optical and electrical properties. CdS crystallizes in a cubic zinc blende and/or hexagonal wurtzite structure with lattice parameters  $a=5.825 \text{ \AA}$ , and  $a=4.136 \text{ \AA}$ ,  $c=6.716 \text{ \AA}$ , respectively [10]. CdS films with cubic structure grow perpendicular to the (111) plane, while the hexagonal structure is textured in the [002] orientation.

The optical transmission of CdS is approximately 80 - 90% at  $\lambda > 520 \text{ nm}$ , and the room temperature energy band gap ( $E_g$ ) value for bulk CdS is 2.5 eV [11], with a temperature coefficient in the range of  $(3.4 - 5.1) \cdot 10^{-4} \text{ eV/K}$  [10]. For CdS thin films, there is a wide spread of reports on  $E_g$  values that varies from 2.2 eV [12] to 2.6 eV [13] depending on the deposition technique, deposition parameters and post-deposition treatments [14, 15].

The specific conductivity of CdS is approximately  $10^{-7} \text{ \Omega}^{-1} \cdot \text{cm}^{-1}$  at room temperature [16], and its resistivity ranges from  $10^{-3} \text{ \Omega} \cdot \text{cm}$  to  $10^8 \text{ \Omega} \cdot \text{cm}$  [17]. Room temperature mobility for holes was as high as  $48 \text{ cm}^2/(\text{V} \cdot \text{s})$  [10], while for electrons the value was up to  $2.42 \cdot 10^3 \text{ cm}^2/(\text{V} \cdot \text{s})$  [18]. CdS is invariably an n-type semiconductor due to the asymmetry in the energetic dislocations of the conduction and valence bands [17].

Six types of isolated native defects are considered for CdS: Cd and S vacancies, Cd and S interstitials, Cd and S anti-sites [19]. In addition to the intrinsic dopants, CdS can be doped with B, Al, Ga, In, Cl, Br and I to obtain an enhanced conductivity and/or with Cu, Ag and Au acceptors to obtain the compensation of donor dopants. H, O and related complexes, as (OH) group, can also be incorporated, acting mainly as shallow donors in CdS [20].

## 1.2. Reported preparation methods for CdS thin films

Thin films of CdS have been prepared by various deposition techniques: physical vapor deposition (PVD), close spaced sublimation (CSS), radio frequency (RF) sputtering, screen printing, pulsed laser evaporation, CBD, electrodeposition, spray pyrolysis, successive ionic layer adsorption reaction, and metal organic chemical vapor deposition. For comparison, we will provide a review of the reported work on CdS thin films grown by some of the most commonly used methods, which are further analyzed.

### 1.2.1. Chemical deposition methods

CBD: In recent years, high priority has been given to the development of low-cost deposition techniques for CdS thin films, one of which is the CBD method. The first reported compound semiconductor films formed by CBD included PbS, SbS and CuS [21]. The deposition of CdS films by CBD was first reported by Mokrushin in 1961 [22] and has now become the most widely studied material produced by CBD. The range of materials deposited by CBD was gradually extended to include sulfides and

selenides of many metals [23, 24], oxides [25], CdTe [26] and several ternary compounds [27].

CBD was confirmed as a simple and promising technique to deposit CdS for high efficiency polycrystalline thin film solar cells based on CIGS, CdTe or CZTS in both substrate and superstrate configurations.

The traditional CBD setup consists of a magnetic stirrer with controllers for the temperature and stirring rate, a solution container, a bath, a thermometer and a holder for substrates (Fig. 1.1). The deposition of CdS films is carried out using an alkaline aqueous solution composed mainly of a Cd salt (CdCl<sub>2</sub>, CdSO<sub>4</sub>, CdI<sub>2</sub>, etc.), thiourea (SC(NH<sub>2</sub>)<sub>2</sub>) as the sulfur source and ammonia (NH<sub>3</sub>) as the complexing agent. The formation of CdS takes place heterogeneously on the substrate surface or homogeneously in the solution due to the spontaneous precipitation of CdS in the form of secondary particles. Homogeneous deposition is highly undesirable, as it yields powdery and non-adherent films. For better quality films, the heterogeneous process is desirable and achieved by slow deposition of CdS at a low concentration of Cd<sup>2+</sup> and a low rate of S<sup>2-</sup> release by the decomposition of thiourea in the basic solution.

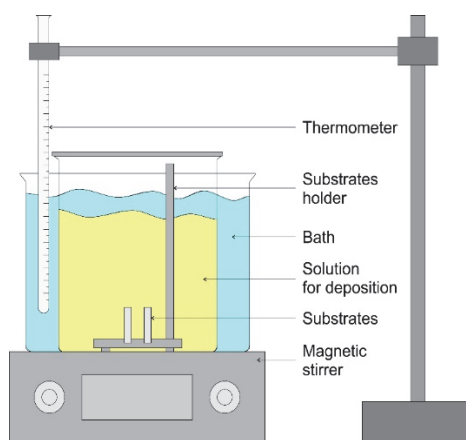


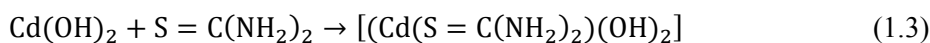
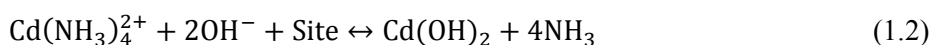
Fig. 1.1. Traditional setup scheme for CBD technique.

The interaction between ions of the cadmium-ammonia complex and thiourea molecules in ammoniacal solution is given by the global reaction (1.1).



The mechanism of CdS growth has been studied by many authors; however, the process model described by Lincot [23] is considered one of the most suitable for the description of the reaction scheme:

1. Reversible adsorption of cadmium hydroxide species (1.2).
2. Formation of a surface complex with thiourea (1.3).
3. Formation of CdS with site regeneration (1.4).





The epitaxial growth process of CdS [23] appears to be strongly dependent on temperature. At room temperature, no deposition occurs within a few hours [15], whereas a small increase of temperature multiplies the growth rate by a factor of 2.5. An increase in ammonia concentration strengthens the complexation of hydroxide ions with cadmium, slowing down the growth rate of CdS [24]. Other important deposition parameters in this technique are the molar concentration of the precursors, pH of solution, deposition time and stirring rate. Moreover, there are several parameters of the post-deposition processing of CBD CdS that also strongly influence the film properties. The details of CBD processing parameters and post-deposition conditions for CdS thin films will be discussed later in Section 1.3.

Chemical spray pyrolysis: The sprayed CdS thin films are deposited at a substrate temperature of 400 °C using a Cd salt and thiourea solution, similar to CBD [7]. Chemically sprayed CdS films have an excellent photoconductivity as well as permeability in the visible range, but the resistivity is approximately  $10^8 \Omega \cdot \text{cm}$  [18], which limits their use as transparent window in solar cells. Annealing or chemical doping is applied as an effective solution in this situation [28]. However, in comparison to CBD CdS films, the out diffusion and evaporation of chlorine from sprayed CdS takes longer and complicates the control of film resistivity [7].

Electrodeposition: Compared with CBD film, CdS films prepared by electrodeposition from an aqueous solution is deposited more slowly, however, the film is denser and has a higher absorption coefficient in the wavelength region of 400 – 1000 nm [29]. Though an alternating current voltage method with a two-electrode cell was proposed to improve the quality of electrodeposited CdS films [30], the control of the deposition process remains an open issue for the electrodeposition of CdS film [31], not to mention the need to control the electrical properties.

### 1.2.2. Physical deposition methods

PVD: For industrial production, in-line vacuum deposition methods such as PVD is preferred for CdS deposition. Co-evaporation, compound evaporation and sputtering are all physical vapor deposition methods. PVD of CdS is usually performed in a high-vacuum thermal evaporation system ( $<10^{-7}$  Torr) from a high-purity powder of CdS at very slow rates (40-400 Å/min) [32, 33]. PVD CdS films are polycrystalline and show continuous coverage and larger grains than CBD films [34]. Moreover, in a solar cell structure, CBD and PVD CdS show different lattice (mis)matches with respect to the absorber. This mismatch is connected to the fact that a CBD CdS layer is a mixture of CdS, Cd–OH and Cd–O, which offers a range of lattice constants that apparently leads to a better lattice match to CIGS than the lattice constants of PVD CdS [6]. As a result, efficiencies of CIGS solar cells achieved by PVD CdS buffer layers hardly exceed 13% [34], whereas those with CBD CdS buffer layers yield efficiencies of approximately 16-17% [1].

CSS: With the CSS technique, CdS films are prepared within several minutes at a pressure below  $10^{-6}$  Torr and with a very low source-to-substrate distance (0.7 cm in [35], 0.2 cm in [36] and 0.03 cm in [37]). The crystallized material has a much lower density of defects, higher degree of crystallinity and larger grain sizes than CBD CdS film. Better crystallinity contributes to a lower stress in the CSS film, however it also contributes to an insufficient driving force to recrystallize CdS during  $\text{CdCl}_2$

treatment. Moreover, due to the large grain size and roughness, CSS CdS films are less able to conform to the substrate during growth than CBD CdS, which might be the reason that solar cells with CBD CdS generally show comparable efficiencies with solar cells that use CSS CdS [38].

RF Sputtering: Sputtered CdS thin films are obtained at substrate temperatures between 25 °C and 320 °C [39], and all CdS thin film properties depend on the sputtering parameters [40]. RF sputtered CdS is a dense and pin-hole free film with a preferential [002] orientation, compared with the random orientation for CSS or CBD CdS. The small grain size, rough surface and defects, located either in the bulk of the CdS or at the CdS/TCO interface, negatively affect the properties of solar cell [41]. Defects of RF sputtered CdS thin films are induced by the sputter process itself due to Ar-ion bombardment of the target material [41, 42].

To summarize, all of the vacuum-based techniques require complex, expensive equipment and strict deposition conditions. In contrast, the wet techniques are characterized by their low cost, simplicity and low temperatures. Among the wet methods, CBD has achieved high popularity and has been widely applied to the manufacture of CdS thin films due to its major advantages:

- low-cost equipment;
- epitaxial growth;
- conformal coating of large area;
- compatibility with a variety of substrates for plating, including plastics;
- low film thicknesses which can be controlled easily by changing the deposition parameters;
- post-deposition treatment in a defined atmosphere or in the presence of CdCl<sub>2</sub>.

Nevertheless, despite the simplicity of the CBD procedure, it is a complicated task to understand the kinetics of the film growth mechanisms involved in the deposition process.

### **1.3. Properties of CBD CdS films**

The physical and electrical properties of CBD CdS films depend on the deposition procedure and post-deposition treatment conditions.

As deposited CBD CdS thin films: In the process of the formation of the film during the deposition steps, the CdS thin film properties are influenced by the following parameters: Cd salt, S/Cd ratio, complexing agent, pH, temperature and duration of deposition, substrate nature and bath geometry.

Small details, such as a constant rate of magnetic stirring and the addition rate of thiourea, also should be considered to obtain uniform CBD CdS films [43]. A review of the CBD CdS properties influenced by the deposition parameters is presented in Table 1.1.

Annealed CBD CdS thin films: CdS thin films deposited by CBD were shown by several authors to have poor crystalline qualities, even to be amorphous, and tend to form the cubic phase [44]. A reorganization of CdS by annealing always favors better quality films [45]. Another problem with CBD films is the high concentration of impurities and the numerous adherent particulates of homogeneously nucleated CdS [46-48]. The presence of these impurities endows the layers with a high speed of recrystallization at low temperatures with major changes in the structural and optical properties [45, 49]. These features make the annealing treatment steps necessary to

improve the properties of CdS thin film. Generally, the beneficial effects of a thermal annealing for CBD CdS films are as follows:

- improvement of crystalline quality by removal of random strain [50-52];
- phase transition and thereby change of the band gap [53];
- improvement of electrical properties, in particular, the reduction of CdS resistivity [9], conferring the required concentration and mobility of electrons to the layers, and good ohmic front contact in the TCO/CdS interface.

In the last few years, several groups have studied the influence of thermal annealing in different atmospheres on the properties of CdS thin films. This influence was shown to be directly dependent on whether the annealing atmosphere is neutral, reducing or oxidizing [44, 49, 53-57], as well as the duration and/or temperature of the annealing process [8, 46]. Generally, neutral annealing brings a significantly improved crystalline quality of the film, while the oxidizing atmosphere assures grain growth and a pinhole free CdS thin film. The presence of H<sub>2</sub> in a reducing atmosphere strongly decreases the concentration of oxygen containing species [58], creates a moderately reducing ambient environment and decreases the concentration of Cd vacancies [59], which are responsible for acceptor centers that participate in the compensation of charge carriers in CdS [60]. A review of CBD CdS properties influenced by the post-deposition treatment is presented in Table 1.2.

*Table 1.1. Influence of deposition parameters on the properties of CBD CdS thin films.*

Deposition parameter	Changes in CdS properties	Ref.
Increase of duration and temperature	<ul style="list-style-type: none"> <li>- Promotes the adherence of colloids and larger particles from the solution;</li> <li>- Increases the pinhole density;</li> <li>- Promotes the cubic-hexagonal transformation with improvement of film crystallinity;</li> <li>- Decreases the E<sub>g</sub>;</li> <li>- Decreases the grain size;</li> <li>- Highest deposition temperature of 85 °C leads to the lowest resistivity and highest mobility.</li> </ul>	[23] [61] [62] [63] [64]
Different Cd salts	<ul style="list-style-type: none"> <li>- Lower release rate of Cd<sup>2+</sup> from Cd(CH<sub>3</sub>COO)<sub>2</sub> in the solution implies higher deposition rates;</li> <li>- CdCl<sub>2</sub> promotes CdS films with relatively larger band gaps and higher quality;</li> <li>- CdI<sub>2</sub> has the lowest initial growth rate.</li> </ul>	[23] [65]
Increase of S/Cd ratio	<ul style="list-style-type: none"> <li>- Increases the E<sub>g</sub>;</li> <li>- Reduces the grain size;</li> <li>- Increases the optical transmission above the threshold;</li> <li>- Improves the coverage of grains.</li> </ul>	[8] [66] [67]
Complexing agent	<ul style="list-style-type: none"> <li>- Ammonium determines the pH of solution;</li> <li>- Tartaric acid improves the quality of CdS film in terms of thickness, uniformity and adherence to the substrate surface.</li> </ul>	[44] [68] [69]

pH	<ul style="list-style-type: none"> <li>– Controls the rate of CdS formation;</li> <li>– Inversely influences the band gap.</li> </ul>	<p>[23] [70] [71] [72]</p>
Nature of substrate	<ul style="list-style-type: none"> <li>– Si substrates suffer structural changes during CdS deposition;</li> <li>– The choice between indium doped tin oxide (ITO) and fluorine doped tin oxide (FTO) is determined primarily by the deposition temperature of CdS and/or the absorber;</li> <li>– For solar cell applications, FTO substrates give excellent reproducibility.</li> </ul>	<p>[37] [73] [74]</p>
Construction of the CBD set up	<ul style="list-style-type: none"> <li>– Keeping a constant pH of solution during the deposition;</li> <li>– Controlling the stirring of solution;</li> <li>– Removing bubbles from the CdS surface;</li> <li>– Improving utilization of Cd species.</li> </ul>	<p>[43] [69] [75]</p>

*Table 1.2. Influence of annealing parameters on the properties of CdS thin films.*

Annealing parameter	Changes in CdS properties	Ref.
Increase of duration and temperature	<ul style="list-style-type: none"> <li>– Increases the rate of changes in the properties of film;</li> <li>– Increases the risk of porosity;</li> <li>– Allows the tuning of <math>E_g</math>;</li> <li>– Decreases the refractive index at a given wavelength;</li> <li>– Contributes to sulfur effusion from the film at higher temperatures.</li> </ul>	<p>[8] [45]</p>
Reducing atmosphere	<ul style="list-style-type: none"> <li>– Requires lower exposure times;</li> <li>– <math>H_2</math> is a strong agent for grain boundary passivation by oxygen removal;</li> <li>– Substantially decreases the resistivity;</li> <li>– Preserves the cubic phase during the entire thermal process.</li> </ul>	<p>[49] [54] [55] [56]</p>
Oxidizing atmosphere	<ul style="list-style-type: none"> <li>– Increases the grain size;</li> <li>– Improves the film crystallinity;</li> <li>– Substantially decreases the <math>E_g</math>;</li> <li>– Creates oxygen containing phases on the CdS surface;</li> <li>– Increases the resistivity of the films.</li> </ul>	<p>[44] [50] [55] [57]</p>

Neutral atmosphere	<ul style="list-style-type: none"> <li>– Improves the film crystallinity;</li> <li>– Reorients the as deposited CdS film;</li> <li>– Decreases the resistivity;</li> <li>– Increases the grain size;</li> <li>– Decreases the number of grain boundaries;</li> <li>– Assures the phase transition from cubic to hexagonal.</li> </ul>	[53] [55]
--------------------	---------------------------------------------------------------------------------------------------------------------------------------------------------------------------------------------------------------------------------------------------------------------------------------------------------------------------------------	--------------

To summarize, a correlation between deposition and post-deposition treatment, capable of conferring suitable properties to CBD CdS films, is still missing. Although plenty of research has been conducted in this direction, there is a lack of commonly accepted understanding for the physico-chemical nature of the processes taking place in the thermal annealing process and the resulting changes of CdS properties. This thermal annealing in a defined atmosphere is an important method to reduce the extent of disorder in CBD CdS and to control the changes in the film properties.

#### 1.4. Application of CBD CdS film in CdTe solar cells

CBD received an important impetus in the PV sector because CdS films chemically deposited on CdTe [76] and CuInSe<sub>2</sub> [77] absorbers were shown to result in superior solar cells compared with the previously studied evaporated CdS [78]. Currently, a CBD CdS buffer layer is also used in monograin and kesterite solar cells [79, 80].

For solar cell applications, CdS films should be conductive, thin and uniform [3]. High conductivity of CdS films increases the built-in potential as an absorber, which in turn improves the photovoltage of the solar cell [81]. Film uniformity avoids shorting pathways between the TCO and the absorber [82]. If thinning raises the transparency of the CdS film and increases short-circuit current [83], then thicker films stop the decrease in  $V_{OC}$  and CdS is not consumed as a result of interdiffusion [84, 85] at the junction interface.

Cell-processing conditions promote this interdiffusion between the absorber and CdS in response to the thermodynamic driving force for alloy formation on each side of the interface. For example, in a CdS/CdTe solar cell, a narrow intermixing between CdS and CdTe allows a smoother transition between both lattices, but the resulting shift of the CdS bandgap reduces the film transmission and lowers the shorter-wavelength quantum efficiency (QE) [4]. CdS intermixing can be minimized by a thermal treatment that would recrystallize the film or by judicious control of device processing [86, 87]. Another proposed strategy to reduce CdS absorption losses was to mix CdS with ZnS in order to increase the bandgap and transmission of the buffer layer. However, as ZnS is chemically less stable than CdS during the CdCl<sub>2</sub> treatment [88], simple mixing has not produced net performance gains [4].

Despite the lower crystallinity of CBD thin films in comparison with other techniques, the CBD CdS films give excellent results for PV applications due to their high relative photoconductivity in the n-type region and better morphological properties, such as low roughness and pinhole density [89]. Furthermore, regardless of toxicity, compatibility or waste aspects, manufacturers of CIGS solar cells preferably apply CBD CdS buffers simply because they result in the highest efficiencies [32].

To summarize, CBD CdS thin films represents a suitable buffer layer for several types of solar cells, but still require some improvements in terms of pinhole free

coverage, reduced absorption and limited interdiffusion with the absorber. Additionally, when applied in a solar cell construction, CBD CdS is highly sensitive to the post-deposition thermal processes due to the high concentration of impurities and defects. A solution for these issues can be the thermal annealing of CBD CdS, which would improve film compactness, minimize the interdiffusion by recrystallizing the film and tailor the properties of CBD CdS to the relevant application.

## 1.5. Summary of the literature overview and aim of the study

The studies reported in the literature on the chemical bath deposition of CdS, and its subsequent thermal annealing as well as the solar cell application of this material can be summarized as follows:

1. A CdS thin film represents an interesting II-VI compound semiconductor in the field of material science due to its properties, such as wide band gap, high transparency, tunable electrical properties, the ability to have a zinc blende or wurtzite structure and the numerous available fabrication techniques.
2. One of the most important applications of CdS is in the fabrication of solar cells. CdS is considered the perfect n-type buffer for CdTe, CIGS and kesterite absorbers in superstrate or substrate configurations.
3. Among the various techniques to produce CdS, the most popular dry methods for CdS thin films are considered to be RF sputtering and thermal evaporation, while the most used wet method is CBD, with the latter having significant advantages in simplicity and low cost. Other major advantages of CBD for CdS can be listed as follows: large area deposition, conformal coating, controllable thickness and compatibility with a variety of applicable substrates.
4. As deposited CBD CdS films tend to form in the cubic phase and have poor crystalline quality. Also these films contain numerous adherent particulates of homogeneously nucleated CdS and a high concentration of impurities, which endows the layers with a high speed of recrystallization at low processing temperatures.
5. A thermal annealing step is required for CBD CdS, as it improves the film crystalline quality, removes the random strain, changes the  $E_g$ , supports the phase transition and improves the electrical properties. In other words, annealing can be used as a tool for the management of CBD CdS properties by adjusting the parameters of the thermal process.
6. For solar cell applications, the thermal annealing of CBD CdS could also solve issues related to shortcutting pathways and interdiffusion at the junction interface.
7. Although the thermal annealing of CBD CdS thin films is widely studied by many groups, a mechanism describing the physico-chemical processes responsible for the changes in CdS properties is still missing. The understanding of such mechanism would help us to control and tailor the properties of CBD CdS thin films for solar cell applications.

On the basis of studies made on CdS thin films and from an application point of view, the aims of the present doctoral thesis were:

1. to prepare CdS thin films by chemical bath deposition and to anneal them in reducing, neutral or oxidizing atmosphere for different durations and temperatures;
2. to study the effect of annealing process on the crystallographic, microstructural, optical and electrical properties of CBD CdS films;
3. to describe the physico-chemical processes responsible for the changes in CdS thin film properties as a result of annealing;
4. to use annealed CdS films in a CdS/CdTe solar cell structure and to show the influence of CdS annealing on the properties of junction.

## 2. EXPERIMENTAL

### 2.1. Chemical bath deposition and thermal treatment of CdS films

Using a traditional CBD setup (Fig. 1.1), CdS thin films were deposited successfully onto different substrates, including glass, ITO/glass, FTO/glass and polyimide. Because of the large number of experiments, data on CdS films on polyimide substrate were not included in this work. The 25 mm × mm glass plates were properly cleaned and immersed in the water solution of 1 mM CdSO<sub>4</sub>, 10 mM thiourea, 0.2 M NH<sub>4</sub>OH and 30 mM (NH<sub>4</sub>)<sub>2</sub>SO<sub>4</sub>. For CdS doping, a low concentration of NH<sub>4</sub>Cl solution (0.1 μM) was added in the deposition bath. The pH, temperature, and agitation speed of the solution were 10.5, 85 °C and 500 rpm, respectively. Different durations of deposition were used to tune the thickness of the CdS films. Except the duration, all other deposition parameters were constant [I].

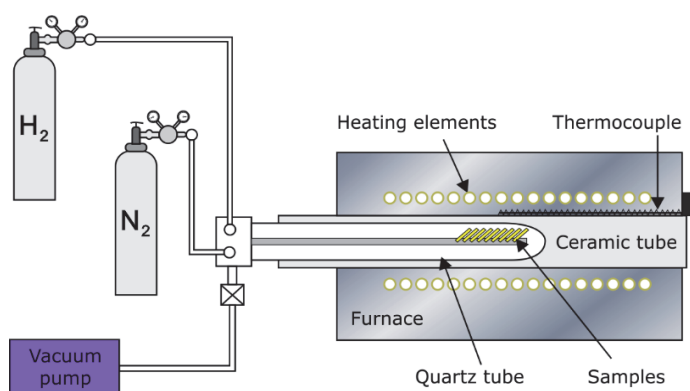


*Fig. 2.1. Scheme of annealing setup.*

After deposition and rinsing with deionized water, all ~ 100 CdS films were vacuum dried in a closed quartz tube at 120 °C for 1 h in order to remove most of the secondary phases of water, hydroxides and organic impurities. At this stage, the CdS films obtained the “as deposited” label. Afterwards, a thermal annealing step was applied in preheated furnace using the same process tube (Fig. 2.1). The vacuumed process tube with CdS samples was filled with 1 atm. hydrogen, nitrogen or a mixture of H<sub>2</sub> and N<sub>2</sub> gases at room temperature then closed and introduced into the cylindrical ceramic tube (Fig. 2.1), where the constant temperature and time were set (Table 2.1). The gas pressure in the process tube was maintained by a standard gas reduction system and was not influenced by the gas expansion at higher temperatures of annealing. Large diameter (55 mm) and volume (1.5 l) of the process tube ensured a gas convection flow so that the reaction products were transported in the colder part of the tube. In the case of air annealing the process tube was opened at the colder part of the quartz tube. A detailed description of the annealing process is presented in papers I-IV.

Table 2.1. Variable parameters of the annealing process for CBD CdS films.

Gas	Annealing parameters	
H <sub>2</sub>	T, °C	200, 250, 300, 350, 400, 450
	Time, min.	3, 5, 10, 20, 30, 60, 120
N <sub>2</sub>	T, °C	250, 400
	Time, min.	10, 30, 60, 120
Air	T, °C	250, 400
	Time, min.	10, 30, 60, 120
5% H <sub>2</sub> + 95% N <sub>2</sub>	T, °C	250, 400
	Time, min.	60

## 2.2. Characterization of CBD CdS films

The morphology, coverage, grain size and elemental composition of CdS films were studied by scanning electron microscopy (SEM), atom force microscopy (AFM) and energy dispersive spectroscopy (EDX). High-resolution SEM apparatus (Zeiss EVO-MA15) was used at an operating voltage of 10 kV. The AFM operated in a “semi-contact” (tapping) mode using the NT-MDT Solver 47 Pro system. The image analysis of AFM 2D images was performed using the Media Cybernetics Image Pro-3.0 program. For the EDX analysis the Rontec EDX XFlash 3001 detector and the Oxford Instruments INCA Energy system were used. The quantitative results were obtained by the help of factory defined standard using the PAP correction – a method for light elements. Due to the low thickness of the CBD CdS films and the strong signal from glass substrate, the amount of oxygen from the EDX data was estimated by subtracting the concentration of SiO<sub>2</sub> from the total oxygen content in the film [I].

The phase composition, crystallographic properties and optical phonons were observed by X-ray diffraction (XRD) and Raman spectroscopy. The XRD measurements were made in the Bragg–Brentano ( $\theta$ – $2\theta$ ) geometry by the Rigaku Ultima IV diffractometer with Cu-K $\alpha$  radiation. The room temperature Raman spectra were recorded in a 180° backscattering geometry by using the Horiba's LabRam HR high resolution spectrometer. The incident laser light with the wavelength of 532 nm was focused on the sample within a spot of 10  $\mu$ m in diameter and the spectral resolution of the spectrometer was about 1.5 cm<sup>-1</sup>. Each spectrum was smoothed with Lorentz fitting and peak position and Full Width at Half Maximum were obtained.

From the XRD patterns, the crystallite size ( $L$ ) was obtained by the Scherrer formula (2.1), where  $B$  is the peak width,  $K$  is the Scherrer constant,  $\lambda$  is the wavelength of X-radiation, and  $\theta$  is  $\frac{1}{2}$  the diffraction angle.

$$B(2\theta) = \frac{K\lambda}{L\cos\theta} \quad (2.1)$$

To determine the interplanar distance ( $d$ ) Bragg's law was applied (2.2), where  $n$  is a positive integer and  $\lambda$  is the wavelength of the incident wave.

$$2d\sin\theta = n\lambda \quad (2.2)$$

The optical characteristics were measured in the wavelength range of 200–2500 nm on the Jasco V-670 UV–vis–NIR spectrophotometer equipped with an integrating sphere. Total optical transmission and reflection spectra were used to determine the transmittance of CdS and the optical thickness. Based on the Tauc relation (2.3), the values of  $E_g$  have been estimated from the  $(\alpha h\nu)^2$  versus  $h\nu$  dependence, by taking the intercept of the extrapolation to zero absorption on a  $h\nu$  axis.

$$h\nu = A(h\nu - E_g)^r \quad (2.3)$$

$\alpha$  is the absorption coefficient, given by  $\alpha = 2.303 \log(T/d)$  ( $d$  here is film thickness and  $T$  is transmission),  $h\nu$  is the photon energy, and the exponent  $r$  denotes the nature of the transition ( $r = 1/2$  for direct allowed transitions).

The electrical properties of the CdS films (resistivity, charge carrier concentration and mobility) were measured in the temperature range of -100 °C to 100 °C, using MMR's Variable Temperature Hall System and a Hall, Van der Pauw Controller H-50. The contact material used for electrical measurements was evaporated indium [II, IV]. In-plane resistivity and charge carrier concentrations were calculated for the thickness (300 - 350 nm) estimated from transmission and reflection spectra and confirmed by SEM analysis. The impurity levels were analyzed by photoluminescence (PL) measurements at room temperature with a green laser (532 nm) and 10 mW density of excitation. PL spectra were registered by a Renishaw - type device with a built-in measuring Raman installation [IV].

### 2.3. Fabrication and characterization of CdS/CdTe solar cells

With the as deposited and annealed CBD CdS films in  $H_2$  and air at 400 °C for 1 h and 2 h, complete CdS/CdTe solar cell devices were fabricated. A 3 – 4  $\mu\text{m}$  thick CdTe layer was deposited by CSS onto the CBD CdS layer (Fig. 2.2) at source and substrate temperatures of 610 °C and 500 °C, respectively. This was followed by a soaking in CdCl<sub>2</sub> solution, air treatment at 420 °C, NP etching and deposition of gold back contact by evaporation. Finally the CdS/CdTe samples were scribed into cells of 5 mm  $\times$  5 mm dimension. More technological details are shown in [V].

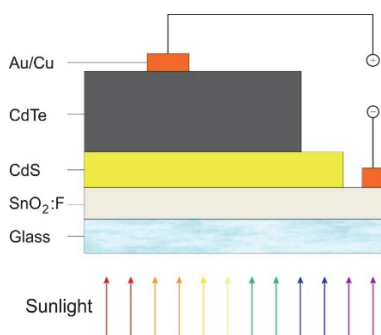


Fig. 2.2. Schematic structure of superstrate CdTe solar cell.

The surface morphology of the cross-section of the CdS/CdTe solar cell was examined by SEM, whereas the performance of the CdS/CdTe solar cells were

characterized by J–V curves and quantum efficiency (QE) measurements under AM1.5 (100 mW/cm<sup>2</sup>) illumination [V].

### 3. RESULTS AND DISCUSSION

The following sections, 3.1 and 3.2, contain a systematic study of the structural, electrical and optical properties of the CBD CdS thin films, altered by thermal processing at various annealing conditions in hydrogen, air and nitrogen gas. The mechanism of physico-chemical processes responsible for the changes in the properties of CBD CdS are proposed. Results have been published in papers I, II, III and IV.

#### 3.1. Properties of CBD CdS films annealed in variable conditions of ambient

##### 3.1.1. Structural properties

Several characteristics for all as deposited and thermally annealed CBD CdS films were revealed by microstructural analysis:

- The surfaces of CBD CdS films may rarely feature large aggregated particles, which were homogeneously formed in the deposition solution. (Fig. 3.1);
- The grains of CBD CdS films have a columnar shape and grow perpendicular to the glass substrate (Fig. 3.2);
- CdS grains have a mean diameter of 260 nm and are formed by small crystallites (Fig. 3.2b), with sizes in the range of 30 to 45 nm (from XRD analysis);
- The oxidizing ambient slightly enhanced the grain growth at 250 °C, while annealing at 400 °C in N<sub>2</sub> and H<sub>2</sub> ambients contracted the grains (Fig. 3.1, Table 3.1).

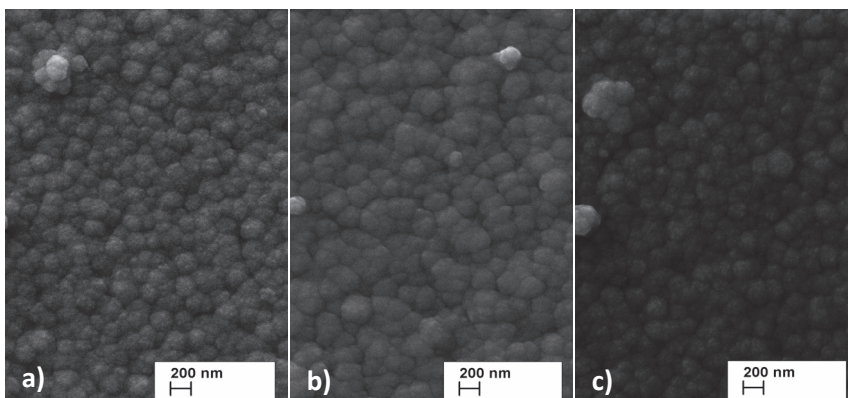


*Fig. 3.1. SEM plane view of as deposited (a) and annealed CdS films – in air at 250 °C (b) and in nitrogen at 400 °C (c) both for 1 h. (A modified version of Figure 1 from [I])*

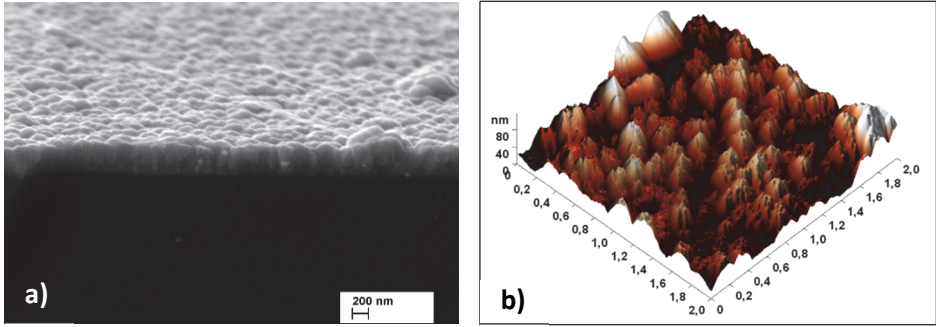


Fig. 3.2. a) SEM cross section view of CdS film annealed in  $H_2$  at 250 °C for 1 h; b) AFM image of as deposited CdS film.

Table 3.1. RMS roughness values for the as deposited and annealed CdS films in different ambient conditions at 250 °C and 400 °C.

Sample name	RMS, nm		
	As dep.	250 °C	400 °C
$H_2$ annealed CdS	17.9	11.7	13.4
$N_2$ annealed CdS		14.8	13.4
Air annealed CdS		16.2	15.4

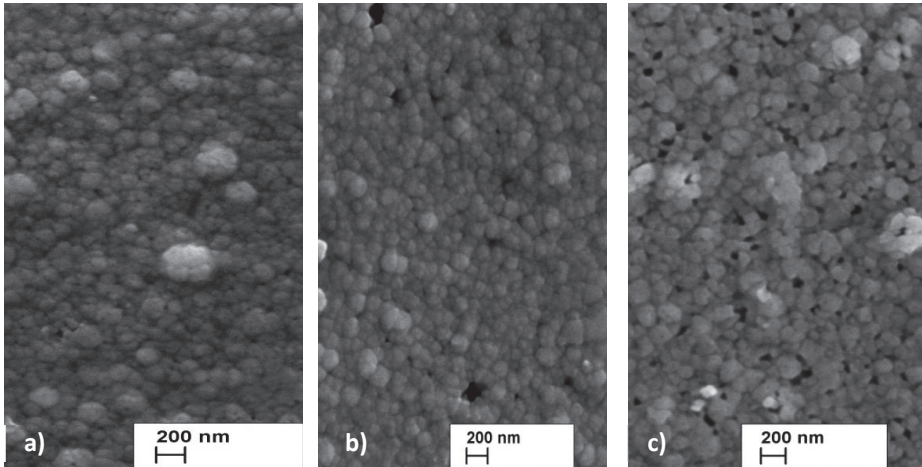


Fig. 3.3. SEM top view of CdS film annealed in  $H_2$  at 450 °C for 10 min (a), 20 min (b) and 60 min (c) [1].

Based on morphology studies of CBD CdS films, we assessed the maximal temperature for thermal annealing of conformal and pinhole free CdS. Annealing for only 10 min at 450 °C generated pinholes in the film, whereas longer processing made it porous (Fig. 3.3). CdS porosity is attributed to the intra-grain recrystallization and sintering of the primary crystallites, resulting in the contraction of grains. Therefore, 400 °C seems to be the highest applicable temperature for thermal annealing that provides low porosity CdS films with suitable properties for the following applications in PV devices.

### 3.1.2. Electrical properties

As we studied CBD CdS thin film as a potential n-type buffer partner for CdTe, CIGS and CZTS p-type absorbers, the electrical properties of CdS films and how are they affected by the thermal annealing process were considered extremely important.

The kinetics of electron density for CdS films annealed in H<sub>2</sub> at temperatures from 200 °C to 400 °C (Fig. 3.4) can be divided into two stages. The first one is characterized by a sharp increase of electron concentration to the level of 10<sup>19</sup> cm<sup>-3</sup>, whereby the growth rate substantially increases with the processing temperature. This fast process, as later will be discussed, corresponds to the interactions in the lattice of crystallites at the atomic level. In the second stage, at 200 – 250 °C, the electron density reaches a plateau, and at higher temperatures (350 – 400 °C), the electron density will slowly decrease with a temperature dependent rate, indicating that this kinetics is limited by diffusion processes. At each annealing temperature, a technologically important plateau of stable electron concentration is reached at 30 min for low annealing temperatures and at 60 min for higher temperatures (Fig. 3.4). These changes in electrical properties are stable to subsequent etching with acetic acid, which indicates that they occur in the bulk of the polycrystalline material and not only at the CdS film surface.

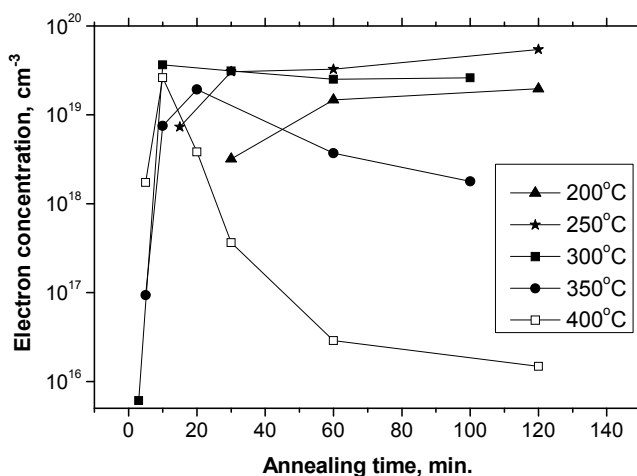


Fig. 3.4. Electron concentration vs annealing time for CBD CdS thin films annealed in H<sub>2</sub> at different temperatures.

Similar to the case of H<sub>2</sub> annealing, a stable electron density is reached for air and nitrogen environments (Fig. 3.5) after 60 min of annealing at 400 °C, while for 250 °C it will stabilize at 30 min. The ambient gas does not influence the general trend of changes in CdS conductivity. Due to the presence of oxygen, the air annealed CdS films will have lower conductivity than H<sub>2</sub> and N<sub>2</sub> annealed samples. The same processes with higher rates take place at 400 °C, and significantly higher resistivity is achieved in air and N<sub>2</sub> annealing (Fig. 3.5) in comparison with the H<sub>2</sub> atmosphere.

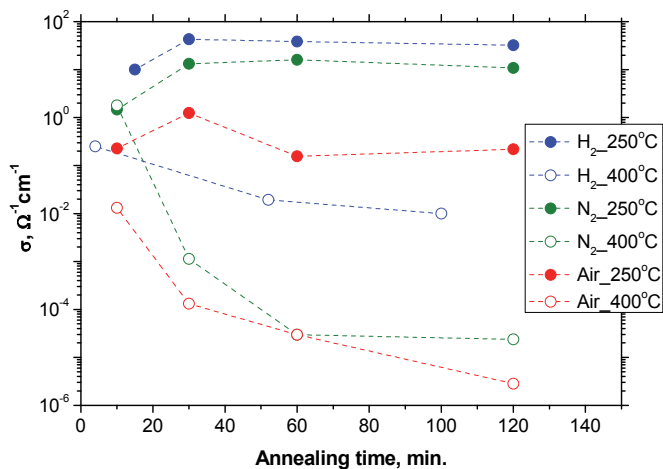


Fig. 3.5. Electrical conductivity of CdS films at room temperature as a function of annealing time, temperature and atmosphere.

The temperature dependence of electrical conductivity (Fig. 3.6) shows that high conductivity of CdS films annealed at low temperatures is generated by shallow donors with activation energies of approximately 10 – 20 meV. The conductivity of such degenerated semiconductor films weakly depends on the measurement temperature. Higher annealing temperatures, approximately 400 °C, remove these shallow donors and the lower conductivity is caused by the deep donors located at approximately 120 meV below the conduction band.

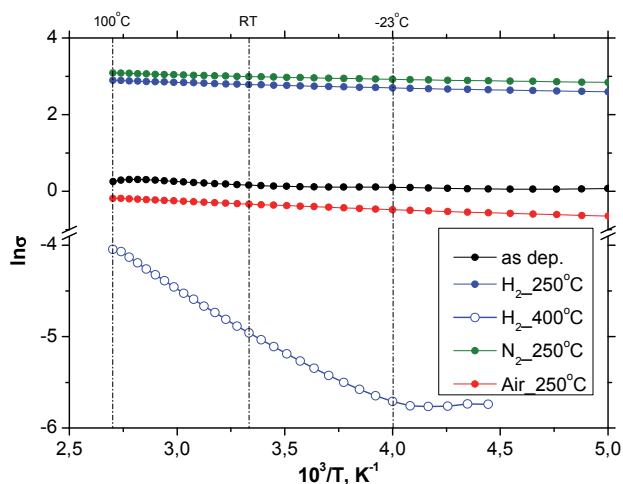


Fig. 3.6. Temperature dependence of electrical conductivity for CdS films annealed for 1 h in H<sub>2</sub>, N<sub>2</sub> and air [IV].

### 3.1.3. Optical band gap

Figure 3.7 shows that the decreasing trend of  $E_g$  becomes more prominent as the annealing temperature increases, and a similar behavior of  $E_g$  is typical for all annealing atmospheres (Fig. 3.8).

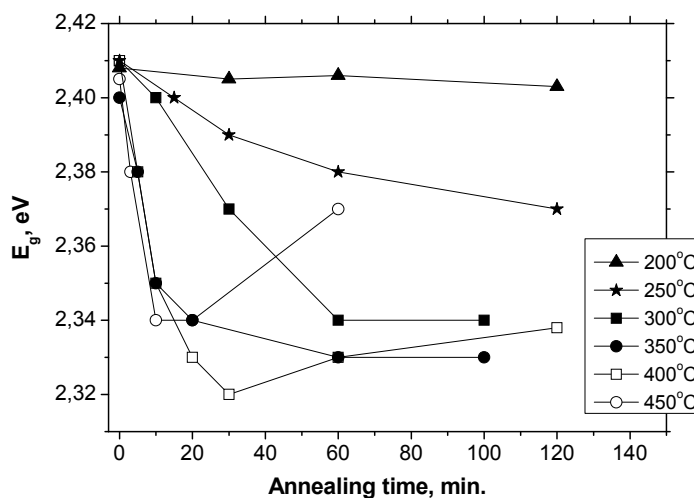


Fig. 3.7. Band gap of H<sub>2</sub> annealed CdS films as a function of annealing time and temperature [I].

The annealing process steadily reduces the  $E_g$  to 2.34 and 2.33 eV for 300 and 350 °C, respectively. The lowest  $E_g$  value (2.32 eV) is reached after 30 min annealing in H<sub>2</sub> at 400 °C. Longer annealing at 400 °C and 450 °C increase the band gap, becoming closer to the  $E_g$  value for bulk CdS (2.42 eV). One can observe a striking similarity between the kinetics of band gap and electrical conductivity for CBD CdS films annealed in different gas environments (Fig. 3.5, 3.8).

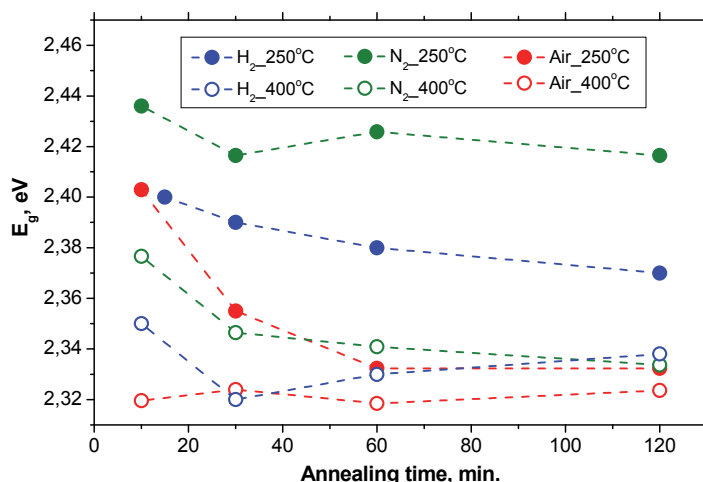


Fig. 3.8. Band gap of CdS films vs annealing time for different ambient conditions and temperatures [IV].

### 3.1.4. XRD and Raman analyses

XRD patterns for H<sub>2</sub> annealed CdS films show no evidence of secondary phases, except a crystalline CdS phase textured in the [111] orientation [I], while annealing in air and nitrogen for 1 h at 400 °C generate a CdSO<sub>3</sub> phase on the CdS surface (Fig.

3.9). After 2 h annealing in nitrogen, this secondary phase is removed, whereas in air annealing it is transformed to CdO.

The main (111) peak located at approximately  $26.4^\circ$  has been treated in the literature as corresponding to both cubic and hexagonal modifications [90]. We analyzed the diffraction patterns in the region of  $26 - 27^\circ$  at higher resolution (Fig. 3.10). Compared with cubic  $26.4^\circ$  and hexagonal  $26.8^\circ$  positions [91, 92], one can see that, for the as deposited film and those annealed at low temperatures in  $H_2$ , the main peak is located close to the hexagonal position. With increasing annealing temperature up to  $400 - 450^\circ C$ , this peak shifts towards the cubic position. For air and  $N_2$  annealed samples, the position of the (111) peak is stabilized at approximately 60 min of  $400^\circ C$  annealing, before reaching the cubic position. This shift is not affected by whether the substrate is glass or ITO (Fig. 3.11) or by the annealing atmosphere (Fig. 3.12).

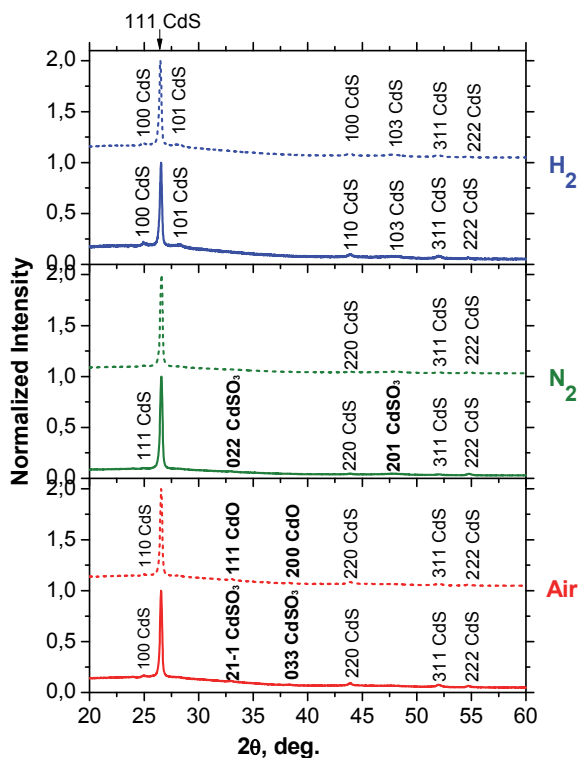


Fig. 3.9. XRD patterns of CdS films annealed at  $400^\circ C$  in  $H_2$ ,  $N_2$  and air for 1 h (solid line) and 2 h (dash line) [IV].

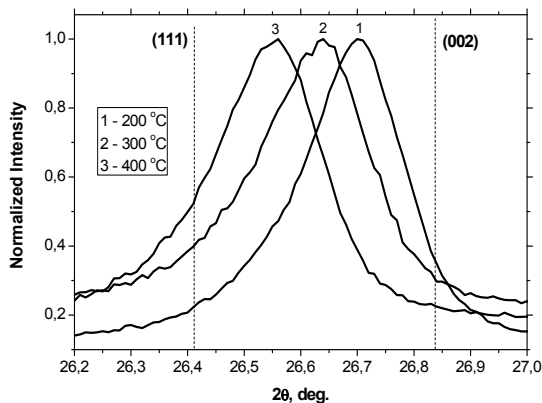


Fig. 3.10. Shift of the (111) peak with increasing annealing temperature for H<sub>2</sub> annealed CdS films. (A modified version of Figure 4 from [I])

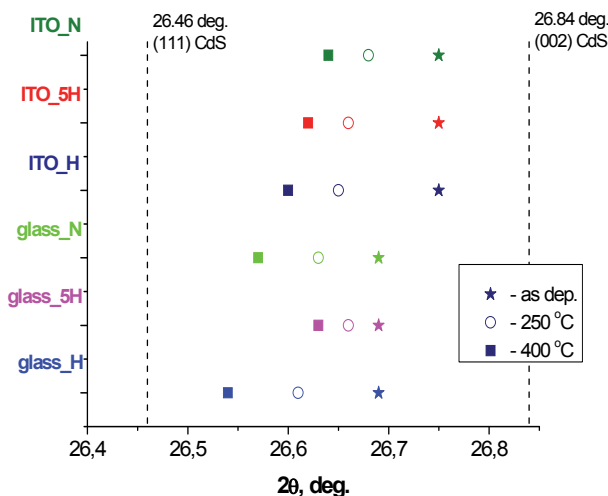


Fig. 3.11. Shift of the (111) peak in dependence of glass or ITO substrate, annealing temperature and ambient (H-hydrogen, N-nitrogen, 5H-5% H<sub>2</sub> with 95% N<sub>2</sub>) [III].

On the other hand, the displacement of the (111) peak to the position corresponding to the cubic CdS structure is accompanied by the lattice relaxation as the interplanar distance and lattice constant become larger when annealing temperature increases (Table 3.2). Additionally, a slight destruction of crystallites is observed, similar to the Metin’s study of nitrogen annealed CdS films [45].

Table 3.2. Crystallite size ( $s$ ), interplanar distance ( $d$ ) and lattice constant ( $a$ ) for CdS layers annealed for 1 h at 400 °C in H<sub>2</sub> [I].

T <sub>anneal</sub> , °C	s, nm	d, Å	$\alpha$ , Å
200	42.9	3.335	5.77
250	42.0	3.338	5.79
300	39.1	3.343	5.79
350	40.3	3.343	5.81
400	40.3	3.354	5.82

The lattice stress shown by XRD [IV] was confirmed by Raman measurements. The 1LO peak (300 cm<sup>-1</sup>) of the as deposited CdS films narrows at 400 °C annealing (Fig. 3.13). Additionally, the decreased intensity of 1LO peak with annealing was attributed to the shift of the crystalline structure to a more cubic phase [IV], which is in accordance with the XRD data

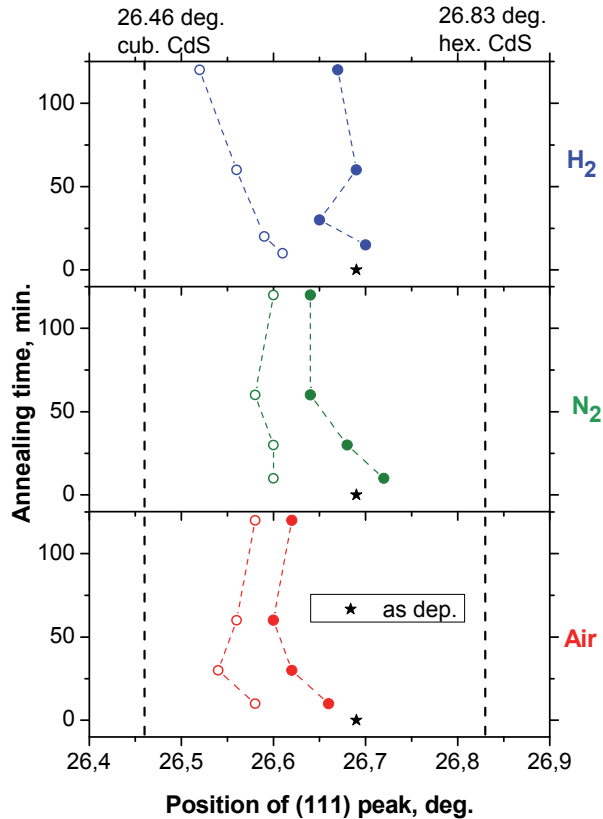


Fig. 3.12. Displacement of the (111) peak vs processing duration at 250 °C (open circles) and 400 °C (solid circles) for different ambient gases: H<sub>2</sub>, N<sub>2</sub>, and air [IV].

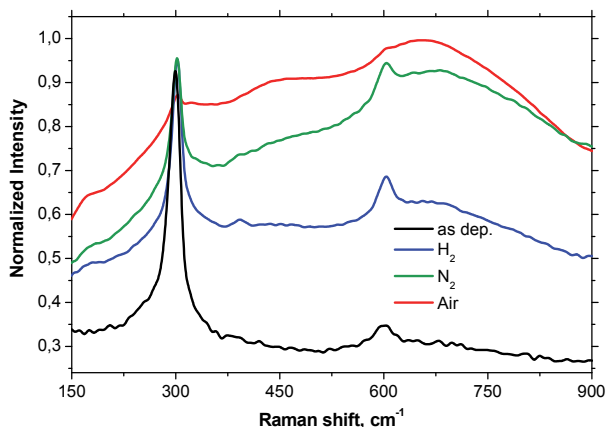


Fig. 3.13. Raman spectra of CdS films annealed at 400 °C for 1 h in different ambient [IV].

### 3.1.5. Elemental analysis

EDX analysis (Table 3.3) indicates that our CBD CdS films are Cd-rich for all annealing temperatures. In addition, for as deposited CdS thin films and those annealed at 200 – 250 °C, strong evidence for O impurity (10 at.%) was found, whereas at higher annealing temperatures, [O] was decreased by 3 – 5 at.%.

Table 3.3. EDX relative atomic concentrations in H<sub>2</sub> annealed CdS thin films vs annealing temperature. Annealing time was 1 h. (A modified version of Table 1 from [I])

Element	Relative atomic concentration, at.%				
	200 °C	250 °C	300 °C	350 °C	400 °C
S	39.4	39.5	39.1	38.6	42.2
Cd	46.8	47.4	46.7	46.5	48.5
O	10.0	11.0	10.0	3.0	5.0

Because our measurement possibilities for the chemical composition of CBD CdS have been limited, we compared our EDX data with results from the literature. Niles and Nair proved an 11 at.% abundance of oxygen by X-ray photoelectron spectroscopy (XPS) [93, 57], while Weber et al. showed the same atomic amount of hydrogen by nuclear reaction analysis [58]. Moreover, Kylner indicated the presence of Cd(OH)<sub>2</sub> and CdO using XPS [94], whereas Danaher claimed an uniform distribution of Cd(OH)<sub>2</sub> and CdO through the film by secondary ion mass spectroscopy [47]. All of these statements confirm our EDX results and indicate the presence of both oxygen and hydrogen in CBD CdS films, most likely as an (OH) group.

### 3.2. Physico-chemistry of the processes in CBD CdS thin films induced by thermal annealing

An as deposited CBD CdS thin film with 300 – 350 nm thickness is characterized by a wide band gap (2.42 eV), high resistivity (600 Ω-cm in dark), high photoconductivity and noticeable PL at approximately 1.65 eV [IV], corresponding

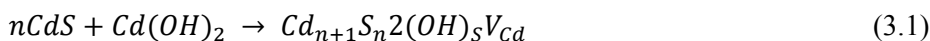
to the well-known complex ( $V_{Cd}D$ ), where D is a donor impurity. Reduction of CBD CdS film resistivity by 3 – 4 orders of magnitude [II] with the creation of high electron density of approximately  $10^{19} \text{ cm}^{-3}$  (Fig. 3.4, 3.5) after 10 min of annealing at relatively low temperatures (200 – 250 °C) represents the most striking result. Such a degenerated semiconductor layer might crucially influence the quality of the p-n junction in a substrate configuration solar cell when it is heated to approximately 200 °C for the sputtering deposition of the i-ZnO/ZnO:Al layer. Therefore, it is extremely important to explain the physico-chemical mechanism behind the changes in the CdS properties.

The high conductivity of CdS films annealed at low temperatures in reducing, oxidizing and neutral atmosphere cannot be explained by the creation of a conductive phase of CdO from residual oxide components [49, 57] because reduction of CdO in  $H_2$  already begins intensively at approximately 200 °C [I]. Moreover, the formation of CdO in the processing solution is prevented by the basic ammonia medium we used for CdS deposition. Additionally, it cannot be explained by the recrystallization of “amorphous” CdS [46], as CdS is deposited in the form of 40 nm sized crystallites [I] and no growth or sintering of these crystallites is observed up to 250 °C. And finally, we will later show that it cannot be explained only by the creation of sulfur vacancies by decomposition of CdS, as proposed in [45, 49].

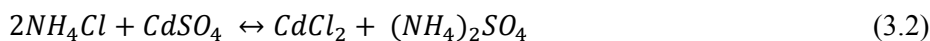
For the explanation of the abrupt fall in resistivity, we raised a hypothesis about the incorporation of cadmium hydroxide into the CdS lattice in the deposition process from a basic ammonia solution [II]. This hypothesis is in accordance with the hydroxide mechanism of CdS formation in the CBD process, where hydroxide clusters act as a catalyst for thiourea decomposition so that CdS formation occurs preferentially on the surface of hydroxide rather than nucleating separately in the solution [27]. Comparing our results to those of other groups (Section 3.1.5), we claim that all oxygen indicated by the EDX analysis in the as deposited CBD CdS (Table 3.3) is present in the (OH) form. The hydroxide group, which is spatially compatible with sulfur (Table 3.4), seems to incorporate into CdS on a sulfur site, acting as a shallow donor [20], thereby forming the cadmium hydroxysulfide as a solid solution of cadmium hydroxide in CdS (3.1).

Table 3.4. Covalent radii of components [95].

Chemical component	Cd	S	O	H	OH	Cl
Covalent radius, pm	144	105	66	31	96	102



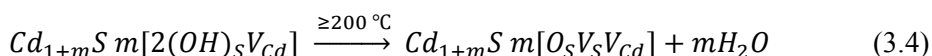
Actually, (OH) incorporates on sulfur site similarly to the scheme of  $Cl_s$  incorporation, introduced in the deposition solution as  $NH_4Cl$  (3.2) (Section 2.1). Both  $CdCl_2$  and  $Cd(OH)_2$  create one  $V_{Cd}$  per every pair of incorporated  $Cl_s$  or  $(OH)_s$  (3.1). In result, the double charged acceptor  $V_{Cd}^{2-}$  compensates the  $(OH)_s^+$  and  $Cl_s^+$  shallow donors, so that the as deposited CBD CdS thin film represents a compensated and resistive n-type semiconductor.



The (3.1) reaction can be written for one mole of CdS, where a very small number  $m$  of Cd(OH)<sub>2</sub> moles is incorporated (3.3).



When CBD CdS undergoes a thermal treatment, at low annealing temperatures, the hydroxide groups become unstable and start to decompose (3.4), releasing water, creating sulfur vacancies ( $V_S^{2+}$ ) and resulting in the transition from cadmium hydroxysulfide to cadmium oxysulfide solid solution, where the isovalent oxygen occupies a sulfur site.



The increase in  $[V_S^{2+}]$  (3.4) implies the reduction of  $[V_{Cd}^{2-}]$ , thereby raising the electrical conductivity of CdS thin films annealed at temperatures  $\geq 200^\circ C$  (Fig. 3.4, 3.5).

Another way of looking at this high density of electrons can be achieved by analyzing the side effects of annealing, such as the precipitation of black Cd noticed on the cold regions of the process tube. Low [96] also had shown, by thermal analysis, that Cd(OH)<sub>2</sub> decomposes to CdO<sub>0.81</sub>, which means that the product of thermal decomposition of Cd(OH)<sub>2</sub> is highly enriched with cadmium. This experimental evidence of Cd precipitation allows us to explain the origin of excess Cd in the annealed samples and the decreased transmittance of the annealed CdS films [IV]. We have to assume that the incorporated Cd(OH)<sub>2</sub> contains less than two (OH) groups. In such an extreme case, the cadmium mono-hydroxide (CdOH) is incorporated into the CdS lattice, which is accompanied by the absence of  $V_{Cd}$ . As a result,  $[V_S^{2+}]$  will be much higher than  $[V_{Cd}^{2-}]$  and, by the thermal destruction of the (OH) group, the CdS lattice reveals a Cd excess. This excess of Cd might enable the impurities of  $(OH)_S^+$  and  $Cl_S^+$  to behave as shallow donors, increasing the electron density of the CdS films at low annealing temperatures (Fig. 3.4). At higher annealing temperatures ( $>300^\circ C$ ), although the destruction of the incorporated hydroxide group is accelerated, the concentration of electrons starts to decrease due to the gradual removal of the shallow donor defects (Fig. 3.6).

The hydroxide group mechanism allows us to explain other CBD CdS properties, such as elemental composition, together with the crystallographic and optical properties of CBD CdS films.

Because incorporated Cd(OH)<sub>2</sub> naturally crystallizes into a hexagonal lattice, whereas CdS and CdO tend to grow in cubic structures, the position of the main XRD peak of the as deposited CdS<sub>1-x</sub>(OH)<sub>x</sub> solid solution is located between the hexagonal and cubic structures (Fig. 3.10). As a result, the structure of crystalline lattice of the as deposited layer and those annealed at low temperatures (200 – 250 °C) is intermediate between hexagonal and cubic modifications with a low lattice constant and a narrow interplanar distance (Table 3.2). Durose at al. attributed the strained crystalline lattice of ball milled CdS to specific disorder [90]. In our case, this disorder could be caused by Cd(OH)<sub>2</sub> incorporated into the CdS lattice during the deposition process. The large  $E_g$  for the as deposited and low-temperature-annealed CdS (Fig. 3.7) is also associated with the incorporated Cd(OH)<sub>2</sub>, which has a high band gap [97].

An increase in the annealing temperature (300 – 350 °C) is likely to accelerate the sintering of the as deposited polycrystalline CdS, and the incorporated Cd(OH)<sub>2</sub> starts to decompose to water and CdO (3.1, 3.3). High water pressure, ~ 10<sup>4</sup> atm. [I], contributes to the cracking of CdS crystallites annealed at up to 350 °C (Table 3.1), whereas the presence of CdO narrows the band gap of CdS to a minimum value of 2.32 eV (Fig. 3.8). Due to the decomposition peculiarity of Cd(OH)<sub>2</sub> the excess of Cd decreased the transmission of CdS and FTO substrates [III] in the range of 400 – 1000 nm [IV]. Additionally, at this region of annealing temperatures, the CdS lattice relaxes with the transition from the intermediate to the cubic structure, confirmed by the shift of the main (111) peak (Fig. 3.10, 3. 11). In other words, the thermal annealing eliminates the lattice disorder generated by incorporated Cd(OH)<sub>2</sub> and reorders the CdS film to the cubic structure.

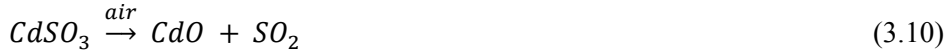
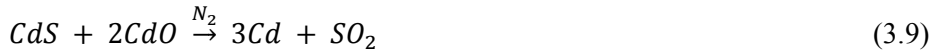
The highest annealing temperatures (>400 °C), together with removal of oxygen and deposit of elemental cadmium observed on the cold walls of process tube, start the out diffusion of chlorine due to high vapor pressure of CdCl<sub>2</sub> (3.2) [98], thereby decreasing the electron density to the level of 10<sup>16</sup> cm<sup>-3</sup>. Some other CdS properties also change in a reverse way: the oxygen content in CdS is slowly increased compared with 350 °C (Table 3.3), the lattice constant (Table 3.2) and E<sub>g</sub> (Fig. 3.7) are restored to the intrinsic values for pure CdS, and the crystallite size starts to increase (Table 3.2). At this temperature region, the oxygen out diffusion is slowed by the closing cracks and retention of oxygen containing phases (Fig. 3.9) in the bulk of the polycrystalline material. The increasing E<sub>g</sub> values for longer annealing at 400 °C and 450 °C may be also explained by the appearance of the (100) and (101) wurtzite peaks in the XRD patterns of CdS films annealed at these temperatures [I].

This phenomenological model is applicable to CdS annealed in various environments with small differences. Because air is more active than H<sub>2</sub> ambient, air annealing shows a deeper removal of oxygen. This is connected with the interaction between CdS, oxygen and CdCl<sub>2</sub> (3.5) proposed by McCandless in [3]. Due to the CdCl<sub>2</sub> flux (3.2) and the high solubility of both cadmium oxygen containing phases and CdS in the CdCl<sub>2</sub> flux [99], the oxygen diffuses into the melted phase and at 400 °C CdSO<sub>3</sub> and CdO are extracted for both air and nitrogen annealed films (3.6, 3.7). The appearance of the CdSO<sub>3</sub> phase instead of CdSO<sub>4</sub>, both being also shown by extended and near-edge x-ray absorption fine structures in [100], might be explained by the limited access of oxygen in the 1.5 l semi closed process tube. This is supported by the out diffusion of Cd, which creates reducing conditions on the film surface.



For longer annealing in N<sub>2</sub>, these oxygen containing phases expelled as metallic Cd and SO<sub>2</sub> (3.8, 3.9), while for longer annealing in air at 400 °C, Cd forms CdO on the CdS surface (3.10).





Because of these oxygen containing phases (Fig. 3.9) on the grain boundaries acting as sources of oxygen back diffusion, the shift of the main (111) peak for CdS films annealed in air and N<sub>2</sub> was stabilized before reaching the position corresponding to the cubic structure (Fig. 3.12).

To summarize, CBD CdS film with a high concentration of electrons (10<sup>19</sup> cm<sup>-3</sup>) was obtained after 10 min of thermal annealing in H<sub>2</sub> at only 200 - 250 °C. As an explanation for the changing properties of CdS films, the incorporation of hydroxide group in the CdS crystalline lattice during deposition process and its destruction during annealing process was proposed.

Due to incorporation of hydroxide group:

- the created Cl<sub>s</sub><sup>+</sup> and (OH)<sub>s</sub><sup>+</sup> shallow donors are compensated by the double charged acceptor V<sub>Cd</sub><sup>2-</sup>, so that the as deposited CBD CdS thin film represents a compensated and resistive n-type semiconductor;
- the lattice parameter and interplanar distance of CdS thin film are lower than values corresponding to bulk cubic CdS, both indicating a stressed crystalline lattice with the main (111) XRD peak located between the positions corresponding to hexagonal and cubic structures;
- the band gap of 2.41 eV, stable up to 250 °C annealing temperatures, is also attributed to the wide band gap of the incorporated Cd(OH)<sub>2</sub>.

Due to the destruction of the incorporated hydroxide group:

- the water is released, the sulfur vacancies V<sub>S</sub><sup>2+</sup> are created and the transition from cadmium hydroxysulfide to cadmium oxysulfide solid solution takes place;
- the increase in [V<sub>S</sub><sup>2+</sup>] implies the reduction of [V<sub>Cd</sub><sup>2-</sup>], thereby Cl<sub>s</sub><sup>+</sup> and (OH)<sub>s</sub><sup>+</sup> shallow donors increase the CdS film electron density at 200 – 250 °C annealing temperatures;
- at annealing temperatures higher than 300 °C the decrease in electron concentration of CdS films is attributed to the removal by out diffusion and evaporation of both excess Cd and chlorine dopant due to high vapor pressure of both Cd and CdCl<sub>2</sub> [98];
- the crystalline lattice relaxes with increasing annealing temperature and the main (111) XRD peak shifts towards the position corresponding to the cubic structure of bulk CdS;
- the systematic decrease of crystallites size demonstrates their cracking due to the evaporation of water in the rapid thermal process in preheated furnace at 200 – 350 °C, while from 400 °C it starts to increase due to higher rate of solid state diffusion;
- the out diffusion of oxygen and Cd at annealing temperatures higher than 400 °C restores the bulk values of the lattice constant and E<sub>g</sub> for pure CdS.

The nature of the annealing gas does not modify the trend of changes in CdS properties, but it influences the removal of trace oxygen from CdS films: annealing processes in air and N<sub>2</sub> create a stable CdS<sub>1-y</sub>O<sub>y</sub> solid solution in the CdS films, while H<sub>2</sub> annealing completely removes the oxides, resulting in pure CdS films (Fig. 3.9).

The presence of trace oxygen in CdS lattice has an important impact on the electrical behavior of CdS as buffer layer in solar cells because, when 66 pm oxygen

atom incorporates on the site of 107 pm sulfur atom [95], the sulfur sub-lattice contracts and the Cd sub-lattice responds with the formation of cadmium vacancies - the acceptor defects that participates in the compensation of charge carriers in the CdS buffer layer. In this sense, by varying the conditions of temperature, duration and environment, annealing can be a convenient and appropriate method to control the oxygen content in the CBD CdS thin films.

### 3.3. Application of annealed CBD CdS film in a CdS/CdTe solar cell

Because each annealing atmosphere brings both positive and negative effects to the properties of the CdS films needed for PV applications (Section 1.4), in this section we illustrate the direct influence of CdS annealing on the final parameters of a CdS/CdTe solar cell in the superstrate configuration (Fig. 2.2).

From the various annealing conditions used in our investigations, CBD CdS films annealed in H<sub>2</sub> and air at 400 °C for 60 min were chosen for application in CdS/CdTe solar cell [V], and as deposited CdS films were used as a reference. The N<sub>2</sub> annealed CdS film was excluded from this experiment because it had the lowest transmittance in comparison to the other two annealed films [III].

The surface view of CdS films, uncovered by CdTe (Fig. 3.14), was registered after absorber deposition and CdCl<sub>2</sub> treatment (Fig. 3.15). For air annealed CdS, the presence of oxygen containing phases, together with co-deposited chloride, improved the film recrystallization, increasing the grain size. From the analysis of the annealed CBD CdS properties, H<sub>2</sub> annealing was the appropriate thermal treatment for the removal of impurities from CdS films and for the destruction of hydroxide components incorporated during deposition.

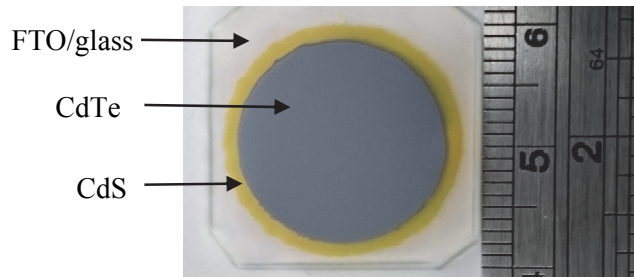


*Fig. 3.14. Plan view of CdS/CdTe solar cell on glass/FTO substrate.*

Nevertheless, because H<sub>2</sub> also removes the oxygen compounds from CdS grain boundaries, additional thermal shocks during absorber preparation have left them open in the form of short-cutting pathways between CdTe and FTO (Fig. 3.15). Therefore, to evaluate the net influence of the annealed CdS film on the solar cell, all the structures were sectioned into 5×5 mm<sup>2</sup> regions.

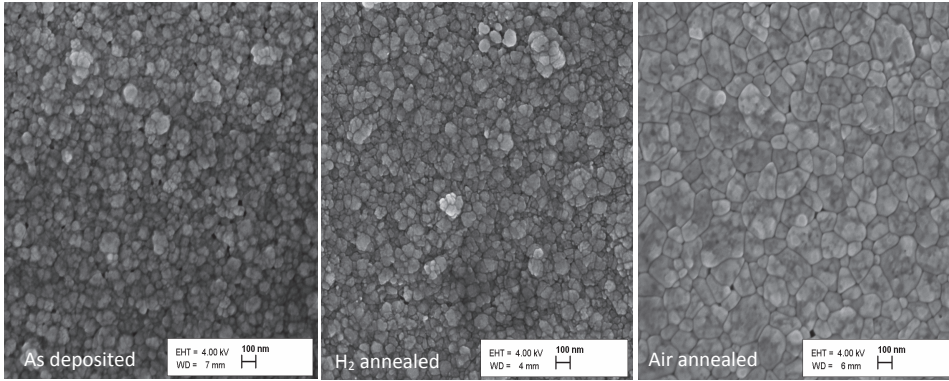


Fig. 3.15. SEM images of the as deposited and annealed CdS films after deposition and CdCl<sub>2</sub> treatment of CdTe [V].

A solar cell with an as deposited CdS film is characterized by the lowest short-circuit current ( $J_{SC}$ ), open-circuit voltage ( $V_{OC}$ ), fill factor ( $FF$ ) and efficiency values (Table 3.5), emphasizing the necessity of annealing the CBD CdS film before its application in a superstrate CdTe solar cell. The solar cell based on air annealed CdS film shows better performance compared with the cells based on as deposited and H<sub>2</sub> annealed CdS film (Fig. 3.16), although the air annealed CdS had lower band gap than the other studied films (Fig. 3.8).

Table 3.5. Parameters of CdS/CdTe solar cells with as deposited and annealed CBD CdS films [V]. For comparison, cell parameters for the best solar cell of our laboratory (with CSS CdS) are included [101].

CdS film	$V_{OC}$ , V	$J_{SC}$ , mA/cm <sup>2</sup>	FF, %	Eff, %
CBD, as deposited	525.7	17.7	39.1	3.6
CBD, H <sub>2</sub> annealed	535.7	18.2	46.4	4.5
CBD, air annealed	777.4	23.4	62.7	11.4
CSS	810.0	23.0	62.0	11.6

A reducing factor of solar cell performance could be the Cd precipitate, appearing in CdS films as a result of H<sub>2</sub> annealing, and decreasing the transmittance of CdS and FTO [V]. On the other hand, the improvement of solar cell parameters is attributed to the oxygen containing phases such as CdSO<sub>3</sub> (Fig. 3.9) that reside on the grain surfaces as active components (3.5-3.7) for the following 420 °C CdCl<sub>2</sub> treatment of the CdS/CdTe solar cell. In the case of H<sub>2</sub> annealing, the smaller grain size of low-oxygen-containing CdS films implies a faster intermixing at the CdS/CdTe interface after CdCl<sub>2</sub> treatment [84, 102], leading to a significant consumption of the CdS layer. When the as deposited films are annealed in air, CdS consumption is reduced, and Te intermixing with CdS layer is minimized [103].

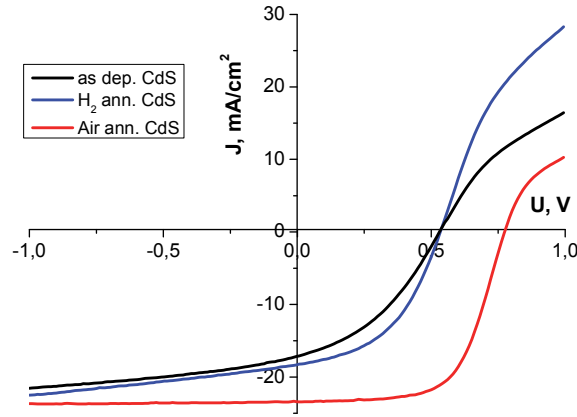


Fig. 3.16. *J-V characteristics of CdS/CdTe solar cells with as deposited and annealed CBD CdS films [V].*

Therefore, in a solar cell structure, the presence of oxygen containing phases on the grain boundaries in the CdS buffer layer is considered beneficial. As for the presence of CdSO<sub>3</sub>, it is an active component due to the presence of sulfur in the fourth oxidation state, which makes its interaction with CdS and CdCl<sub>2</sub> possible for the formation of SCl<sub>2</sub> (3.11, 3.12). SCl<sub>2</sub> is an important reaction component that contributes to the mass transfer of CdS by the formation of sulfur pieces (3.13).



Interestingly, we obtained similar efficiency values (Table 3.5) for two CdTe solar cells - one with a CBD CdS film and another – with a CSS CdS film [101]. The latter CdS film was of much higher quality in terms of larger grains and lack of porosity. This achievement indicates the importance of CdS annealing in general and the impact of oxygen containing phases on the junction formation. The components of the CdCl<sub>2</sub> flux have to be closer to the junction of the solar cell as they accelerate the mass transfer between the polycrystalline phases of both CdS and CdTe for the formation of an effective CdS/CdTe heterojunction.

In other words, during the CdCl<sub>2</sub> treatment of a solar cell, applied in air at 420 °C at the back side of the CdTe layer, the flux penetration through the absorber will be enhanced by the presence of oxygen containing phases from CdS. Therefore, annealing in air for a CBD CdS film looks to be a solution, as it brings the oxygen and incorporated chlorine from CdS to the region of junction formation. The effect of oxygen on the CdS/CdTe interface has also been applied in [2, 46] by introducing oxygen into the CdS sputtering process.

Nevertheless, the film uniformity remains an issue for CBD CdS, which is firstly affected by annealing and then by the high temperature processes of CdTe fabrication (Fig. 3.15). We looked closer at these uniformities, shown by SEM cross section imaging of solar cells, and identified two types of peeling. The peeling from the CdS surface (Fig. 3.17a) seems to be caused by the undesirable conglomerates on the surface of the CdS film (Fig. 3.1). Peeling from the FTO surface (Fig. 3.17b) is generated only in the case of H<sub>2</sub> annealed CdS; its origin is still unclear and requires further investigation.

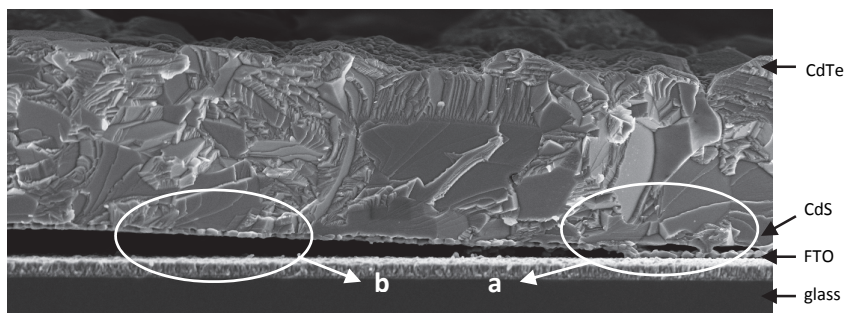


*Fig. 3.17. Cross section of a “bad contact” region of a CdS/CdTe solar cell: peeling from CdS surface (a), peeling from FTO surface (b) [V].*

To summarize, each annealing condition studied for CBD CdS thin films improves the performance of superstrate solar cells.

H<sub>2</sub> annealing removes the oxygen compounds from the grain boundaries and opens them as shortcutting pathways through CdS layer, thereby decreasing device parameters. CdS/CdTe solar cells with air annealed CBD CdS show the highest performance: 23.4 mA/cm<sup>2</sup> current density and 11.4% efficiency. The simultaneous presence of both oxygen and CdCl<sub>2</sub> from CdTe thermal activation contribute to the recrystallization and sintering of the highly textured columnar CBD CdS. Moreover, annealing in air of CBD CdS assures the presence of oxy-chloride components at both sides of the CdTe absorber, contributing to the formation of an effective junction.

Although our CdS films show similar performances to CSS CdS when included in a CdTe solar cell, the porosity of the annealed CBD CdS, which intensifies during CdTe deposition and CdCl<sub>2</sub> thermal treatment, remains an issue to resolve.

## CONCLUSIONS

The systematic study of changes in the properties of CBD CdS thin films allowed an understanding and description of the physico-chemical processes occurring during thermal annealing.

1. We claim that in the deposition process, the hydroxide group incorporates into the CdS lattice on the sulfur site, resulting in the formation of cadmium hydroxysulfide solid solution. The explanation of the simultaneous changes in structural, optical and electrical properties that occur as a result of thermal annealing of CdS thin films is based on this claim.
2. During thermal processing, the hydroxide groups seem to decompose to water and O<sub>s</sub>, resulting in the cracking of crystallites and the formation of a cadmium oxysulfide solid solution which contains V<sub>S</sub>.
3. The increase of [V<sub>S</sub><sup>2+</sup>] creates an excess of elemental Cd as precipitates resulting in a sharp increase of electron density at 200 °C annealing temperature.
4. At 350 – 400 °C annealing temperatures, the density of electrons exponentially decreases, indicating that the kinetics is limited by the slow out diffusion of Cd and dopants such as chlorine.
5. As the oxygen content in the sulfur sub-lattice decreases with increasing annealing temperature, the crystalline lattice of CdS thin films transforms to a stable cubic structure.
6. The nature of the annealing ambient does not modify the trend of the changes in the CdS properties, but it influences the removal of trace oxygen from the CdS films.
7. The chlorine dopant, introduced in the process of deposition, do not provide optimal structural, optical and electrical properties of the CBD CdS film for application in CdTe solar cell. The thermal annealings were proved to be appropriate technological tools for controlling the properties of CdS thin films and improving the performance of CdS/CdTe device.

In result of the present work the effect of annealing on the properties of CBD CdS thin films, which is still considered controversial, have received an unambiguous physico-chemical explanation.

## ACKNOWLEDGEMENTS

First of all I am grateful to Dr. Tamara Potlog from Moldova State University for connecting me with Estonia in 2010 and for opening the opportunity to study at Tallinn University of Technology. I express my sincerest gratitude to my first supervisor Dr. Jaan Hiie for his unconditional support, guidance and understanding during my doctoral studies. I am thankful to Dr. Malle Krunk, Leading Research Scientist and Laboratory Manager, for her support and useful discussions, to Dr. Valdek Mikli for SEM and EDX analysis, to Dr. Arvo Mere and his students for technical supervision, to Nicolae Spalatu for solar cell preparation, to Dr. Taavi Raadik for support with Raman and photoluminescence measurements, to Dr. Vello Valdna for useful discussions and to Dr. Atanas Katerski for his support and useful collaboration.

I wish to thank Prof. Andres Öpik, the Dean of the Faculty of Chemical and Materials Technology up to 31.08.2014 and the Head of the doctoral school "Functional materials and technologies" in Tallinn University of Technology for providing the opportunity to participate in the PhD studies at the faculty and in the graduate school; and Prof. Enn Mellikov, Head of the Department of Materials Science up to 2015, for the opportunity to use high-end research equipment within the Department.

The work was financially supported by European Social Fund's Doctoral Studies and Internationalization Program DoRa5 and DoRa8; European Union through 7th FP project FLEXSOLCELL (GA-2008-230861); Estonian Ministry of Education and Research (IUT19-4, SF0140092s08); Estonian Science Foundation (ETF9142); European Union through the European Regional Development Fund: Project TK114 (Centre of Excellence "Mesosystems: Theory and Applications", TK114, 3.2.0101.11-0029) and AR12118 ("Efficient plasmonic absorbers for solar cells", 3.2.1101.12-0023); FMTDK graduate school "Functional materials and technologies" receiving funding from the European Social Fund under Project 1.2.0401.09-0079 in Estonia.

My warmest thanks belong to my family.

Natalia Maticiuc

## ABSTRACT

Interest in CdS thin films has been raised by their successful application as buffer layers in CdTe, CIGS and kesterite solar cells. Although a CdS thin film possesses several advantages in comparison to Zn based buffers, issues such as controllable properties and shortcutting pathways through the film remain open.

These internationally recognized issues have represented some of the main goals of the FP7 Project "Development of Flexible Single and Tandem II-VI-Based High Efficiency Thin Film Solar Cells" (FLEXSOLCELL) between Tallinn University of Technology, Moldova State University, and Trieste University from Italy. In the frame of FLEXCSOLCELL the creation of thinner and more uniform CdS thin films by chemical bath deposition (CBD) has been one of the improvement routes for CdS/CdTe solar cell. This deposition method was chosen due to its major advantages over other techniques: epitaxial growth, conformal coating and controllable thickness of the film, and also because the Department of Material Science from Tallinn University of Technology has a long experience in the chemical deposition processes of semiconductor thin films.

This PhD research has been done in the Laboratory of Thin Film Chemical Technologies with the main financial support from Doctoral Studies and Internationalisation Programme "DoRa", Estonian Ministry of Education and Research (IUT19-4, SF0140092s08) and FP7 Project "FLEXSOLCELL".

The aim of the thesis is to study systematically the impact of post-deposition thermal treatment variables on the optical, structural and electrical properties of CdS thin films, an understanding of which is essential for device applications.

The thesis is based on five publications and it is divided into three Chapters. Following the introduction, Chapter 1 includes a literature overview describing the main properties of CdS, deposition methods for CdS films, the properties of CBD CdS thin films and solar cells based on a CdTe absorber with CBD CdS as a buffer layer. Chapter 2 briefly describes the preparation, annealing and characterization of CBD CdS thin films, as well as the fabrication and characterization of CdS/CdTe solar cells. Chapter 3 is divided into three sections and includes the results and a discussion of CdS properties, followed by the application of annealed CBD CdS thin films in practical devices.

CdS thin films were prepared by CBD in a basic ammonia solution with  $\text{CdSO}_4$  as the Cd source, thiourea as the sulfur source, and a low concentration of  $\text{NH}_4\text{Cl}$  as dopant. Afterwards, the films were annealed at temperatures from 200 to 450 °C in different environments, including hydrogen, nitrogen and air as source of oxygen. The work covered approximately 100 samples and every experimental point represents a new CdS thin film annealed at unrepeated conditions.

Based on energy dispersive X-ray spectrometry, X-ray diffraction, and band gap studies, the mechanisms of the changes in CdS thin film properties were systematically studied. It was assumed that cadmium hydroxide incorporates into the CdS thin film during chemical bath deposition, forming the cadmium hydroxysulfide alloy as a compensated semiconductor with a stressed crystalline lattice. The destruction of the hydroxide group which intensifies at 300 °C annealing implies the cracking of crystallites due to the escape of water and the creation of an excess of Cd, resulting in the transition from cadmium hydroxysulfide to a cadmium oxysulfide solid solution. This excess Cd decreases the concentration of cadmium vacancies so that  $N_D \gg N_A$ , and enables the impurities of  $(\text{OH})_S^+$  and  $\text{Cl}_S^+$  to behave as shallow

donors, increasing the electron density of the CdS films at low annealing temperatures (200 – 300 °C). At higher annealing temperatures (350 – 400 °C), the out diffusion of Cd is enhanced and the isovalent oxygen contracts the sulfur sub-lattice due to smaller size of oxygen compared to sulfur; in result the concentration of cadmium vacancies increases and the conductivity of CdS thin films is reduced. Additionally, due to the reduced content of oxygen in the sulfur sub-lattice, the bulk values of the lattice constant and  $E_g$  for pure CdS thin films are restored and the CdS lattice transforms from an intermediate to a cubic structure.

The nature of the annealing gas does not modify the trend of changes in the CdS properties, but it influences the removal of trace oxygen from the CdS films. Annealing processes in air and  $N_2$  create a stable cadmium oxysulfide solid solution in CdS films, whereas  $H_2$  annealing completely removes the oxygen containing phases and the dopants such as chlorine, resulting in pure resistive CdS films with sphalerite structure. The presence of oxygen as isovalent dopant in the CdS lattice has an important impact on the final parameters of the CdS/CdTe solar cell. A CdS/CdTe solar cell with air annealed CBD CdS shows the highest performance due to the presence of oxygen containing phases on CdS surface, which in the  $CdCl_2$  treatment process promote the mass transfer of junction components, contributing to the sintering and formation of an effective junction.

The systematic study of changes in structural, optical and electrical properties of annealed CBD CdS thin films as a result of thermal treatment allowed us to describe the physico-chemical mechanism of the processes. We have demonstrated that varying the conditions of temperature, duration and environment of annealing is a convenient and appropriate technological tool for controlling the properties of CdS thin films. Moreover, because the properties of CBD CdS thin films are drastically changed by the annealing in the temperature interval from i-ZnO/ZnO:Al sputtering (200 °C) up to temperatures of CdTe processing (>400 °C), the results of present work are highly important for the technological development of both substrate CIGS and superstrate CdTe solar cells, respectively.

## KOKKUVÕTE

CdS õhukesed kiled pakuvad huvi tänu rakendamisele puhverkihtidena CdTe, CIGS ja CZTS päikesepatareides. Ehkki CdS õhukestel kiledel on rida eeliseid, võrreldes Zn baasil ehitatud puhverkiledega, vajavad omaduste kontrollitavus ja lühised läbi kile detailsemat uurimist.

Need rahvusvaheliselt tõdetud probleemid kuulusid FP7 projekti "Kõrgefektiivsete paindlike õhukesekileliste mono- ja tandemiirideliste päikesepatareide arendamine II-VI tüüpi ühendite baasil" (FLEXSOLCELL) eesmärkide hulka. Projekti partneriteks olid Tallinna Tehnikaülikool, Moldova Riiklik Ülikool ja Trieste Ülikool Itaalias. FLEXSOLCELL raames õhemate ja ühtlasemate CdS kilede valmistamine keemilise vannsadestamise meetodil (CBD) oli üheks CdS/CdTe päikesepatareide täiustamise teeks. See sadestamise meetod valiti tänu olulistele eelistele võrreldes teiste meetoditega: epitaksiaalne kasv, ühtlane katmisvõime ja kile paksuse kontrollitavus, aga ka tänu pooljuhtkilede keemiliste sadestusmeetodite pikaajalisele viljelemisele Tallinna Tehnikaülikooli Materjaliteaduse instituudis.

Käesolev PhD uurimus sooritati Õhukeste Kilede Keemilise Tehnoloogia Laboratooriumis Doktoritõpingute ja Rahvusvahelistumise Programmi "DoRa", Eesti Teadus- ja Haridusministeeriumi (IUT19-4, SF0140092s08) ja FP7 projekti "FLEXSOLCELL" toel.

Töö eesmärgiks oli süstemaatiliselt uurida sadestusjärgse termilise käsitluse mõju CdS õhukeste kilede optilistele, struktuursetele ja elektrilistele omadustele, et saadud seaduspärasusi rakendada seadmetes.

Teesid baseeruvad viiel publikatsioonil ja sisaldavad kolm peatükki. Sissejuhatusel järgneb I peatükk kirjandusülevaatega, mis käsitleb CdS põhilisi omadusi, CdS kilede sadestamise meetodeid, CBD CdS õhukeste kilede omadusi ja CdTe absorberile ning CBD CDS puhverkilele ehitatud päikesepatareid. II peatükk kirjeldab lühidalt CBD CdS õhukeste kilede valmistamise, lõõmutamise ja mõõtmise meetodeid. III peatükk on jaotatud kolme sektsiooni, millest esimene sisaldab CdS omaduste uurimustulemusi, teine tulemuste arutelu ning analüüsi ja kolmas käsitleb CBD CdS õhukeste kilede rakendustulemusi tegelikes seadmetes.

Õhukesed CdS kiled sadestati CdSO<sub>4</sub> ja tiokarbamiidi ammoniakaalses vesilahuses (pH 10,3) NH<sub>4</sub>Cl juuresolekul 0,1%. Saadud kiled lõõmutati temperatuurivahemikus 200 – 400 °C vesiniku, lämmastiku ja õhu gaasilistes keskkondades. Töö rajaneb ligikaudu 100 proovile ja iga eksperimentaalne punkt vastab uuele CdS kilele lõõmutatuna kordumatutes tingimustes.

Termilise käsitluse tulemusel CdS õhukestes kiledes tekkivate muutuste mehhanismi süstemaatiline uurimine baseerus energia dispersioon röntgenspektroskoopia, röntgendifraktomeetria ja optilise keelutsooni laiuse mõõtmismeetoditel. Töö tulemusena leiti, et sadestamise protsessis kaadmiumhüdrosiid suure tõenäosusega ehitub CdS kristallvõresse, moodustades kaadmiumhüdrosiisulfiidse tahke lahuse kui kompenseeritud pooljuhi, mille võre on CdS suhtes pinge all. Termilisel käsitlusel hüdroksiidgrupp laguneb, eriti intensiivistudes 300 °C piirkonnas, millega kaasneb veeauru eraldumine, kristallitide pragunemine ning Cd liia tekkimine. Tulemuseks on hüdroksiisulfiidi transformeerumine kaadmiumoksisulfiidseks tahkeks lahuseks. Cd ülekaalu toimele väheneb kaadmiumi vakantside kontsentratsioon nii, et  $N_D \gg N_A$ , mistõttu (OH)<sub>s</sub><sup>+</sup> ja Cl<sub>s</sub><sup>+</sup> defektid kui madalad doonorid emiteerivad elektronid juhtivustsooni,

suurendades elektronide tihedust kiles juba madalatel lõõmutustemperatuuridel. Lõõmutustemperatuuri kasvamisel elektrijuhtivus CdS kiledes hakkab vähenema, mis on ühest küljest seotud Cd väljadifusiooni intensiivistumisega ja teisest küljest isovalentse hapniku kontsentratsiooni jätkuva suurenemisega, mis soodustab kaadmiumi vakantside kontsentratsiooni tõusu väävli alavõre kokkutõmbumise arvel. Ka hapniku väljadifusioon suureneb, mistõttu võre konstant ja keelutsooni laiuse väärtused puhtale kaadmiumsulfiidile taastuvad ning CdS võre läheb üle heksagonaalse ja kuubilise vahepealsest kuubilisse struktuuri.

Lõõmutusgaasi iseloom ei muuda muutuste trendi CdS kiledes, aga mõjutab hapniku jääkide eemaldumist. Lõõmutusprotsessid õhus ja lämmastikus tekitavad CdS kiledes stabiilse oksisulfiidse tahke lahuse. Lõõmutamine vesinikus eemaldab täielikult oksiidid ja lenduvad lisandid nagu kloor, andes puhta kõrge takistusega ja sfaleriitse struktuuriga CdS kile. Hapnik isovalentse lisandina CdS võres soodustab kaadmiumi vakantside suuremat kontsentratsiooni ja on olulise mõjuga CdS/CdTe päikesepatarei omadustele. Õhus eellõõmutatud CBD CdS rakendamine CdS/CdTe päikesepatarei tehnoloogias on soodsaim võrreldes teiste gaasiliste keskkondadega tänu aktiivsete oksiidide tekkimisele kile pinnal, mis soodustavad CdCl<sub>2</sub> juuresolekul vaba väävli sisalduse suurenemist sulandajas ja intensiivistavad massiülekanne nii kile paakumisprotsessis kui ka efektiivse siirde moodustumisel.

Termiliselt käsitletud CBD CdS õhukeste kilede struktuursete, optiliste ja elektriliste omaduste süstemaatiline muutumine võimaldas kirjeldada lõõmutusprotsessi füsikokeemiat. Me näitasime, et lõõmutuse temperatuuri, aja ja keskkonna varieerimine on oluline tehnoloogiline vahend CdS õhukeste kilede omaduste kontrollimiseks. Kuna CBD CdS kile omadused muutuvad drastiliselt juba i-ZnO/ZnO:Al katoodpihustamise madalatest kuni CdTe sadestamise kõrgete temperatuurideni, siis käesoleva töö tulemused on väga olulised nii CIGS kui ka CdTe päikesepatareide tehnoloogiate arendustele.

## REFERENCES

1. M.A. Green, K. Emery, Y. Hishikawa, W. Warta, E.D. Dunlop, Solar cell efficiency tables (version 46), *Prog. Photovolt: Res. Appl.* **23** (2015) 805–812.
2. A. Romeo, D.L. Batzner, H. Zogg, C. Vignali, A.N. Tiwari, Influence of CdS growth process on structural and photovoltaic properties of CdTe/CdS solar cells, *Sol. Energy Mater. Sol. Cells* **67** (2001) 311-321.
3. B.E. McCandless, R.W. Birkmire, Influence of window and absorber layer processing on device operation in superstrate thin films CdTe solar cells. In: Proceedings of the 28th IEEE PVSC: 2000 Sep 15-22; New York, USA.
4. M. Burgelman, Cadmium telluride thin films solar cells: characterization, fabrication and modelling. J. Poortmans, V. Arkhipov, editors. Thin film solar cells fabrication, characterization and applications, Chichester: John Wiley & Sons Ltd.; 2006, 277-314.
5. D. Schmid, M. Ruckh, F. Grunwald, H.W. Schock, Chalcopyrite/defect chalcopyrite heterojunctions on the basis of CuInSe<sub>2</sub>, *J. Appl. Phys.* **73** (1993) 2902-2909.
6. A. Kylner, Effect of impurities in the CdS buffer layer on the performance of the Cu(In,Ga)Se<sub>2</sub> thin film solar cell, *J. Electrochem. Soc.* **146** (1999) 1816-1823.
7. J. Hiie, T. Dedova, V. Valdna, K. Muska, Comparative study of nano-structured CdS thin films prepared by CBD and spray pyrolysis: Annealing effect, *Thin Solid Films* **511-512** (2006) 443-447.
8. J. Hiie, K. Muska, V. Valdna, V. Mikli, A. Taklaja, A. Gavrilov, Thermal annealing effect on structural and electrical properties of chemical bath-deposited CdS films, *Thin Solid Films* **516** (2008) 7008-7012.
9. J. Hiie, F. Quinci, V. Lughi, V. Sergio, V. Valdna, V. Mikli et al., Chlorine doping of cadmium sulfide on the example of CBD CdS, *Mater. Res. Soc. Symp. Proc.* **1165** (2009) 1165-M08-17.
10. S. Adachi, Properties of group-IV, III-V and II-VI semiconductors, Chichester: John Wiley & Sons, Ltd; 2005.
11. J.I. Pankove, Optical Processes in Semiconductors, New York: Dover Publications Inc., 1971.
12. S.A. Al Kuhaimi, Influence of preparation technique on the structural, optical and electrical properties of polycrystalline CdS films, *Vacuum* **51** (1998) 349-355.
13. P.J. George, A. Sanchez, P.K. Nair, M.T.S Nair, Doping of chemically deposited intrinsic CdS thin films to n type by thermal diffusion of indium *Appl. Phys. Lett.* **66** (1995) 3624-3626.
14. G. Hodes, A. Yaron, F. Decker, and P. Motisuke, Three-dimensional quantum-size effect in chemically deposited cadmium selenide films, *Phys. Rev. B* **36** (1987) 4215-4221.
15. M.B. Ortuno-Lopez, M. Sotelo-Lerma, A. Mendoza-Galvan, R. Ramirez-Bon, Optical band gap tuning and study of strain in CdS thin films, *Vacuum* **76** (2004) 181-184.
16. P.P. Hankare, P.A. Chate, D.J. Sathe, CdS thin film: Synthesis and characterization, *Solid State Sci.* **11** (2009) 1226-1228.

17. A.L. Fahrenbruch, R.H. Bube, Fundamentals of solar cells, New York: Academic Press, 1983.
18. D. Cha, S. Kim, N.K. Huang, Study on electrical properties of films prepared by chemical pyrolysis deposition, *Mater. Sci. Eng.* **B106** (2004) 63-68.
19. K. Nishidate, T. Sato, Y. Matsukura, M. Baba, M. Hasegawa, Density-functional electronic structure calculations for native defects and Cu impurities in CdS, *Phys. Rev. B* **74** (2006) 035210.
20. J.B. Varley, V. Lordi, Electrical properties of point defects in CdS and ZnS, *Appl. Phys. Lett.* **103** (2013) 102103.
21. C. Puscher, Ueber ein neues und billiges Verfahren, ohne Anwendung von Farben verschiedene Metalle (wie Gold, Silber, Kupfer, Argentan, Messing, Tombak, Eisen, Zink) mit prachtvollen Lüsterfarben zu überziehen, *Dingl. J.* **190** (1869) 421.
22. S. G. Mokrushin, Y. V. Tkachev, Formation of Cc 18 at the boundary of solid and liquid phases, *Kolloidn. Zh.* **23** (1961) 438-441 (*In Russian*).
23. R. Ortega-Borges, D. Lincot, Mechanism of chemical bath deposition of cadmium sulfide thin films in the ammonia-thiourea system, *J. Electrochem. Soc.* **140** (1993) 3464-3473.
24. S. Gorer, G. Hodes, Quantum size effects in the study of chemical solution deposition mechanisms of semiconductor films, *J. Phys. Chem.* **98** (1994) 5338-5346.
25. A. Ennaoui, M. Weber, R. Scheer, H.J. Lewerenz, Chemical-bath ZnO buffer layer for CuInS<sub>2</sub> thin-film solar cells, *Sol. Energy Mater. Sol. Cells* **54** (1998) 277-286.
26. G. K. Padam, S. K. Gupta, Electron spin resonance and transmission electron microscopy studies of solution-grown CdTe thin films, *Appl. Phys. Lett.* **53** (1998) 865-867.
27. G. Hodes, Chemical solution deposition of semiconductor films, New York: Marcel Dekker Inc., 2003.
28. H. Oumous, H. Hadiri, Optical and electrical properties of annealed CdS thin films obtained from a chemical solution, *Thin Solid Films* **386** (2001) 87-90.
29. C. Lu, L. Zhang, Y. Zhang, S. Liu, G. Liu, Fabrication of CdS/CdSe bilayer thin films by chemical bath deposition and electrodeposition, and their photoelectrochemical properties, *Appl. Surf. Sci.* **319** (2014) 278-284.
30. E. Fatas, P. Herrasti, F. Arjona, E. Garcia Camarero, Characterization of CdS thin films electrodeposited by an alternating current electrolysis method, *J. Electrochem. Soc.* **134** (1987) 2799-2801.
31. J. Nishino, S. Chatani, Y. Uotani, Y. Nosaka, Electrodeposition method for controlled formation of CdS films from aqueous solution, *J. Electroanal. Chem.* **473** (1999) 217-222.
32. D. Abou-Ras, G. Kostorz, A. Romeo, D. Rudmann, A.N. Tiwari, Structural and chemical investigations of CBD- and PVD-CdS buffer layers and interfaces in Cu(In, Ga)Se<sub>2</sub>-based thin film solar cells, *Thin Solid Films* **480-481** (2005) 118-123.
33. L.L. Kazmerski, O. Jamjoum, P.J. Ireland, R.A. Mickelsen, W.S. Chen, Formation, growth, and stability of the CdS/CuInSe<sub>2</sub> interface, *J. Vac. Sci. Technol.* **21** (1982) 486-490.
34. A. Romeo, R. Gysel, S. Buzzi, D. Abou-Ras, D.L. Batzner, D. Rudmann, F. Kurdesau, H. Zogg, A.N. Tiwari, Properties of CIGS solar cells developed

- evaporated II-VI buffer layers. In: Proceedings of Technical Digest of the 14th International Photovoltaic Science and Engineering Conference: 2004 Jan 26-30; Bangkok, Thailand.
35. N. Spalatu, J. Hiie, V. Valdna, M. Caraman, N. Maticiu, V. Mikli, T. Potlog, M. Krunk, V. Lugh, Properties of the CdCl<sub>2</sub> air-annealed CSS CdTe thin films, *Energy Procedia* **44** (2014) 85-95.
  36. A.I. Oliva, O. Solis-Canto, R. Castro-Rodriguez, P. Quintana, Formation of the band gap energy on CdS thin films growth by two different techniques, *Thin Solid Films* **391** (2001) 28-35.
  37. N. Romeo, A. Bosio, V. Canevari, M. Terheggen, L. Vaillant Roca, Comparison of different conducting oxides as substrates for CdS/CdTe thin film solar cells, *Thin Solid Films* **431-432** (2003) 364-368.
  38. H.R. Moutinho, D. Albin, Y. Yan, R.G. Dhere, X. Li, C. Perkins, C.-S. Jiang, B. To, M.M. Al-Jassim, Deposition and properties of CBD and CSS CdS thin films for solar cell application, *Thin Solid Films* **436** (2003) 175-180.
  39. E.M. Feldmeier, A. Fuchs, J. Schaffner, H.-J. Schimper, A. Klein, W. Jaegermann, Comparison between the structural, morphological and optical properties of CdS layers prepared by close space sublimation and RF magnetron sputtering for CdTe solar cells, *Thin Solid Films* **519** (2011) 7596-7599.
  40. B.-S. Moon, J.-H. Lee, H. Jung, Comparative studies of the properties of CdS films deposited on different substrates by R.F. sputtering, *Thin Solid Films* **511-512** (2006) 299-303.
  41. H. Hernandez-Contreras, G. Contreras-Puente, J. Aguilar-Hernandez, A. Morales-Acevedo, J. Vidal-Larramendi, O. Vigil-Galan, CdS and CdTe large area thin films processed by radio-frequency planar magnetron sputtering, *Thin Solid Films* **403-404** (2002) 148-152.
  42. J.-H. Lee, D.-J. Lee, Effects of CdCl<sub>2</sub> treatment on the properties of CdS films prepared by r.f. magnetron sputtering, *Thin Solid Films* **515** (2007) 6055-6059.
  43. G. Sasikala, P. Thilakan, C. Subramanian, Modification in the chemical bath deposition apparatus, growth and characterization of CdS semiconducting thin films for photovoltaic applications, *Sol. Energy Mater. Sol. Cells* **62** (2000) 275-293.
  44. H. El Maliki, J.C. Bernede, S. Marsillac, J. Pinel, X. Castel, J. Pouzet, Study of the influence of annealing on the properties of CBD-CdS thin films, *Appl. Surf. Sci.* **205** (2003) 65-79.
  45. H. Metin, R. Esen, Annealing studies on CBD grown CdS thin films, *J. Crystal Growth.* **258** (2003) 141-148.
  46. X. Wu, Y. Yan, R.G. Dhere, Y. Zhang, J. Zhou, C. Perkins, B. To, Nanostructured CdS:O film: preparation, properties, and application, *Phys. Status Solidi (c)* **1** (2004) 1062-1066.
  47. W.J. Danaher, L.E. Lyons, G.C. Morris, Some properties of thin films of chemically deposited cadmium sulphide, *Sol. Energy Mater.* **12** (1985) 137-148.
  48. B.E. McCandles, R.W. Birkmire, Influence of window and absorber layer processing on device operation in superstrate thin film CdTe solar cells. In: Proceedings of the 28th IEEE Photovoltaic Special Conference: 2000, Sept 15-22; Anchorage, USA.

49. O. Vigil, O. Zelaya-Angel, Y. Rodriguez, Changes of the structural and optical properties of cubic CdS films on annealing in H<sub>2</sub> and air atmospheres, *Semicond. Sci. Technol.* **15** (2000) 259-262.
50. D.S. Boyle, A. Bayer, M.R. Heinrich, O. Robbe, P. O'Brien, Novel approach to the chemical bath deposition of chalcogenide semiconductors, *Thin Solid Films* **361-362** (2000) 150-154.
51. K. Senthil, D. Mangalaraj, Sa.K. Narayandass, Structural and optical properties of CdS thin films, *Appl. Surf. Sci.* **169-170** (2001) 476-479.
52. M. Ichimura, F. Goto, E. Arai, Structural and optical characterization of CdS films grown by photochemical deposition, *J. Appl. Phys.* **85** (1999) 7411-7417.
53. S. Mishra, A. Ingale, U.N. Roy, A. Gupta, Study of annealing-induced changes in CdS thin films using X-ray diffraction and Raman spectroscopy, *Thin Solid Films* **516** (2007) 91-98.
54. L.M. Fraas, W.P. Bleha, P. Braatz, Recrystallization of thermally evaporated CdS film via an H<sub>2</sub>-S heat-treatment process, *J. Appl. Phys.* **46** (1975) 491-495.
55. S.A. Tomas, O. Vigil, J.J. Alvarado-Gil, R. Lozada-Morales, O. Zelaya-Angel, H. Vargas, A. Ferreira da Silva, Influence of thermal annealings in different atmospheres on the band-gap shift and resistivity of CdS thin films, *J. Appl. Phys.* **78** (1995) 2204-2207.
56. H. Kim, D. Kim, Influence of CdS heat treatment on the microstructure of CdS and the performance of CdS/CdTe solar cells, *Sol. Energy Mater. Sol. Cells* **67** (2001) 297-304.
57. M.T.S. Nair, P.K. Nair, R.A. Zingaro, E.A. Meyers, Conversion of chemically deposited photosensitive CdS thin films to n-type by air annealing and ion exchange reaction, *J. Appl. Phys.* **75** (1994) 1557-1564.
58. M. Weber, J. Krauser, A. Weidinger, J. Bruns, C.-H. Fischer, W. Bohne, J. Rohrich, R. Scherr, Hydrogen impurities in chemical bath deposited CdS, *J. Electrochem. Soc.* **146** (1999) 2131-2138.
59. H.H. Woodbury, Stoichiometric effects of O<sub>2</sub> on CdS, *J. Phys. Solids* **27** (1966) 1257-1261.
60. M. Aven, J.S. Prener, Physics and Chemistry of II-VI Compounds, Schenectady: General Electric Research and Development center, 1967.
61. E. Çetinörgü, C. Gümüş, R. Esen, Effects of deposition time and temperature on the optical properties of air-annealed chemical bath deposited CdS films, *Thin Solid Films* **515** (2006) 1688-1693.
62. F. Liu, Y. Lai, J. Liu, B. Wang, S. Kuang, Z. Zhang, J. Li, Y. Liu, Characterization of chemical bath deposited CdS thin films at different deposition temperature, *J. Alloys Compd.* **493** (2010) 305-308.
63. P.K. Nair, J. Campos, M.T.S. Nair, Opto-electronic characteristics of chemically deposited cadmium sulphide thin films, *Semicond. Sci. Technol.* **3** (1988) 134-145.
64. M.A. Contreras, M.J. Romero, B. To, F. Haseon, R. Noufi, S. Ward, K. Ramanathan, Optimization of CBD CdS process in high-efficiency Cu(In,Ga)Se<sub>2</sub>-based solar cells, *Thin Solid Films* **403-404** (2002) 204-211.
65. M. Cao, Y. Sun, J. Wu, X. Chen, N. Dai, Effects of cadmium salts on the structure, morphology and optical properties of acidic chemical bath deposited CdS thin films, *J. Alloys Compd.* **508** (2010) 297-300.

66. O. Vigil-Galan, A. Arias-Carbajal, R. Mendoza-Perez, G. Santana-Rodriguez, J. Sastre-Hernandez, J. C. Alonso, E. Moreno-Garcia, G. Contreras-Puente, A. Morales-Acevedo, Improving the efficiency of CdS/CdTe solar cells by varying the thiourea/CdCl<sub>2</sub> ratio in the CdS chemical bath, *Semicond. Sci. Technol.* **20** (2005) 819-822.
67. R. Mendoza-Perez, G. Santana-Rodriguez, J. Sastre-Hernandez, A. Morales-Acevedo, A. Arias-Carbajal, O. Vigil-Galan, J.C. Alonso, G. Contreras-Puente, Effects of thiourea concentration on CdS thin films grown by chemical bath deposition for CdTe solar cells, *Thin Solid Films* **480–481** (2005) 173-176.
68. P. Roy, S. Kumar Srivastava, A new approach towards the growth of cadmium sulphide thin film by CBD method and its characterization, *Mater. Chem. Phys.* **95** (2006) 235-241.
69. M.D. Archbold, D.P. Halliday, K. Durose, T.P.A. Hase, D.S. Boyle, S. Mazzamuto, N. Romeo, A. Bosio, Development of low temperature approaches to device quality CdS: A modified geometry for solution growth of thin films and their characterization, *Thin Solid Films* **515** (2007) 2954-2957.
70. R. Ochoa-Landin, M.G. Sandoval-Paz, M.B. Ortuno-Lopez, M. Sotelo-Lerma, R. Ramirez-Bon, Observations on the influence of pH control on the properties of chemically deposited CdS films in an ammonia-free system, *J. Phys. Chem. Solids* **70** (2009) 1034-1041.
71. A. Kariper, E. Guneri, F. Gode, C. Gumus, T. Ozpozan, The structural, electrical and optical properties of CdS thin films as a function of pH, *Mater. Chem. Phys.* **129** (2011) 183-188.
72. E. Yucel, N. Guler, Y. Yucel, Optimization of deposition conditions of CdS thin films using response surface methodology, *J. Alloys Compd.* **589** (2014) 207-212.
73. A.I. Oliva, R. Castro-Rodriguez, O. Ceh, P. Bartolo-Perez, F. Caballero-Briones, V. Sosa, First stages of growth of CdS films on different substrates, *Appl. Surf. Sci.* **148** (1999) 42-49.
74. R.W. Birkmire, E. Eser, Polycrystalline thin film solar cells: Present status and future potential, *Annu. Rev. Mater. Sci.* **27** (1997) 625-53.
75. B. E. McCandless, W.N. Shafarman, Chemical surface deposition of ultra-thin cadmium sulfide films for high performance and cadmium utilization. In: Proceedings of the 3rd World Conference on Photovoltaic Energy Conversion: 2003 May 11-18; Osaka, Japan.
76. T.L. Chu, S.S. Chu, C. Ferekides, C.Q. Wu, J. Brit, C. Wang, 13.4% efficient thin film CdS/CdTe solar cells, *J. Appl. Phys.* **70** (1991) 7608-7612.
77. B.M. Basol, V.K. Kapur, R.C. Kullberg, High-efficiency CuInSe solar cells prepared by the two-stage process, *Solar Cells* **27** (1989) 299-306.
78. P.K. Nair, M.T.S. Nair, Prospects of chemically deposited CdS thin films in solar cell applications, *Solar Cells* **22** (1987) 103-112.
79. E. Mellikov, D. Meissner, T. Varema, M. Altosaar, M. Kauk, O. Volobujeva, J. Raudoja, K. Timmo, M. Danilson, Monograin materials for solar cells, *Sol. Energy Mater. Sol. Cells* **93** (2009) 65-68.
80. W. Wang, M.T. Winkler, O. Gunawan, T. Gokmen, T.K. Todorov, Y. Zhu, D.B. Mitzi, Device characteristics of CZTSSe thin-film solar cells with 12.6% efficiency, *Adv. Energy Mater.* **4** (2014) 1301465.

81. J. Fritsche, D. Kraft, A. Thißen, T. Mayer, A. Klein, W. Jaegermann, Band energy diagram of CdTe thin film solar cells, *Thin Solid Films* **403-404** (2002) 252-257.
82. B.E. McCandless, K.D. Dobson, Processing options for CdTe thin film solar cells, *Solar Energy* **77** (2004) 839-856.
83. B.L. Williams, J.D. Major, L. Bowen, L. Phillips, G. Zoppi, I. Forbes, K. Durose, Challenges and prospects for developing CdS/CdTe substrate solar cells on Mo foils, *Sol. Energy Mater. Sol. Cells* **124** (2014) 31-38.
84. B. McCandless, M. Engelmann, R. Birkmire, Interdiffusion of CdS/CdTe thin films: modelling and x-ray diffraction line profiles, *J. Appl. Phys.* **89** (2001) 988-994.
85. Y. Yan, D. Albin, M.M. Al-Jassim, Do grain boundaries assist S diffusion in polycrystalline CdS/CdTe heterojunctions?, *Appl. Phys. Lett.* **78** (2001) 171-173.
86. X. Wu, High-efficiency polycrystalline CdTe thin-film solar cells, *Solar energy* **77** (2004) 803-814.
87. A.A. Taylor, J.D. Major, G. Kartopu, D. Lamb, J. Duenow, R.G. Dhere, Z. Maeder, S.J.C. Irvine, K. Durose, B.G. Mendis, A comparative study of microstructural stability and Sulphur diffusion in CdS/CdTe photovoltaic devices, *Sol. Energy Mater. Sol. Cells* **141** (2015) 341-349.
88. I. Oladeji, L. Chow, C. Ferekides, V. Viswanathan, Z. Zhao, Metal/CdTe/CdS/Cd<sub>1-x</sub>Zn<sub>x</sub>/TCO/glass: A new CdTe thin film solar cell structure, *Sol. Energy Mater. Sol. Cells* **61** (2000) 203-211.
89. M.E. Calixto, M.L. Albor-Aguilera, M. Tufino-Velazquez, G. Contreras-Puente, A. Morales-Acevedo, Chemical bath deposited CdS for CdTe and Cu(In,Ga)Se<sub>2</sub> thin film solar cells processing, in: L.A. Kosyachenko, editor. *Solar Cells - Thin-Film Technologies*, Rijeka: InTech; 2011, 237-252.
90. K. Durose, A.T. Fellows, A.W. Brinkman, G.J. Russell, J. Woods, Structural aspects of ball milled CdS and CdSe, *J. Mater. Sci.* **20** (1985) 3783-3789.
91. ICDD file no: 01-089-0440, Bibl.: D. Rodic, V. Spasojevic, A. Bajorek, P.J. Onnerund, *Magn. Mater.* **152** (1996) 159.
92. ICDD file no: 01-074-9665, Bibl.: H. Sowa, *Solid State Sci.* **7** (2005) 73.
93. D.W. Niles, G. Herdt, M. Al-Jassim, An x-ray photoelectron spectroscopy investigation of O impurity chemistry in CdS thin films grown by chemical bath deposition, *J. Appl. Phys.* **81** (4) (1997) 1978-1984.
94. A. Kylner, A. Rockett, L. Stolt, Oxygen in solution grown CdS films for thin film solar cells, *Solid State Phenom.* **51-52** (1996) 533-540.
95. B. Cordero, V. Gómez, A.E. Platero-Prats, M. Revés, J. Echeverría, E. Cremades, F. Barragán, S. Alvarez, Covalent radii revisited, *Dalton Trans.* (2008) 2832-2838.
96. M.J.D. Low, A.M. Kamel, The thermal decomposition of cadmium hydroxide, *J. Phys. Chem.* **69** (1965) 450-457.
97. T.P. Gujar, V.R. Shinde, W.-Y. Kim, K.-D. Jung, C.D. Lokhande, O.-S. Joo, Formation of CdO films from chemically deposited Cd(OH)<sub>2</sub> films as a precursor, *Appl. Surf. Sci.* **254** (2008) 3813-3818.
98. D.R. Lide, *CRC Handbook of Chemistry and Physics*, Boca Raton, FL: CRC Press; 2005.

99. M.B. Loginova, J.V. Andreev, Melting diagrams of systems  $\text{CdCl}_2\text{-CdX}$ . *Inorg. Mater.* **6** (1970) 1885-1886 (*In Russian*).
100. Y.L. Soo, W.H. Sun, S.C. Weng, Y.S. Lin, L. Chang, L.Y. Jang, X. Wu, Y. Yan, Local environment surrounding S and Cd in CdS:O thin film photovoltaic materials probed by x-ray absorption fine structures, *Appl. Phys. Lett.* **89** (2006) 131908.
101. N. Spalatu, J. Hiie, V. Mikli, M. Krunks, V. Valdna, N. Maticiuc, T. Raadik, M. Caraman., Effect of  $\text{CdCl}_2$  annealing treatment on structural and optoelectronic properties of close spaced sublimation CdTe/CdS thin film solar cells vs deposition conditions, *Thin Solid Films* **582** (2015) 128-133.
102. J. Han, C. Liao, T. Jiang, G. Fu, V. Krishnakumar, C. Spanheimer, G. Haindl, K. Zhao, A. Klein, W. Jaegermann, Annealing effects on the chemical deposited CdS films and the electrical properties of CdS/CdTe solar cells, *Mater. Res. Bull.* **46** (2011)194–198.
103. D.S. Albin, Y. Yan, M.M. Al-Jassim, The effect of oxygen on interface microstructure evolution in CdS/CdTe solar cells, *Prog. Photovolt.: Res. Appl.* **10** (2002) 309–322.

**PAPER I**

**N. Maticiuc**, J. Hiie, V. Mikli, T. Potlog, V. Valdna, Structural and optical properties of cadmium sulfide thin films modified by hydrogen annealing, *Mater. Sci. Semicond. Process.* 26 (2014) 169–174.





Contents lists available at ScienceDirect

## Materials Science in Semiconductor Processing

journal homepage: [www.elsevier.com/locate/mssp](http://www.elsevier.com/locate/mssp)

## Structural and optical properties of cadmium sulfide thin films modified by hydrogen annealing

Natalia Maticiu<sup>a,\*</sup>, Jaan Hiie<sup>a</sup>, Valdek Mikli<sup>a</sup>, Tamara Potlog<sup>b</sup>, Vello Valdna<sup>a</sup><sup>a</sup> Tallinn University of Technology, Ehitajate tee 5, Tallinn 19086, Estonia<sup>b</sup> Moldova State University, A. Mateevici street 60, Chisinau MD-2009, Republic of Moldova

## ARTICLE INFO

## Keywords:

CdS film  
Optical properties  
Structural properties  
X-ray diffraction  
Cd(OH)<sub>2</sub> incorporation

## ABSTRACT

This paper provides a systematic study of structural and optical properties of cadmium sulfide (CdS) films annealed under hydrogen (H<sub>2</sub>) in a wide range of temperatures (200–450 °C) and times (3–120 min). The aim is to present the properties of the CdS film as a function of hydrogen annealing conditions and to discuss the mechanism behind these changes. The stressed cubic lattice of as-deposited CdS film was relaxed by increasing the temperature and the time of H<sub>2</sub> annealing. The surface porosity of CdS films revealed the highest temperature and duration applicable to H<sub>2</sub> annealing. The dependence of the band gap as a function of annealing conditions is discussed. The origin of changed optical properties accompanying the shrinkage of the lattice is explained by the incorporation of the hydroxide group on the sulfur site in the CdS lattice during the deposition process and its decomposition after 300 °C. A relationship between CdS properties and the decomposition process of Cd(OH)<sub>2</sub> to water and CdO during annealing in H<sub>2</sub> was established at different low, moderate and high temperatures of annealing.

© 2014 Elsevier Ltd. All rights reserved.

## 1. Introduction

Cadmium sulfide (CdS) is an important n-type semiconductor material which plays a key role in the fabrication of thin film solar cells. It has been successfully used as a window/buffer layer in the production of both CdTe and CIGS solar cells with record efficiencies [1].

Among various processes, chemical bath deposition (CBD) is one of the most advantageous due to low cost, low temperature processing and its suitability for forming large area thin films. However, a major problem is that the CBD film contains numerous adherent particulates of homogeneously nucleated CdS and other bath reaction products [2–4]. The presence of these impurities entails the layers with a high speed of recrystallization already at

low temperatures with major changes in the structural and optical properties [5,6]. A possible method to control these changes and reduce the extent of disorder is the thermal annealing in a defined atmosphere. CdS layers have been annealed in oxidizing [7,8], reducing [5,8,9] and neutral [8,10] atmospheres. Several studies have covered the influence of each type of annealing on the properties of CdS.

Generally, the neutral annealing brings reorientation of an as-deposited CdS film with a significantly improved crystalline quality. Tomas et al. [8] have shown that the Ar+S<sub>2</sub> annealing diminishes the resistivity by increasing the grain size, therefore the number of grain boundaries decreases in the films. Also, the Ar annealing increases the grain size and produces a large amount of sulfur vacancies as a consequence of the non-equilibrium conditions. On the other hand, annealing in a neutral atmosphere leads to phase transition from the metastable cubic phase of CdS to the stable hexagonal phase [10]. Besides increased grain size and improved crystallinity of CdS annealed in an

\* Corresponding author. Tel.: +372 620 3366; fax: +372 620 2020.  
E-mail address: [nataliamaticiu@yahoo.com](mailto:nataliamaticiu@yahoo.com) (N. Maticiu).

oxidizing ambient, Haider et al. [7] have reported a substantial decrease in the band gap. Moreover, the presence of oxygen creates both CdO and CdSO<sub>4</sub> layers on the surface, slightly increasing the resistivity of the films as compared to the neutral atmosphere [8]. The thermal treatments in a reducing atmosphere have the advantage of containing H<sub>2</sub>, which is a strong agent for grain boundary passivation by oxygen removal. The presence of H<sub>2</sub> causes the resistivity to decrease by 4 orders of magnitude [11] compared to the neutral case [8]. Only CdS samples exposed to H<sub>2</sub> and air atmosphere preserve the same structural cubic phase during the complete thermal process [5]. The cubic structure increases the potential applicability of CdS for optoelectronic devices, because many semiconductors such as InP [12] also have a cubic structure. Annealing in H<sub>2</sub> is important as it requires lower exposure times and was shown by several authors [9,13,14] to have visible consequences for technological applications in solar cells.

Still, the pin-holes and irreproducibility are a concern for reliable CdS films [15]. To find the thermal process that produces CBD CdS films with the best combination of high band gap and low resistivity is the main task regarding to this semiconductor material. In addition, the mechanism that explains the microstructure and optical behavior as a function of annealing conditions is not completely understood.

The aim of this paper is to present the structural and optical properties of a CBD CdS film as a function of hydrogen annealing in a large range of temperature and time. Conditions of H<sub>2</sub> annealing for high transparency, band gap and porosity free CdS thin films will be analyzed. In comparison with previous works [2–8] on CdS films, the mechanism of changes in CdS properties on the basis of Cd(OH)<sub>2</sub> presence is discussed here.

## 2. Material and methods

Polycrystalline CdS films were deposited on 25 mm × 25 mm soda-lime glass substrates. The plates were properly cleaned and immersed in the chemical bath which consisted in a water solution of 1 mM CdSO<sub>4</sub>, 10 mM thiourea, 0.2 M NH<sub>4</sub>OH and 30 mM (NH<sub>4</sub>)<sub>2</sub>SO<sub>4</sub>. For CdS doping [16], a low concentration of NH<sub>4</sub>Cl solution (0.1 μM) was added in the deposition bath. The temperature and agitation speed of the solution were 85 °C and 500 rpm, respectively. One deposition lasted for 30 min, but for thicker CdS films the process was repeated thrice. After deposition vacuum drying at 120 °C was applied to remove most of the secondary phases of water, hydroxides and organic impurities. This drying was the last stage of preparation for the so-called as-deposited CdS layers. Each layer was annealed then in hydrogen ambient under different conditions. The vacuumed process tube with samples was filled with 1 atm hydrogen gas at room temperature then closed and introduced into a cylindrical furnace where the constant temperature and time were set. Annealing temperature varied in the range of 200 °C to 450 °C while annealing lasted from 3 up to 120 min. The hydrogen pressure in the process tube was maintained by a standard gas reduction system and was not influenced by

expansion of gas at high temperatures of annealing. Large diameter (55 mm) and volume (1500 ml) of the process tube ensured an excess of H<sub>2</sub> and the gas convection flow so that the reaction products were transported to the colder part of the tube.

Crystallographic investigations were performed using the X-ray diffraction (XRD) technique. The measurements were made in the Bragg–Brentano ( $\theta$ – $2\theta$ ) geometry by the Rigaku Ultima IV diffractometer with Cu-K $\alpha$  radiation. Crystallite size, lattice constant and interplanar distance were computed by the PDXL software (Version 14.0.3) on the Rigaku system. The optical characteristics were measured in the wavelength range of 200–2500 nm on the Jasco V-670 UV–vis–NIR spectrophotometer equipped with an integrating sphere. Total optical transmission and reflection spectra were used to determine the transmittance of CdS and the optical thickness; by calculation of the absorption coefficient, the band gap was obtained. Surface morphology of CdS films was examined by scanning electron microscopy (SEM). High-resolution SEM apparatus (Zeiss EVO-MA15) was used at an operating voltage of 10 kV. Surface topographies of the layers were studied by AFM using the NT-MDT Solver 47 Pro system operated in a “semi-contact” (tapping) mode. The image analysis of AFM 2D images was performed using the Media Cybernetics ImagePro-3.0 program. The elemental composition of films was determined by means of energy dispersive spectroscopy (EDX) analysis, using the Rontec EDX XFlash 3001 detector and the Oxford Instruments INCA Energy system. The quantitative results were obtained by the help of factory defined standard using the PAP correction – a method for light elements.

## 3. Results

CdS films grew in a columnar structure, perpendicular to the glass substrate (Fig. 1a). Independent of annealing conditions, up to 400 °C the surface view of the CdS layer remained unchanged (Fig. 1c and d). However, Fig. 1b shows that the H<sub>2</sub> annealing generated the recrystallization process which improved the contact between the vertical grains, smoothing the CdS film surface. Already after 10 min annealing at 450 °C pores appeared in the film surface; at longer annealing the CdS porosity clearly increased (Fig. 2). The CdS porosity might be caused by the contraction of the layer which in turn was triggered by the sintering process at high temperature annealing. The same processes were attributed to reduced thickness of CdS layers at high temperature of annealing (Table 1).

EDX analysis revealed a complex composition of CdS films which became stoichiometric when the annealing temperature increased (Table 1). The sulfur deficiency was found characteristic for all CdS films, the highest deficiency being detected at 300 °C annealing. The difference in Cd and S concentrations in the annealed layers could be assigned to the presence of residual oxygen and hydrogen impurities [3,17]. Data in Table 1 show that CdS thin films were transparent to the signals of Si, O and Na from the glass substrate, especially the layers annealed at 450 °C. By subtracting the concentration of SiO<sub>2</sub> from the total oxygen content, the concentration of oxygen in CdS films was

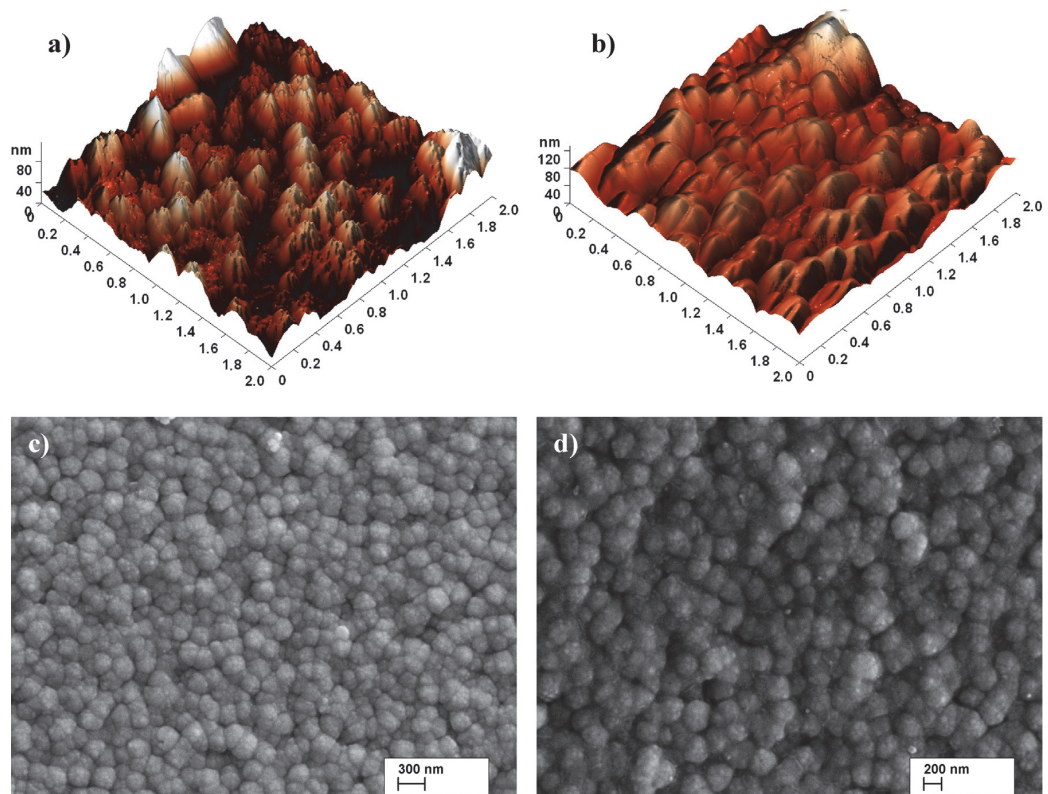


Fig. 1. AFM images and SEM top views of as-deposited (a, c) and annealed at 400 °C (b, d) CdS layers.

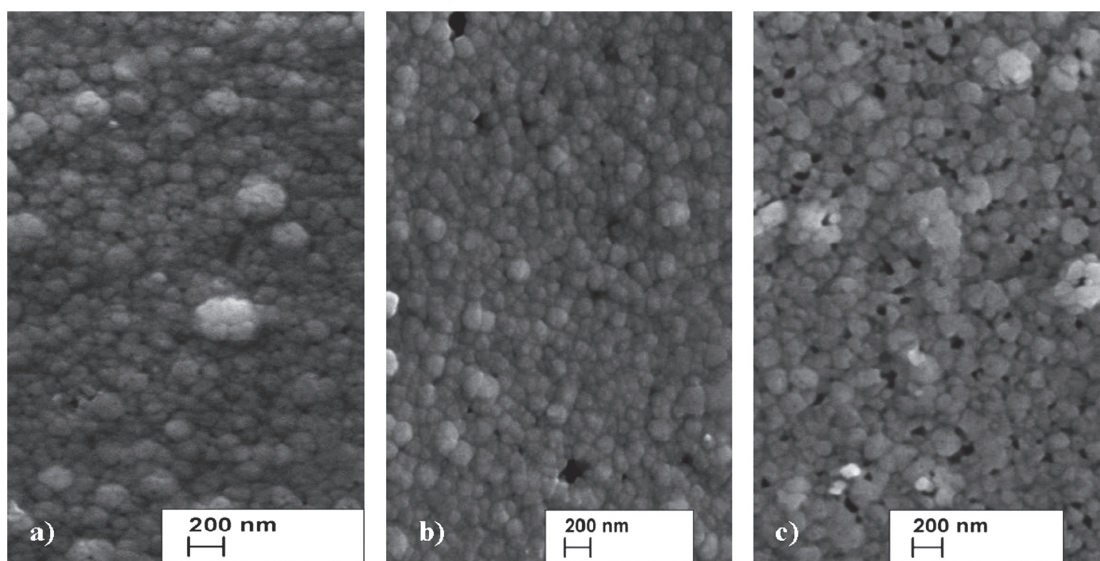
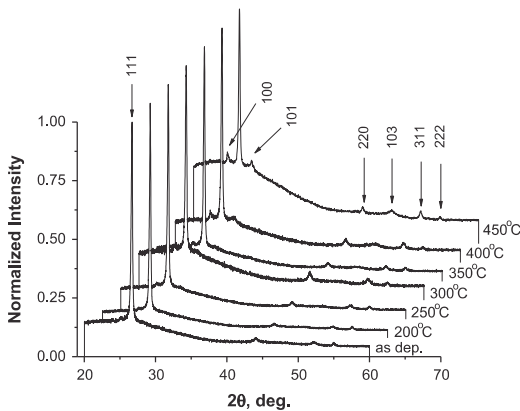


Fig. 2. SEM top view images of CdS film annealed at 450 °C during 10 min (a), 20 min (b) and 60 min (c).

**Table 1**

The thickness ( $t$ ) and the relative concentrations of elements in CdS thin films (by EDX) depending on the annealing temperature when duration was 1 h.

$T_{\text{anneal}}$ ( $^{\circ}\text{C}$ )	$t$ (nm)	O	Na	Si	S	Cd	[O]–2[Si]
as-dep	357.3	12.6	0.1	1.1	39.4	46.8	10
200	346.1	12.4	0.1	0.6	39.5	47.4	11
250	312.6	12.9	0.2	1.1	39.1	46.7	10
300	295.9	10.7	0.5	3.7	38.6	46.5	3
350	334.9	7.8	0.3	1.2	42.2	48.5	5
400	304.5	5.2	0.7	1.2	43.6	49.3	3
450	235.6	10.6	2.3	6.5	37.8	42.8	0



**Fig. 3.** XRD spectra of as-deposited and annealed CdS films for 1 h at different annealing temperatures.

estimated. Strong evidence of O impurity (10%) was found for as-deposited CdS thin films and those annealed at 200–250  $^{\circ}\text{C}$  while at higher annealing temperature its concentration decreased. A similar result was obtained by Niles using the XPS method and attributed to Cd–O bonds [17].

**Fig. 3** shows the XRD pattern of CdS thin films. The noisy signal of the 450  $^{\circ}\text{C}$  annealed sample may be caused by the pores into CdS film deposited on the amorphous glass. In contrast to the commonly accepted transformation of CdS cubic to hexagonal modification during annealing [18], the prevalence of the cubic CdS phase is shown here. This might be due to the presumably incorporated Cd(OH)<sub>2</sub> into the CdS lattice. In **Fig. 4** the vertical lines depict the exact values for hexagonal (26.83 $^{\circ}$ ) and cubic (26.46 $^{\circ}$ ) orientations of bulk CdS [19]. In the annealing process the 26.65 $^{\circ}$  main peak of CdS is shifted toward the 26.48 $^{\circ}$  cubic peak (**Fig. 4**), reaching at 450  $^{\circ}\text{C}$ .

This represents clear experimental evidence that the lattice structure of as-deposited CdS was under stress due to the mixed phase, while longer annealing at higher temperatures led to a pure cubic phase. The lattice constant ( $a$ ), interplanar distance ( $d$ ) and crystallite size ( $s$ ) were obtained from the X-ray diffractogram for the (111) peak. As the annealing temperature was raised from 200 to 450  $^{\circ}\text{C}$ , the increase of  $a$  and  $d$  towards the characteristic value of cubic-CdS [19] was observed. In parallel, a decrease of the crystallite size from 43 to 39 nm

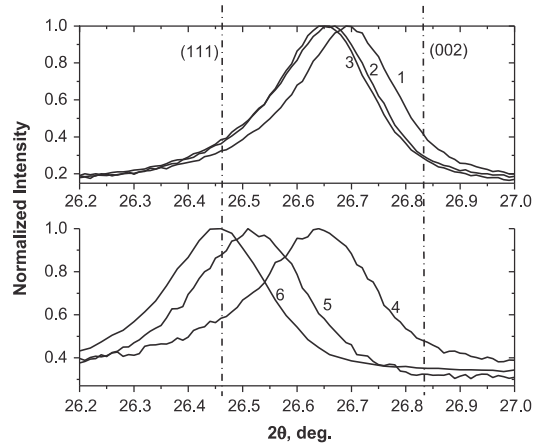


**Fig. 4.** Shift of (111) peak with increasing annealing time and temperature: as-deposited CdS films (1); annealed at 250  $^{\circ}\text{C}$  for 30 min (2) and 120 min (3); annealed at 450  $^{\circ}\text{C}$  for 10 min (4), 20 min (5) and 60 min (6).

**Table 2**

Crystallite size  $s$ , interplanar distance  $d$  and lattice constant  $a$  for CdS layers annealed in H<sub>2</sub> for 1 h at different temperatures.

$T_{\text{anneal}}$ ( $^{\circ}\text{C}$ )	$s$ (nm)	$d$ ( $\text{\AA}$ )	$A$ ( $\text{\AA}$ )
200	42.92	3.335	5.77
250	42.02	3.338	5.79
300	39.13	3.343	5.79
350	40.32	3.343	5.81
400	40.32	3.354	5.82
450	39.33	3.364	5.84

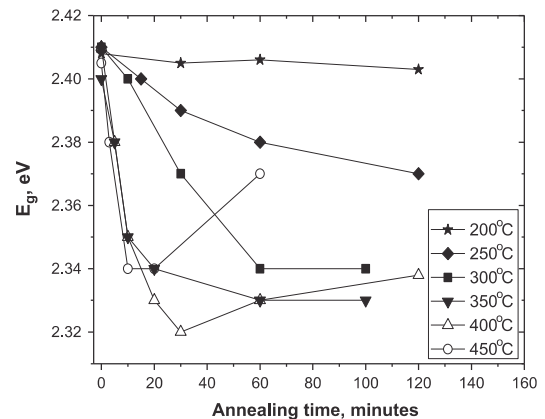


**Fig. 5.** Band gap of CdS films as a function of annealing time and temperature.

and from 42 to 35 nm was noticed for 20–30 and 60 min annealing, respectively.

The optical band gap ( $E_g$ ) values obtained by the extrapolation of absorption dependence are presented in **Fig. 5**, which shows that the changing trend of  $E_g$  became more prominent as the annealing temperature increased.

The 2.41 eV band gap of as-deposited CdS films was close to the 2.42 eV value of bulk CdS while the annealing process steadily reduced it to 2.34 and 2.33 eV for 300 and 350 °C temperatures, respectively. The lowest  $E_g$  value (2.32 eV) was reached after 30 min annealing at 400 °C. Longer annealing returned the band gap to the direction of  $E_g$  value for bulk CdS, which could be connected with the CdS wurtzite modification peaks of XRD pattern (Fig. 3).

## 4. Discussion

In the analysis of the CdS properties, different features were found to be characteristic for distinct annealing temperature and time. These differences could be explained assuming the hypothesis of cadmium hydroxide ( $\text{Cd}(\text{OH})_2$ ) incorporation into the CdS lattice on the sulfur site in the deposition process. The presence of the hydroxide group in as-deposited CBD CdS thin films was also admitted by Danaher et al. [3] and spectrometrically confirmed by Kylner et al. [2]. In order to better characterize the processes that occur in CdS films during annealing, three regions of annealing temperatures were delimited: low, moderate and high temperatures.

### 4.1. Low annealing temperatures 200–250 °C

The hydroxide group in CdS samples annealed at low temperatures is suggested by the O impurity (10 at%) in Table 1. This incorporation rises to low  $a$  and  $d$  for as-deposited CdS layers (Table 2) and a stressed crystalline lattice between hexagonal and cubic (Fig. 4). Gibson et al. called such a structure “polytype”, made of a nearly random stacking sequence of hexagonal planes [20]. This is due to the specific dislocations discussed by Durose et al. in [21], which in our case occur when  $\text{Cd}(\text{OH})_2$  is incorporated into CdS lattice during the deposition process. Elimination of these dislocations through annealing will order the structure of CdS film to a cubic lattice. The high value of  $E_g$  for as-deposited CdS might be explained by the large band gap of incorporated  $\text{Cd}(\text{OH})_2$ , which at low temperatures is not yet decomposed [22].

### 4.2. Moderate annealing temperatures 300–350 °C

Further increase in the annealing temperature is likely to accelerate the sintering of as-deposited polycrystalline CdS. According to [23], starting at 300 °C  $\text{Cd}(\text{OH})_2$  decomposes to water and CdO. The latter was experimentally confirmed by the condensation of Cd black deposit on the cold walls of the process tube. When  $\text{Cd}(\text{OH})_2$  decomposes, the high pressure of water  $\sim 10^4$  atm. [23] contributes to the destruction of CdS crystallites (Table 2). In this temperature region the relaxation of CdS lattice with transition to the pure CdS cubic structure is confirmed by the shift of the main XRD peak (Fig. 4). A similar shift was observed by Ortega-Lopez et al. in [24], where the increased strain in the CdS lattice was achieved when the amount of Cd ions in the solution was increased. We associate the behavior of optical band gap of CBD CdS thin films during the process of hydrogen annealing at moderate temperatures (Fig. 5) with transition from  $(\text{OH})_S$

substitution to  $\text{O}_S$  in the sulfur sub-lattice. As the dimensions of oxygen atom are smaller than dimensions of sulfur, this transition is accompanied by the shrinking of the lattice and narrowing of the band gap. Due to the decomposition peculiarity of  $\text{Cd}(\text{OH})_2$  [25] the above-described process involves formation of excess cadmium precipitates (Table 1).

### 4.3. High annealing temperatures 400–450 °C

At the highest temperatures of annealing CdS layers are more pure. Due to the out-diffusion of oxygen and cadmium the lattice constant and band gap restore to the intrinsic values for pure CdS. The minimum value of  $E_g$  coincides with the destruction of primary crystallites in CdS along with the increase of both  $a$  and  $d$  (Table 2). Also, the appearance of (100) and (101) wurtzite peaks in the XRD pattern of CdS film annealed at 400 °C and 450 °C (Fig. 3) may explain the increasing of  $E_g$  values for longer annealing at these temperatures. These findings support previous research into the electrical properties of CBD CdS films [11].

Due to the intra-grain recrystallization, sintering and contraction of the grains, CdS films became porous when annealed in the range of 400–450 °C. This leads to the conclusion that 400 °C seems to be the highest temperature for  $\text{H}_2$  annealing that provides non-porous CdS layers with suitable properties for photovoltaic goals.

## 5. Conclusions

The hypothesis of incorporation of hydroxide group in the CdS crystalline lattice during the deposition process and its destruction during the hydrogen annealing process was raised to explain the changes of CdS film properties. The stressed cubic lattice of as-deposited film was relaxed by the  $\text{H}_2$  annealing which also provided CdS layers with a more cubic phase. The stability of the cubic CdS phase remained up to high temperatures of annealing when wurtzite modification of CdS film was revealed by XRD characterization. Crystallite size of CdS systematically decreased when the temperature and time of annealing were increased. The dependence of the band-gap as the function of time and temperature of annealing was analyzed on the basis of  $\text{Cd}(\text{OH})_2$  decomposition and transition from  $(\text{OH})_S$  substitution to  $\text{O}_S$  in the sulfur sub-lattice of CdS.

Our practical findings suggest that the annealing in  $\text{H}_2$  ambient implies the recrystallization of CdS film improving its surface, its stoichiometry and decreasing the level of impurities. The highest applicable temperature for annealing CdS films in  $\text{H}_2$  should be considered as 400 °C since at 450 °C the CdS film became porous. Also, a 60-min annealing ensures more stable properties with insignificant changes in properties for longer annealing.

## Acknowledgments

This study was supported by European Social Fund's Doctoral Studies and Internationalization Program Dora,

by the European Union through the 7th FP project FLEX-SOLCELL (GA-2008-230861), by the European Regional Development Fund (Centre of Excellence “Mesosystems: Theory and Applications”, TK114), by Estonian Science Foundation Grant ETF9142, by Estonian Ministry of Education and Research through Program AR10128 and Target Financing Project SF0140092s08.

## References

- [1] M.A. Green, K. Emery, Y. Hishikawa, W. Warta, E.D. Dunlop, *Prog. Photovolt.* 21 (2013) 1.
- [2] A. Klyner, A. Rockett, L. Stolt, *Solid State Phenom.* 51–52 (1996) 533.
- [3] W.J. Danaher, L.E. Lyons, G.C. Morris, *Sol. Energy Mater.* 12 (2) (1985) 137.
- [4] B.E. McCandles, R.W. Birkmire, in: *Proceedings of the 28th IEEE Photovoltaic Special Conference, 2000*, p. 491.
- [5] O. Vigil, O. Zelaya-Angel, Y. Rodriguez, *Semicond. Sci. Technol.* 15 (2000) 259.
- [6] H. Metin, R. Esen, *Semicond. Sci. Technol.* 18 (2003) 647.
- [7] A.J. Haider, A.M. Mousa, S.M.H. Al-Jawad, *Semicond. Sci. Technol.* 8 (4) (2008) 326.
- [8] S.A. Tomas, O. Vigil, J.J. Alvarado-Gil, R. Lozada-Morales, O. Zelaya-Angel, H. Vargas, A. Ferreira da Silva, *J. Appl. Phys.* 78 (4) (1995) 2204.
- [9] H. Kim, D. Kim, *Sol. Energy Mater. Sol. Cells* 67 (2001) 297.
- [10] S. Mishra, A. Ingale, U.N. Roy, A. Gupta, *Thin Solid Films* 516 (2007) 91.
- [11] N. Maticiu, J. Hiie, T. Potlog, V. Valdna, A. Gavrilov, *Mater. Res. Soc. Symp. Proc.* 1324 (2012) 69.
- [12] M. Purica, E. Budianu, E. Rusu, P. Arabadji, *Thin Solid Films* 511–512 (2006) 468.
- [13] J. Han, C. Liao, T. Jiang, G. Fu, V. Krishnakumar, C. Spanheimer, G. Haindl, K. Zhao, A. Klein, W. Jaegermann, *Mater. Res. Bull.* 46 (2) (2011) 194.
- [14] C.S. Ferekides, D. Marinskiy, V. Viswanathan, B. Tetali, V. Palekis, P. Selvaraj, D.L. Morel, *Thin Solid Films* 361–362 (2000) 520.
- [15] A. Romeo, D.L. Bätzner, H. Zogg, C. Vignali, A.N. Tiwari, *Sol. Energy Mater. Sol. Cells* 67 (2001) 311.
- [16] N. Maticiu, J. Hiie, T. Raadik, A. Graf, A. Gavrilov, *Thin Solid Films* 535 (2013) 184–187.
- [17] D.W. Niles, G. Herdt, M. Al-Jassim, *J. Appl. Phys.* 81 (4) (1997) 1978.
- [18] S. Kalhe, S.K. Kulkarni, A.S. Nigavekar, S.K. Sharma, *Sol. Energy Mater.* 10 (1984) 47.
- [19] International Centre for Diffraction Data (ICDD), PDF-2 Release 2008.
- [20] P.N. Gibson, M.E. Özsan, J.M. Sherborne, D. Lincot, P. Cowache, in: *Proceedings of the 2nd World Conference on Photovoltaic Solar Energy Conversion, 1998*, p. 1089.
- [21] K. Durose, A.T. Fellows, A.W. Brinkman, G.J. Russell, J. Woods, *J. Mater. Sci.* 20 (1985) 3783.
- [22] T.P. Gujar, V.R. Shinde, W.Y. Kim, K.D. Jung, C.D. Lokhande, O.S. Joo, *Appl. Surf. Sci.* 254 (2008) 3813.
- [23] Database of HSC Chemistry Ver. 4.0., Outokumpu Research Oy, Pori, Finland.
- [24] M.B. Ortuno-Lopez, M. Sotelo-Lerma, A. Mendoza-Galvan, R. Ramirez-Bon, *Vacuum* 76 (2004) 181.
- [25] M.J.D. Low, A.M. Kamel, *J. Phys. Chem.* 69 (2) (1965) 450.

## **PAPER II**

**N. Maticiuc**, J. Hiie, T. Potlog, V. Valdna, A. Gavrilo, Influence of annealing in H<sub>2</sub> atmosphere on the electrical properties of thin film CdS, Mater. Res. Soc. Symp. Proc. 1324 (2012) 69.



## Influence of Annealing in H<sub>2</sub> Atmosphere on the Electrical Properties of Thin Film CdS

Natalia Maticiu<sup>1,2</sup>, Jaan Hiie<sup>1</sup>, Tamara Potlog<sup>2</sup>, Vello Valdna<sup>1</sup>, Aleksei Gavrilov<sup>1</sup>

<sup>1</sup>Department of Materials Science, Tallinn University of Technology, 5 Ehitajate tee, Tallinn, 19086, Estonia.

<sup>2</sup>Department of Applied Physics and Informatics, Moldova State University, 60 A. Mateevici street, Chisinau, MD 2009, Moldova.

### ABSTRACT

Chemical bath-deposited (CBD) thin film CdS has been widely used as a buffer and n-type window layer in CdS/CIGS and CdS/CdTe thin film solar cells. Annealing of CBD CdS assigns to the layers required concentration and mobility of electrons, crystallinity, structural stability and perfect Ohmic front contact in TCO/CdS interface. But always annealing reduces band gap ( $E_g$ ) of solution-deposited CdS and lowers current density of the CdS/CdTe PV device due to optical absorption within the CdS layer.

We have studied systematically dynamics of changes in CBD CdS/glass thin film structural, optical and electrical properties in annealing process in H<sub>2</sub> ambient at normal pressure in pre-heated ceramic tubular furnace. Here we'll present electrical, characterization results of annealed CBD CdS/glass thin films, 300 nm thick. The films were deposited with thiourea from ammoniacal 1 mM dilute solution of CdSO<sub>4</sub> and 0.001 at. % of NH<sub>4</sub>Cl relative to Cd for Cl doping.

We found high concentration of electrons 1-4 E19 cm<sup>-3</sup> in the layers annealed at 200 - 450 °C, while for 200 °C the long time of annealing over 60 min is needed, but for high temperature region 350 - 450 °C only for short 10 min annealing this concentration region of electrons was achieved. In the high temperature region rapid decrease of electron concentration and conductivity will go on with increasing annealing temperature and time. Mobility of electrons will decrease from 9 to 5 cm<sup>2</sup>/V·s in the annealing region 200-350 °C, which is probably connected with disordering of lattice. On the basis of acquired results we propose an hypothesis about substitutional incorporation of OH group on S site in CdS lattice in deposition process and that (OH)<sub>s</sub> complex defect acts as a donor defect like Cl and we believe that the both defects are responsible for changes of thin film CdS electrical, optical and structural properties in the annealing process. Thermal annealing in hydrogen atmosphere is a convenient and appropriate method for precise control of CdS thin film electrical properties, and also for creation of n/n<sup>+</sup> CdS window layers in the substrate configuration of a solar cell.

### INTRODUCTION

CdS thin films are used as n-type window layers in CdTe [1] and CIGS [2] based solar cells due to wide band gap, high transparency and reasonable mobility of electrons. The performance of solar cells that use chemically deposited CdS are superior to those using evaporated CdS films [3]. This is primarily due to a shift of the absorption edge of the film to shorter wavelengths, in comparison with PVD (physical vapor deposited) CdS [4] – an advantage in the role of as deposited CBD CdS thin films as window materials in CIGS based substrate type heterojunction

solar cells [2]. However, CBD CdS performs well also in annealed superstrate configuration FTO/CdS/CdTe solar cells [5], though in annealing process the band gap decreases from about 2.45 eV to 2.2 eV resulting in lower photovoltaic response of solar cell [1] due to increased absorption in window layer. The formation of heterojunction depends on concentration and conductivity of charge carriers and on the quality of interface between n- and p- type components of the junction. Several authors have found that annealing of CBD CdS thin films at low temperatures 120 – 200 °C improves solar cell parameters [6, 7]. These circumstances impose for further more detailed investigations of CdS annealing processes.

In [8] we described results of systematic investigations of changes in structural and optical properties of CBD CdS resulting from post-deposition thermal treatment in hydrogen ambient and trying to understand the solution chemistry and how the properties of CdS thin films could be tailored for control of the final solar cell characteristics. In this work we report the influence of the annealing on electrical properties of CdS thin films deposited by CBD method.

## EXPERIMENT

CdS thin films were deposited on glass substrates in a hermetically closed glass jar in water solution of CdSO<sub>4</sub> (1 mM), thiourea (10 mM), NH<sub>4</sub>OH (0.2 M), (NH<sub>4</sub>)<sub>2</sub>SO<sub>4</sub> (0.03 M) and relative to Cd 0.001 at % NH<sub>4</sub>Cl at 80 °C. All samples were deposited three times. The CBD CdS layers were washed and dried at 120 °C in vacuum and these layers serve as initial samples (as deposited in the text) for annealing in a preheated tubular furnace in a quartz process tube under 1 atm of H<sub>2</sub> in the temperature range of 200 – 450 °C for 3 - 120 minutes. The heat treatment in H<sub>2</sub> provides reducing atmosphere for deoxidation of CdS layers, as well its normal pressure inhibits evaporation of chlorine dopant from CdS. It has to be emphasized that each experimental point of annealing has been made with new as deposited samples. The CdS thin films were characterized by x-ray diffraction (XRD) in the  $\omega$  - 2 $\nu$  configuration (Cu- $k\alpha$ ) (Rigaku X-ray - LAST IV), scanning electron microscopy (SEM) (Zeiss EVO MA-15), energy-dispersive x-ray spectroscopy (EDS) (Link Analytical AN 10000), optical reflection and transmission on Jasco-V-670 type spectrophotometer. Sheet resistance and Hall effect were measured by Van der Paw four probe method at room temperature. In-plane resistivity and charge carrier concentrations were calculated for the thicknesses (280 - 430 nm) estimated from transmission and reflection data.

## RESULTS

At all annealing temperatures a rapid decrease of resistivity of annealed samples by 4-5 orders of magnitude and acceleration of the decay rate with increasing of annealing temperature has been observed, as shown in Figure 1. The abrupt decay in 10 minutes is followed by slow changes of resistivity at longer annealing times and could be divided into three sub-regions of moderate (200-250 °C), intermediate (250-350 °C) and high (350-450 °C) temperatures. In the low temperature area at 200 °C the lowest resistivity of 0.02  $\Omega$ -cm is achieved and stabilized at 60 min. annealing time. The stabilization time is shortening at higher temperatures. In intermediate region, after the rapid decrease, the resistivity will increase in growing rate with increasing of annealing temperature.

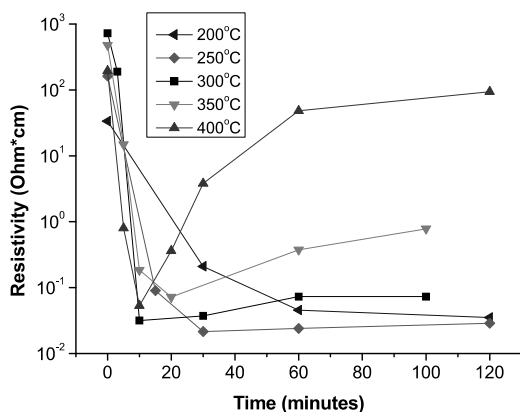


**Figure 1.** Resistivity of CdS layers versus annealing temperature and time.

Hall mobility was measured for samples with sheet resistance lower than  $3 \text{ k}\Omega/\square$ , see Table 1. Lowest values of mobility lie in the intermediate region of annealing temperature. Concentration of electrons is very high,  $> 10^{19} \text{ cm}^{-3}$ , for low and intermediate regions of temperatures.

**Table 1.** Electrical properties of annealed CdS thin films. (The first number in the name of sample corresponds to the annealing temperature, °C – and annealing time in minutes)

Sample (°C-min)	Thick-ness (nm)	Sheet Resistance ( $\text{k}\Omega/\square$ )	Electron Mobility ( $\text{cm}^2/\text{V}\cdot\text{s}$ )	Resistivity ( $\times 10^{-2}, \Omega\cdot\text{cm}$ )	Electron Concentration ( $\times 10^{19}, \text{cm}^{-3}$ )
200 - 60	430	$1.06 \pm 0.01$	$9.3 \pm 0.4$	$4.57 \pm 0.01$	$1.5 \pm 0.1$
200 - 120	420	$0.839 \pm 0.003$	$9.0 \pm 1.5$	$3.52 \pm 0.02$	$2.0 \pm 0.3$
250 - 30	370	$0.582 \pm 0.004$	$9.5 \pm 0.6$	$2.15 \pm 0.02$	$3.1 \pm 0.2$
250 - 60	370	$0.648 \pm 0.002$	$8.0 \pm 0.7$	$2.40 \pm 0.01$	$3.3 \pm 0.3$
250 - 120	370	$0.776 \pm 0.007$	$4.0 \pm 1.5$	$2.88 \pm 0.02$	$4.1 \pm 1.5$
300 - 10	280	$1.13 \pm 0.01$	$5.4 \pm 0.8$	$3.17 \pm 0.01$	$3.7 \pm 0.6$
300 - 60	280	$2.61 \pm 0.01$	$3.5 \pm 0.2$	$7.31 \pm 0.03$	$2.46 \pm 0.15$
300 - 100	290	$2.51 \pm 0.02$	$3.8 \pm 0.2$	$7.27 \pm 0.05$	$2.28 \pm 0.15$
350 - 20	370	$1.95 \pm 0.02$	$4.5 \pm 0.2$	$7.22 \pm 0.15$	$1.9 \pm 0.1$
400 - 10	390	$1.36 \pm 0.01$	$4.5 \pm 0.2$	$5.03 \pm 0.02$	$2.76 \pm 0.15$

## DISCUSSION

The most striking result is creation of high concentration of electrons  $4.1 \cdot 10^{19} \text{ cm}^{-3}$  at moderate annealing temperatures 200 – 250 °C, see Table 1. An abrupt decrease of resistivity and increase of electron concentration in CBD CdS thin films annealed in hydrogen or in vacuum at the same moderate temperatures has also been observed by [9, 10]. It should be mentioned that this fact may be a possible reason for formation of reverse diode in the  $n^+$ -CdS/i-ZnO/ZnO:Al window region of CIGS type substrate configuration solar cells like in the case for  $n^+$ -CdO/n-CdS/ITO interface described by Durose [11].

The high concentration of electrons corresponds to the high density of shallow donors in CdS lattice and the resistivity of such degenerated semiconductor layers does not depend on temperature (Figure 2). The high conductivity cannot be explained by creation of conductive phase of CdO from the residual oxide components, because reduction of CdO begins intensively from 200 °C [12]. Also it can not explained by creation of sulfur vacancies because long H<sub>2</sub> annealing at high temperature region results in high resistivity film, which has very low intensity of photoluminescence below band gap energy [13] indicating to the absence of impurities and complexes with cadmium vacancies, as potential acceptors.

Temperature dependence of conductivity for CdS thin film annealed at 400 °C has an activation energy of 0.2 eV over room temperature, which indicates to the presence of deep donors (Figure 2).

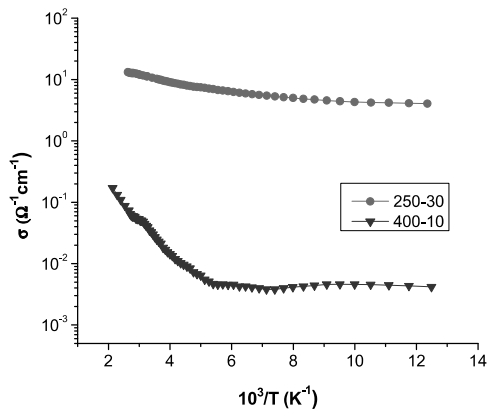
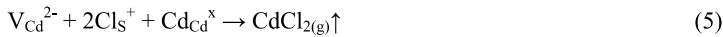
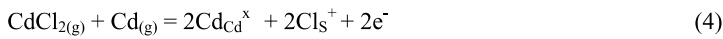
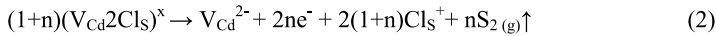


**Figure 2.** Conductivity of CdS thin films annealed at 250 and 400 °C versus reverse temperature of measurement,  $10^3/T \text{ (K}^{-1}\text{)}$ .

Increase in annealing temperature accelerates the fall of resistivity. As a working hypothesis, incorporation of cadmium hydroxychloride into CdS lattice on sulfur site in deposition process from basic ammonia solution, is assumed. Presence of hydroxide group in as deposited CBD CdS thin films has been spectrometrically (FTIR) confirmed by Kylvner [14]. Sulfur, chlorine and hydroxide group are spatially compatible, their atomic sizes are about 100 pm, for oxygen 60 pm (compare densities of cubic modifications of CdS  $4.82 \text{ g/cm}^3$  and CdO  $8.2 \text{ g/cm}^3$ ), and for hydrogen 30 pm. The hydroxide and chloride ions on sulfur site form electrically neutral defect

complexes  $V_{Cd}2Cl_s$  and  $V_{Cd}2(OH)_s$ . Increase in annealing temperature accelerates sintering of as deposited polycrystalline CdS and retention of larger quantities of chloride and hydroxide impurities, which would otherwise evaporate and decompose. Upon decomposition of two hydroxide groups in CdS lattice one water molecule will be released and one sulfur vacancy created. Annihilation of sulfur and cadmium vacancies creates two donor centers of  $Cl_s^+$  and  $(OH)_s^+$ . These substitutional impurities on sulfur site behave as shallow donors contributing at room temperature to the decrease of resistivity. The concentration of chloride and hydroxide impurities, saved in as deposited CdS, depends on post-deposition temperature of vacuum drying. At high temperature region of annealing, due to destruction of hydroxide group and out diffusion of chlorine and removal by evaporation, the concentration of electrons decreases.

Incorporation of cadmium chloride could be sketched with equations 1 – 5:



For all annealing temperatures until 400 °C a technologically important stability region could be envisaged, for example at 400 °C it will be 60 minutes or longer. All annealed samples have been electrically stable over a year.

Thermal annealing in hydrogen atmosphere is a convenient and appropriate method for precise control of CdS thin film electrical properties, and also for creation of n/n<sup>+</sup> CdS window layers in the substrate configuration of a solar cell.

## CONCLUSIONS

Thermal annealing in hydrogen atmosphere is a convenient and appropriate method for precise control of CdS thin film electrical properties, and also for creation of n/n<sup>+</sup> CdS window layers in the substrate configuration of a solar cell.

## ACKNOWLEDGMENTS

This work has been supported by EU 7<sup>th</sup> FP project FLEXSOLCELL GA-2008-230861, by Estonian Science Foundation grants 7241 and 7608, and by Estonian National Target Financing Nos SF0140092s08, and SF0140099s08.

## REFERENCES

1. X. Wu, *Solar Energy* **77**, 803–814 (2004).
2. I. Repins, M. Contreras, M. Romero, Y. Yan, W. Metzger, J. Li, S. Johnston, B. Egaas, C. DeHart, J. Scharf, B. E. McCandless and R. Noufi, *PVSC'08 33<sup>rd</sup> IEEE Proc.*, 1–6 (2008).
3. M. T. S. Nair, P. K. Nair, R. A. Zingaro and E. A. Meyers, *J.Appl.Phys.*, **75(3)**, 1557–1564 (1994).
4. D. Abou-Ras, G. Kostorz, A. Romeo, D. Rudmann and A.N. Tiwari, *Thin Solid Films*, **480–481**, 118–123 (2005).
5. R. G. Dhere, J. N. Duenow, A. Duda, S. Glynn, J. Li, W. K. Metzger, H. Moutinho and T. A. Gessert, *Mater. Res. Soc. Symp. Proc.*, **1165**, 1165-M02-08 (2009).
6. T. Sakurai, N. Ishida, S. Ishizuka, M. M. Islam, A. Kasai, K. Matsubara, K. Sakurai, A. Yamada, K. Akimoto and S. Niki, *Thin Solid Films*, **516**, 7036–7040 (2008).
7. Y. D. Chung, D. H. Cho, N. M. Park, K. S. Lee and J. Kim, *Current Applied Physics*, **11**, S65-S67 (2011).
8. N. Maticiuc, T. Potlog, J. Hiie, V. Mikli, N. Pöldme, T. Raadik, V. Valdna, A. Mere, A. Gavrilov, F. Quinci, V. Lughì and V. Sergo, *Moldavian Journal of the Physical Sciences*, **9(3-4)**, 275-279 (2010).
9. J. Hiie, K. Muska, V. Valdna, V. Mikli, A. Taklaja and A. Gavrilov, *Thin Solid Films*, **516**, 7007-7012 (2008).
10. E. Vasco, E. Puron and O. de Melo, *Material Letters*, **25**, 205-207 (1995).
11. M. K. Al Turkestani and K. Durose, *Sol. Energy Mat. & Solar Cells*, **95**, 491-496 (2011).
12. HSC Chemistry 4.0, Chemical Reaction and Equilibrium Software with extensive Thermochemical Database (1999).
13. J. Hiie, F. Quinci, V. Lughì, V. Sergo, V. Valdna, V. Mikli, E. Kärber and T. Raadik, *Mater. Res. Soc. Symp. Proc.*, **1165**, 1165-M08-17 (2009).
14. A. Kylner, A. Rockett and L. Stolt, *Sol.Stat. Phenom.*, **51-52**, 533-540 (1996).

## **PAPER III**

**N. Maticiuc**, J. Hiie, Annealing effect on CdS films: transition from glass to ITO, IOP Conf. Ser.: Mater. Sci. Eng. 49 (2013) 012061.



# Annealing effect on CdS films: transition from glass to ITO

Natalia Maticiu<sup>\*</sup> and Jaan Hiie

Tallinn University of Technology, Ehitajate tee 5, Tallinn, Estonia

**Abstract.** Structural and optical properties of CdS films deposited on glass and ITO substrates and annealed in H<sub>2</sub>, N<sub>2</sub> or H<sub>2</sub>+N<sub>2</sub> atmospheres at 250 °C and 400 °C were compared. The optical thickness 405±10 nm of the CdS films was found not to be influenced by any annealing conditions or substrate. The as deposited films on both substrates had similar diffraction patterns with one narrow peak corresponding to the (111) cubic plane at 2θ 26.70° and 26.75°, respectively. Higher density of nucleation centres on the ITO surface generated denser CdS films. In the annealing process of CdS/ITO a slower shift of both (111) peak and lattice constant was observed in the direction of pure zinc blende modification. Similar values of band gap and transmittance were determined for as-deposited CdS while annealing at 400 °C decreased transmittance by 5% and 16% for CdS on glass and ITO, respectively. Transmittance dropped because of the destruction of hydroxide group in the CdS lattice, the formation of cadmium excess and the reduction of SnO<sub>2</sub> to black SnO in the ITO structure.

## 1. Introduction

CdTe- and CIGS- based photovoltaic solar cells in a superstrate configuration are made on glass substrates coated by transparent conductive oxide (TCO) like tin oxide (SnO<sub>2</sub>) or indium tin oxide (ITO) over which CdS layer is deposited. Combined TCO–CdS window layers [1–4] and the effect of these bilayers on the final photovoltaic response [5] had been studied by many authors. Usually TCO-coated glass substrates with suitable photovoltaic quality are commercially available, while the optimization of CdS thin films remains in progress at laboratory scale.

As an optimization route for CdS thin film, annealing in different atmospheres at certain time-pressure-temperature conditions may be used. In [6] we studied the properties of CdS/glass thin films after H<sub>2</sub> annealing. A relationship between annealing conditions and desirable properties of CdS on glass was obtained: temperatures up to 400 °C had a weak influence on the morphological and optical properties; 1h annealing was enough to reach stable electrical properties; CdS films annealed at 250 – 400 °C had resistivity in the region of  $2.3 \cdot 10^{-2} - 6.1 \Omega \cdot \text{cm}$ , respectively. It is interesting to verify if the knowledge gained about the properties of annealed CdS/glass may be applied for the annealed CdS/ITO/glass structures. Similar studies have shown the influence of annealing in air [7] or nitrogen [8] on CdS properties when deposited on different substrates such as glass, ITO, SnO<sub>2</sub> or other materials. However, information about CdS/ITO/glass bilayers annealed in H<sub>2</sub> atmosphere is scarce. This paper compares the optical, structural and electrical properties of CdS layers deposited on glass and ITO substrates and annealed in H<sub>2</sub>, N<sub>2</sub> and H<sub>2</sub>+N<sub>2</sub> gases.

---

<sup>\*</sup>Corresponding author. Tel.: +372 620 3366

E-mail address: [nataliamaticiu@yahoo.com](mailto:nataliamaticiu@yahoo.com) (N. Maticiu)



## 2. Experiment

Polycrystalline CdS films were deposited by chemical bath deposition (CBD) on both uncoated soda-lime glass and commercial ITO coated glass substrates. The plates were accurately cleaned and immersed in the deposition solution. The temperature and agitation speed of the solution were 85 °C and 500 rpm, respectively. One deposition lasted for 30 minutes, but for thicker CdS films the process was repeated three times. After deposition the films were vacuum dried at 120 °C to remove most of the secondary phases of water, hydroxides and organic impurities. This drying was the last stage of preparation for the so-called as-deposited CdS layers. We choose the thermal treatment conditions based on our investigation on H<sub>2</sub> annealing of CdS/glass: normal pressure, 1 h duration at 250 °C and 400 °C. For comparison, annealing in N<sub>2</sub> and H<sub>2</sub>+N<sub>2</sub> (H<sub>2</sub> concentration of was 5%) was also applied.

Crystallographic investigations were performed using the X-ray diffraction (XRD) technique in the Bragg-Brentano ( $\theta$ - $2\theta$ ) geometry by a Rigaku Ultima IV diffractometer with Cu-K $\alpha$  radiation. Crystallite size, lattice constant and interplanar distance were computed by the PDXL software (Version 1.4.0.3) on the Rigaku system. The optical characteristics were evaluated at room temperature in the range of 200–2500 nm on the Jasco V-670 UV-VIS spectrophotometer equipped with an integrating sphere. Total optical transmission and reflection spectra were used to determine the band gap and optical thickness of CdS.

## 3. Results and discussions

Optical properties were analyzed on the basis of transmittance spectra and  $E_g$  values shown in figure 1a and table 1, respectively.

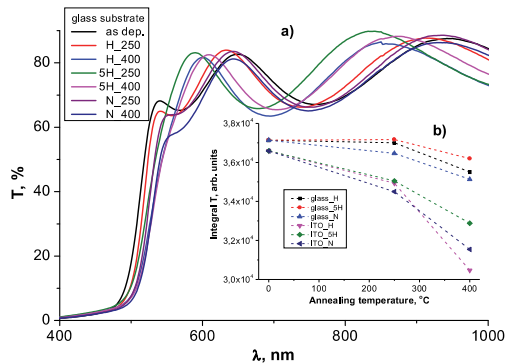


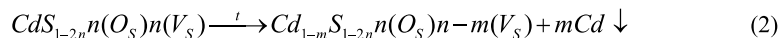
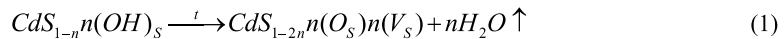
**Figure 1.** a) Optical transmittance spectra of the CdS films. b) Calculated integral transmittance of CdS/glass and CdS/ITO as a function of annealing temperature and ambient.

**Table 1.** Band gap ( $E_g$ ), lattice constant ( $a$ ), interplanar distance ( $d$ ) and crystallite size ( $S$ ) of the CdS films deposited on different substrates and annealed in H<sub>2</sub> (H), N<sub>2</sub> (N) and H<sub>2</sub>+N<sub>2</sub> (5H) ambient.

Substrate →	$E_g$ , eV		$a$ , Å		$d$ , Å		$S$ , Å	
	glass	ITO	glass	ITO	glass	ITO	glass	ITO
as deposited	2.454	2.464	5.783	5.775	3.337	3.330	405.2	428.0
H-250 °C	2.412	2.373	5.803	5.793	3.346	3.341	428.3	457.0
H-400 °C	2.364	2.379	5.821	5.804	3.354	3.347	391.3	394.3
5H-250 °C	2.391	2.373	5.792	5.790	3.340	3.340	430.9	460.0
5H-400 °C	2.348	2.365	5.806	5.802	3.345	3.346	377.4	364.0
N-250 °C	2.377	2.376	5.797	5.787	3.344	3.338	420.0	472.0
N-400 °C	2.352	2.367	5.806	5.797	3.351	3.343	368.3	347.7

Almost similar changes of band gap were found for CdS on glass and ITO substrates, independent of the annealing atmosphere. When the annealing temperature increased, the band gap of CdS/glass gradually decreased for all three atmospheres from 2.45 eV (as-deposited CdS) to 2.35 eV (annealed at 400 °C). With ITO the  $E_g$  of CdS reached a constant value (2.375 eV) for  $N_2$ -containing ambients at both annealing temperatures (table 1).

We estimated the integral transmittance in the region of 500-1000 nm as the area under the T plot (figure 1b). With a glass substrate a similar trend of CdS transmittance was observed for all annealing gases - a slow decrease at 250 °C followed by an abrupt decrease at 400 °C (~5 %). However, the lowest transmittance was emphasized for a CdS sample annealed in  $N_2$ . The decreased transmittance of CdS could be explained by hydroxide group incorporated into the CdS lattice the destruction of which starts at 300 °C [6]. Independent of the annealing atmosphere, the hydroxide group incorporated into the CdS lattice leads to the formation of  $CdS_{1-n}(OH)_s$  solid alloy. When temperature is applied,  $H_2O$  evaporates and Cd precipitate [9] is formed (1, 2).



When CdS/glass was annealed, the Cd precipitate (2) decreased the transmittance of CdS (figure 1b). However, in the presence of  $H_2$  the CdO decomposes, as oxygen is eliminated by the release of  $H_2O$ , and CdS band gap increases [6]. Therefore, the CdS transmittance was higher after the  $H_2$  annealing than that of  $N_2$  one. This reveals an advantage of  $H_2$  annealing for CdS films.

For a CdS film on ITO, the transmittance decreased faster up to 250 °C than with the glass case. Thus, the contribution of Cd precipitate (2) to the decomposition of  $SnO_2$  should be taken into account (3, 4). Both products of reaction (3) resulted in the reduced transmittance of the CdS/ITO bilayer.



Still, when CdS/ITO was annealed at 400 °C in  $H_2$ , the transmittance decreased by 16% compared to as-deposited CdS. A new reaction (5) may compete with (3) due to higher activity of the  $H_2$  compared to the metallic Cd from CdS. These processes resulted in the blackening of the ITO substrate and an abrupt drop of CdS transmittance.



The transmittance behavior of CdS on both glass and ITO substrates suggested that  $H_2+N_2$  mixture instead of pure  $H_2$  or  $N_2$  gases is needed for annealing.

The structural properties of CdS were analyzed based on XRD measurement results. Similar XRD patterns with one narrow (111) diffraction peak of the cubic plane at 26.70° and 26.75° were found for CdS films on glass and ITO substrates, respectively. Figure 2 shows that both peaks are in the close proximity of the (002) hexagonal plane at 26.83°. Twice higher (111) peak of CdS/ITO than that of CdS/glass suggests a more oriented CdS film. This is attributed to the strong influence of the oriented crystalline surface of ITO. The high density of nucleation centers on ITO generates a denser CdS film, which might also explain the decreased transmittance of CdS on ITO (figure 1b).

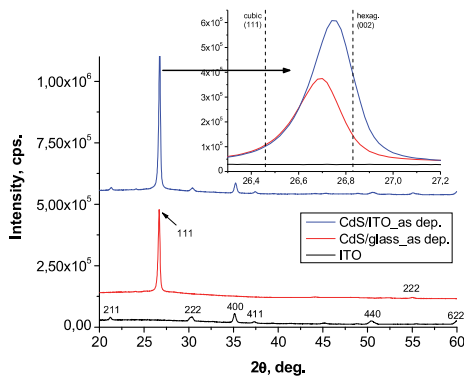


**Figure 2.** XRD pattern of as-deposited CdS on glass and ITO substrates.

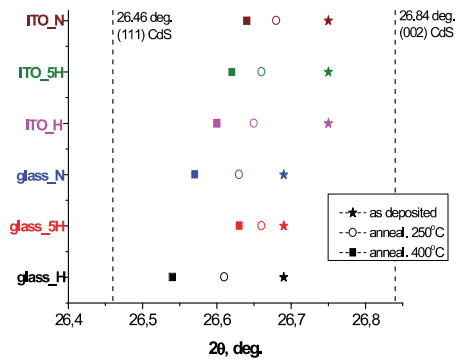


**Figure 3.** Influence of annealing conditions on the shift of the main (111) peak of CdS.

Interestingly for both substrates, the main (111) peak shifted in the direction of the zinc blende CdS plane at  $26.46^\circ$  in all three ambients when the annealing temperature increased (figure 3). However, a slower shift of the main cubic peak and lattice constant (table 1) in the direction of zinc blende modification of CdS was found in the case of the ITO substrate during annealing. The shift of this main peak infers that the stressed lattice of as-deposited CdS relaxed during annealing at 250 - 400 °C, after which a more pure cubic CdS phase was obtained. The comparison between the three annealing atmospheres in the case of glass substrate shows that the  $H_2$  ambient contributed to a more cubic structure of CdS, while the  $H_2+N_2$  ambient had a weak influence on the CdS lattice. In the case of the ITO substrate no significant differences were found when CdS was annealed at higher temperatures.

#### 4. Conclusions

An abrupt reduction of transmittance was found for CdS/ITO annealed in  $H_2$  at 400 °C. This might limit the applicability of CBD CdS for superstrate solar cells. We minimized the transmittance by annealing CdS/ITO in a mixture of  $H_2 + N_2$ . The oriented ITO contributes to denser CdS films. The typical shift of the main (111) peak is characteristic for CdS on both glass and ITO. Generally, the structural and optical properties of CdS films on glass and ITO are quite similar.

#### Acknowledgements

Support by DoRa, 7FP GA-2008-230861, TK114, ETF9142, AR10128, SF0140092s08.

#### References

- [1] Oliva A I, Castro-Rodriguez R, Ceh O, Bartolo-Perez P, Caballero-Briones F, Sosa V 1999 *Appl. Surf. Sci.* **148** 42
- [2] Schaffner J, Feldmeier E, Swirschuk A, Schimper H-J, Klein A, Jaegermann W 2011 *Thin Solid Films* **519** 7556
- [3] Lee J-H 2007 *Thin Solid Films* **515** 6089
- [4] Castro-Rodriguez R, Oliva A I, Sosa V, Caballero-Briones F 2000 *Appl. Surf. Sci.* **161** 340
- [5] Romeo N, Bosio A, Canevari V, Terheggen M, Vaillant Roca L 2003 *Thin Solid Films* **431** 364
- [6] Maticiu N, Hiie J, Potlog T, Valdna V, Gavrilo A 2012 *Mater. Res. Soc. Symp. Proc.* **1324** 69
- [7] Martinez M A, Guillen C, Herrero J 1999 *Appl. Surf. Sci.* **140** 182
- [8] Metin H, Erat S, Durmus S, Ari M 2010 *Appl. Surf. Sci.* **256** 5076
- [9] Moreno M S, Varela A, Otero-Diaz L C 1997 *Phys. Rev. B* **56(9)** 5186

## **PAPER IV**

**N. Maticiuc**, M. Kukk, N. Spalatu, T. Potlog, M. Krunks, V. Valdna, J. Hiie, Comparative study of CdS films annealed in neutral, oxidizing and reducing atmospheres, *Energy Procedia* 44 (2014) 77–84.



E-MRS Spring Meeting 2013 Symposium D - Advanced Inorganic Materials and Structures for Photovoltaics, 27-31 May 2013, Strasbourg, France

## Comparative study of CdS films annealed in neutral, oxidizing and reducing atmospheres

Natalia Maticiu<sup>a\*</sup>, Mart Kuk<sup>a</sup>, Nicolae Spalatu<sup>b</sup>, Tamara Potlog<sup>b</sup>, Malle Krunks<sup>a</sup>, Vello Valdna<sup>a</sup>, Jaan Hiie<sup>a</sup>

<sup>a</sup>Department of Materials Science, Tallinn University of Technology, 5 Ehitajate tee, 19086 Tallinn, Estonia

<sup>b</sup>Faculty of Physics, Moldova State University, 60 A. Mateevici str., 2009 Chişinău, Moldova

---

### Abstract

Chemical bath deposited CdS:Cl thin films on glass substrates were annealed in H<sub>2</sub>, N<sub>2</sub> and air at 250 °C and 400 °C, and then characterized by XRD, Van der Paw, Raman, photoluminescence and transmittance - reflectance spectroscopy.

Different properties of CdS film are found depending on the neutral, reducing or oxidizing annealing gas. Strong activity of chlorine as a flux and dopant agent is observed in the air- annealed CdS films. This is expressed by the strongest photoluminescence intensity of the 2.24 eV peak. Oxygen containing phases CdSO<sub>3</sub> and CdO are shown by XRD patterns for air- and N<sub>2</sub>- annealed CdS films at 400 °C. Longest N<sub>2</sub> annealing generated pure CdS layers, similarly with the H<sub>2</sub>- annealed ones. Also, the H<sub>2</sub> annealing shows a shift of the main (111) CdS peak toward the pure cubic modification proportionally with the annealing time, while N<sub>2</sub> and air annealing fixed the peak at intermediate cubic-hexagonal position. This could be explained by incorporation of oxygen in CdS lattice for N<sub>2</sub> and air annealing, supported by the presence of oxide phases in CdS XRD patterns. H<sub>2</sub> annealing removes the incorporated oxygen from the lattice and oxide phases from the grain boundaries, leaving pure CdS films. Behavior of CdS structural properties unambiguously demonstrates the incorporation of hydroxide group and oxygen into the CdS crystallite lattice and explains the changes of structural, optical and electrical properties of CdS films in the annealing process.

© 2013 The Authors. Published by Elsevier Ltd.

Selection and peer-review under responsibility of The European Materials Research Society (E-MRS)

*Keywords:* CdS, H<sub>2</sub> annealing; N<sub>2</sub> annealing; air annealing; structural properties; optical properties; electrical properties.

---

\* Corresponding author. Tel.: +372-620-3366; fax: +372-620-2020.

E-mail address: [nataliamaticiu@yahoo.com](mailto:nataliamaticiu@yahoo.com)

## 1. Introduction

CdS thin film is widely used as n-type semiconductor partner and buffer layer in thin film chalcogenide solar cells [1]. Among possible deposition methods, chemical bath deposition (CBD) is one of the most suitable due to its low cost, low temperature processing and possibility to form large area films. As deposited CBD CdS layers have a high speed of recrystallization already at low temperatures with major changes in structural and optical properties [2,3]. A possible way to control these changes and reduce the extent of disorder in CdS films may be the thermal annealing in a defined atmosphere. The importance of CdS properties control is revealed by the application of CdS films in substrate configuration solar cells. For instance, in CIGS solar cell the i-ZnO and ZnO:Al layers are sputtered on CdS at 200 °C in O<sub>2</sub>+Ar or Ar ambient [4], influencing the properties of underlying CdS film and final parameters of the solar cell [5,6].

Generally, the influence of annealing ambient on CdS film properties was studied by many authors. The neutral (N<sub>2</sub>, Ar containing) annealing brings reorientation of as deposited CdS films with a significantly improved crystalline quality, diminishes their resistivity by increasing the grain size and decreasing the number of grain boundaries in CdS films [7]. Also, such an annealing leads to phase transition from the metastable cubic phase to a stable hexagonal phase of CdS [8], which is undesirable when stacking CdS film with a cubic CdTe absorber. Besides increased grain size and improved crystallinity of CdS films annealed in oxidizing (O<sub>2</sub> containing) ambient, a substantial decrease in the band gap have been reported [9]. The thermal treatment in a reducing atmosphere of H<sub>2</sub> has the advantage to eliminate the chemisorbed oxygen and oxides. Annealing in the presence of H<sub>2</sub> preserves the same structural cubic phase during the complete thermal process [2] and decreases the resistivity by 4 orders of magnitude [10] compared to the neutral case [7].

However, a deep study of the mechanisms and understanding of annealing processes in CBD CdS films depending on reducing, oxidizing and neutral atmospheres is still missing. Here we present the analysis of structural, optical and electrical properties of CdS films and the mechanisms responsible for their changes when annealing in different ambient is applied.

## 2. Experimental

CdS thin films were prepared by CBD, the experimental details being presented elsewhere [10]. After the deposition and vacuum drying CdS films were annealed in a closed process tube in three different atmospheres at normal pressure: hydrogen, nitrogen and air. Every annealing lasted 1h and the annealing temperatures were established at 250 °C and 400 °C.

CdS layers were characterized by X-ray diffraction (XRD), photoluminescence (PL), Raman, optical transmission - reflection spectra, Van der Pauw and Hall Effect techniques. XRD measurements were performed in the Bragg - Brentano (θ-2θ) geometry using a Rigaku Ultima IV diffractometer with Cu Kα radiation. Crystallite size and lattice constants were calculated using the software PDXL Version 1.4.0.3 on the Rigaku system. The optical total transmittance and reflectance spectra of CdS films were obtained in the wavelength range of 200 – 2500 nm on a Jasco V-670 UV-VIS-NIR spectrophotometer equipped with an integrating sphere. The PL was measured at room temperature (RT) with a green laser (532 nm) and 10 mW density of excitation. Spectra were registered by a Renishaw - type device with a built-in measuring Raman installation. The RT Raman spectra were recorded in a 180° backscattering geometry by using the Horiba's LabRam HR high resolution spectrometer. The incident laser light with the wavelength of 532 nm was focused on the sample within a spot of 10 μm in diameter and the spectral resolution of the spectrometer was about 1.5 cm<sup>-1</sup>. Each spectrum was smoothed with Lorentz fitting and peak position and Full Width at Half Maximum (FWHM) were obtained. The electrical properties of the CdS films (resistivity, charge carrier concentration and mobility) were measured in the temperature range of -100 °C to +100 °C, using MMR's Variable Temperature Hall System and a Hall, Van der Pauw Controller H-50. The contact material used for electrical measurements was evaporated indium.

### 3. Results and discussions

CdS films grown on glass substrates and annealed in air,  $N_2$  or  $H_2$  were adherent, yellowish and reflecting. Independently of the annealing ambient, all the films annealed at 400 °C were more dark-yellowish compared to those annealed at 250 °C.

#### 3.1. Structural properties

Structural properties of CdS thin films were analyzed on the basis of XRD and Raman measurements. At low annealing temperature (250 °C) the XRD patterns do not reveal any additional phases except CdS. At higher annealing temperature (400 °C) in air and nitrogen  $CdSO_3$  and  $CdO$  phases were found (Fig. 1a).  $CdSO_3$  which appeared during nitrogen annealing for 60 minutes has disappeared at longer annealing for 120 minutes, while in air  $CdSO_3$  was transformed to  $CdO$ . Only annealing in hydrogen resulted in pure CdS (Fig. 1a).

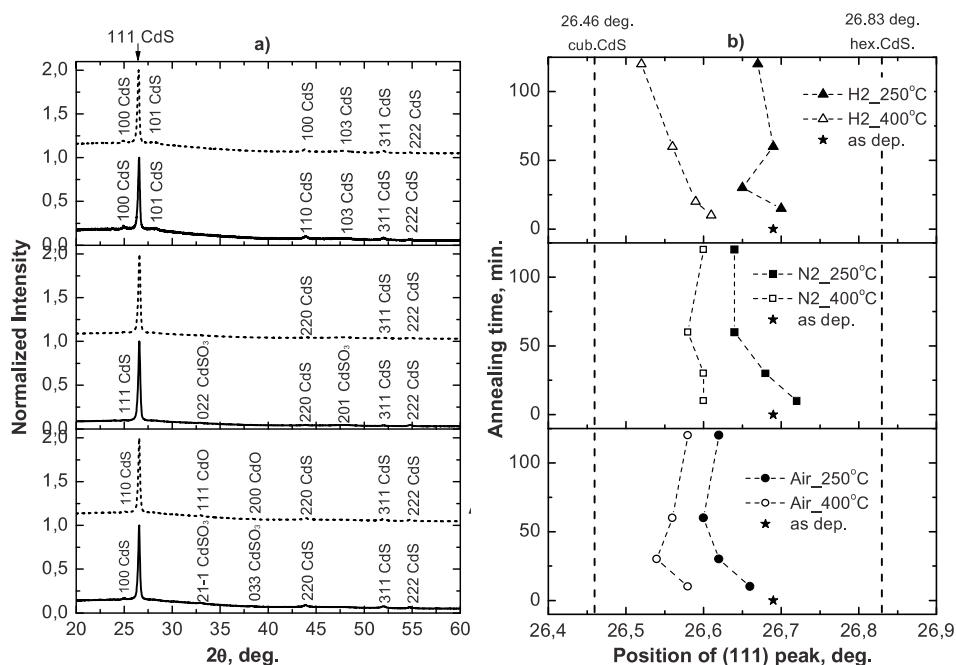


Fig. 1. (a) XRD pattern of CdS films annealed at 400 °C in  $H_2$ ,  $N_2$  and air for 1h (solid line) and 2h (dash line); (b) Shift of the main (111) peak in dependence of annealing ambient, temperature and duration

By high resolution analysis was shown the shift of the main (111) peak toward the cubic modification of CdS (Fig. 1b). In  $H_2$  annealing process we explain this shift by the decomposition of incorporated OH group, creation of oxygen on sulfur site and by removal of oxygen from the crystalline lattice [10]. While atomic size of sulfur and OH group are similar, the atomic size of oxygen is smaller (compare the densities of cubic CdS 4.8 g/cm<sup>3</sup> and CdO 8.1 g/cm<sup>3</sup> [11]) and causes contraction of CdS lattice [12], like sulfur in CdTe [13] and boron in silicon [14]. In air

and  $N_2$  the shift of the (111) peak is stabilized for 60 minutes annealing (Fig. 1b), which corresponds to the remained traces of oxygen in the CdS lattice and supported by the presence of oxide phases (Fig. 1a).

The traces of oxygen are present even in  $H_2$ - annealed CdS and only at 450 °C annealing the main peak reaches the position of pure cubic modification ( $26.46^\circ$ ) for CdS [10]. However, as the air ambient is more active it showed a deeper removal of oxygen compared to  $H_2$ ; this could be attributed to  $CdCl_2$  dopant added in the deposition process of CdS. Due to the presence of  $CdCl_2$  flux and high solubility of both cadmium oxides and CdS in  $CdCl_2$  flux [15], the oxygen diffuses into the melted phase and at high temperature  $CdSO_3$  and CdO are extracted.

The complex composition of as deposited CdS films [16] involves the formation of oxides like CdO and  $CdSO_3$  in neutral and oxidizing atmospheres of annealing (1, 2).



In  $N_2$  annealing process, depending on the temperature and time, the oxides are expelled as metallic Cd and  $SO_2$  (3, 4), while in  $H_2$  ambient Cd and water are expelled (5, 6). The metallic Cd was confirmed by the black deposit on cold walls of the process tube. In air Cd forms on CdS surface CdO (7) as the most stable phase (Fig. 1a).



Raman spectra of CdS films annealed in different atmospheres (Fig. 2) present a well-resolved line at approximately  $300\text{ cm}^{-1}$ , corresponding to the first order scattering of the longitudinal optical (LO) phonon mode.

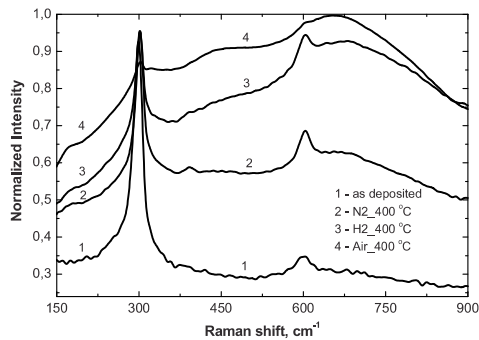


Fig. 2. Raman spectra of CdS films annealed for 1h in different ambients at 400 °C.

The position of this peak is slightly shifted to lower wave numbers (Table 1) with respect to bulk CdS peak ( $305\text{ cm}^{-1}$ ). Several authors explained this shift by the changes of grain size [17,18,19]. The narrowing of the 1LO peak of annealed CdS films (Table 1) is connected to the lattice stress shown by XRD data [12]. The decreased peak intensity with annealing is attributed to the shift of the crystalline structure of CdS films to a more cubic phase [20]. The second-order scattering of LO phonon is also visible at approximately  $600\text{ cm}^{-1}$ .

Both Raman and XRD measurements indicate that CdS films annealed in any atmosphere have a better crystallinity [17] than the as deposited ones. However, we observed at  $\sim 700\text{ cm}^{-1}$  an additional Raman peak that for air-annealed CdS film has higher intensity compared to 2LO peak. This peak may correspond to  $\text{CdSO}_3$  and  $\text{CdO}$  [21,22], both phases representing the oxidation products of annealing at  $400\text{ }^\circ\text{C}$  (Fig. 1a).

Table 1. Position of 1LO peak and its FWHM value in dependence of annealing ambient for CdS films.

Sample	Main peak ( $\text{cm}^{-1}$ )	FWHM ( $\text{cm}^{-1}$ )
As deposited CdS	300.0	19.56
$\text{H}_2$ -annealed CdS	302.4	14.36
$\text{N}_2$ -annealed CdS	302.7	13.39
Air-annealed CdS	302.7	10.15

### 3.2. Optical properties

Transmittance spectra of CdS films (Fig. 3a) show that annealing at low temperature ( $250\text{ }^\circ\text{C}$ ) weakly influenced the optical properties of CdS films. However, air-annealed CdS has lower transmittance in the 500-700 nm region compared to  $\text{N}_2$  and  $\text{H}_2$  ambients. At high temperature ( $400\text{ }^\circ\text{C}$ ) all the atmospheres substantially decrease the CdS transmittance due to the presence of metallic Cd precipitate in the CdS grains. Still, transmittance of the air-annealed CdS remained unchanged due to transformation of metallic Cd to transparent  $\text{CdO}$  (Fig. 1a). Absorption of light in the longer wavelength region is usually caused by crystalline defects such as grain boundaries and dislocations [23].

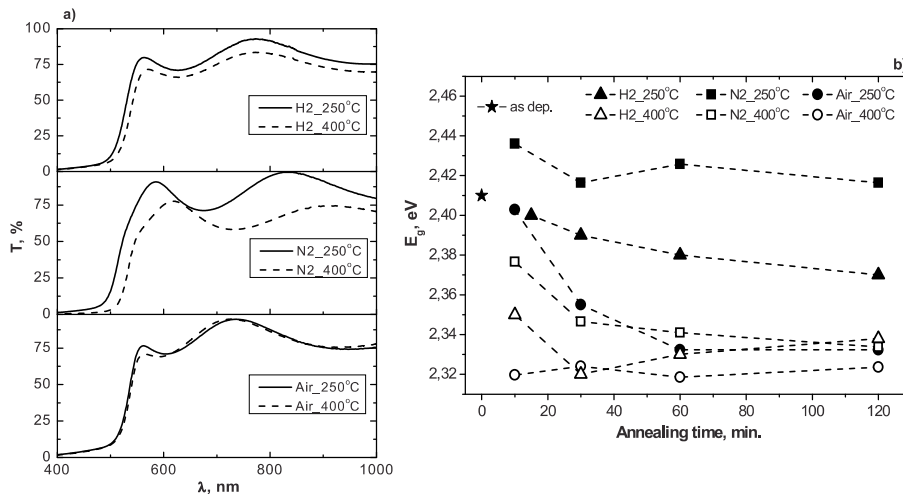


Fig. 3. (a) Transmittance spectra of CdS films annealed at different annealing time and ambient for 1h; (b) Band gap values of CdS films versus annealing time for different ambient and temperature.

Band gap ( $E_g$ ) of CdS films annealed in  $H_2$  and  $N_2$  at low temperature (250 °C) show small decrease with increasing annealing time (Fig. 3b), while for air- annealed CdS  $E_g$  decreased from 2.4 eV to 2.34 eV. Oxygen from the air ambient assured a higher presence of CdO [24] in CdS film, which decreased  $E_g$  already at 250 °C. At 400 °C  $E_g$  decreased faster, lowest value (2.32 eV) being reached for air- annealed CdS. This could be explained by the incorporation of oxygen on the vacant sulfur site appeared in the process of hydroxide group destruction in the CdS lattice. High concentration of oxygen in CdS lattice is also supported by the presence of  $CdSO_3$  and CdO phases for annealing in  $N_2$  and air (Fig. 1a).

### 3.3. Electrical properties

Time dependence of electrical resistivity measured at RT for CdS films shows stable electrical properties after 60 minutes annealing for each annealing temperature and ambient (Fig. 4a). At low annealing temperature the hydroxide group decomposes with formation of excess Cd and  $V_S$ .

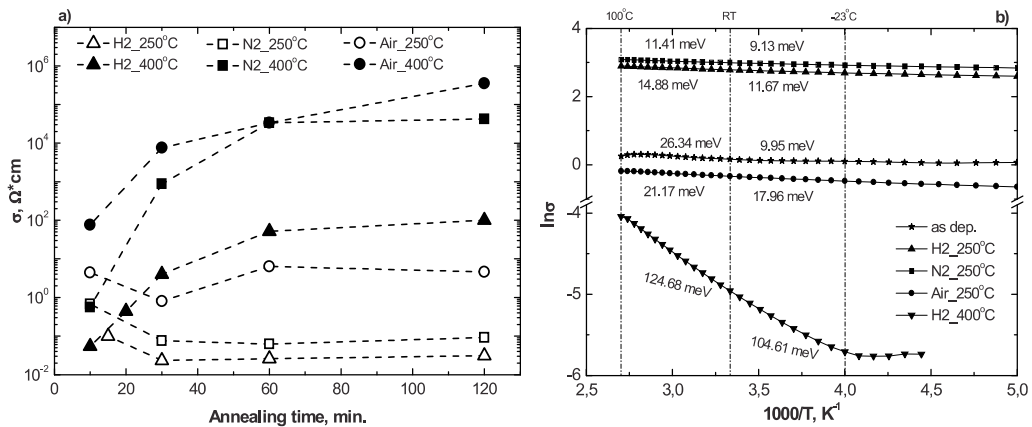


Fig. 4. (a) Electrical resistivity of CdS films at RT as a function of annealing time, temperature and atmosphere. (b) Time dependence of electrical conductivity and activation energy values for CdS films annealed for 1h in  $H_2$ ,  $N_2$  and air.

The high conductivity is controlled by the  $ClS^+$  and  $(OH)_S^+$  shallow donors [10] (considering annihilation of sulfur and cadmium vacancies) at ~9-30 meV under conduction band (Fig. 4b). At 250 °C the process stabilized in 30 minutes for  $N_2$  and  $H_2$  annealing. For air- annealed CdS resistance will be differently increased than for  $H_2$  and  $N_2$  due to incorporated oxygen on sulfur site and its reaction with Cd, forming CdO. Same processes with higher rate take place at annealing temperature 400 °C and significantly higher resistances are achieved in air and  $N_2$  annealing due to the background oxides in CdS (Fig. 1a). At 400 °C annealing, due to full destruction of hydroxide groups and out diffusion of chlorine, the concentration of electrons decreased [10] and CdS conductivity is determined by the deep donor defects at ~120 meV in the region of measurement temperatures 20 - 100 °C (Fig. 7).

The PL spectra (Fig. 5) for all samples consist of two prominent bands at approximately 1.7 eV and 2.24 eV. The 1.7 eV PL band was interpreted [25] in terms of commonly accepted neutral complex  $(V_{Cd}2Cl_S)^0$ . The sharp peak (2.24 eV) corresponds to the emission of donor – acceptor pairs due to the thermal dissociation (8) of the neutral complex to  $Cl_S^+$  donors and  $(V_{Cd}Cl_S)^-$  acceptors [26].



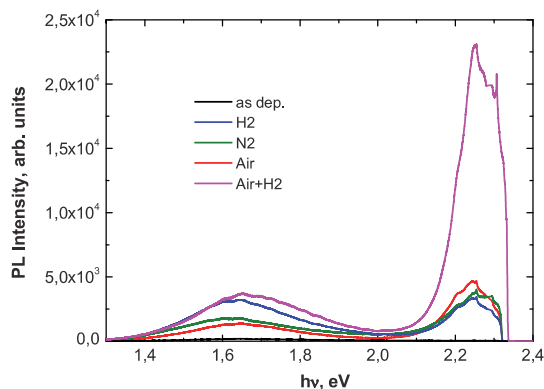


Fig. 5. Photoluminescence spectra of CdS films annealed for 2h in different atmospheres.

The unexpected high PL intensity of air-annealed CdS films is connected with the incorporation of oxygen on  $V_S$  and the spatial compensation of contraction in Cd sub-lattice by  $V_{Cd}$ . The oxygen should enhance formation of  $V_{Cd}$  and therefore to increase the intensity of both PL peaks. However, due to concentration quenching, lower intensity of the 1.7 eV peak (showing the neutral complex concentration) is observed. This explanation is confirmed by one order of magnitude increase of PL peak intensity for the air-annealed CdS film which was over-annealed in  $H_2$  (Fig. 5).

#### 4. Conclusions

Changes in structural, optical and electrical properties of CBD CdS layers in the annealing process are connected with decomposition of OH group incorporated in CdS lattice in the deposition process, with outdiffusion of  $H_2O$  and destruction of crystallites, and with creation of Cd excess resulting in transition from  $CdS_{1-x}(OH)_x$  to  $CdS_{1-y}O_y$  solid solution. Annealing in air and  $N_2$  creates stable  $CdS_{1-y}O_y$  solid solution while  $H_2$  annealing removes the oxides and chloride dopant resulting in pure CdS films. Excess of Cd as precipitate decreases the transmittance while incorporation of oxygen into CdS lattice decreases the band gap of the CdS film. The gained knowledge about influence of annealing conditions on the properties of CdS film will facilitate further investigations on CdS/absorber heterostructures for elaboration of high-quality solar cells.

#### Acknowledgements

This study was supported by European Social Fund's Doctoral Studies and Internationalization Program Dora, by the European Union through the 7th FP project FLEXSOLCELL (GA-2008-230861), by the European Regional Development Fund (Centre of Excellence "Mesosystems: Theory and Applications", TK114), by Estonian Science Foundation Grant ETF9142 and by Estonian Ministry of Education and Research through the program AR10128 and Target Financing projects SF0140092s08 and SF0140099s08.

#### References

- [1] Green MA, Emery K, Hishikawa Y, Warta W, Dunlop ED. Solar cell efficiency tables (version 41). *Prog. Photovoltaics* 2013; 21:1-11.
- [2] Vigil O, Zelaya-Angel O, Rodriguez Y. Changes of the structural and optical properties of cubic CdS films on annealing in  $H_2$  and air atmospheres. *Semicond Sci Technol* 2000; 15:259-262.
- [3] Metin H, Esen R. Annealing effects on optical and crystallographic properties of CBD grown CdS films. *Semicond Sci Technol* 2003; 18:647-654.

- [4] Jiang M, Tang K, Yan X. Characterization of intrinsic ZnO thin film deposited by sputtering and its effects on CIGS solar cells. *J Photonics Energy* 2012; 2:028502.
- [5] Chung Y-D, Cho D-H, Park N-M, Lee K-S, Kim J. Effect of annealing on CdS/CIGS thin-film solar cells. *Curr Appl Phys* 2011; 11:S65-S67.
- [6] Sakurai T, Ishida N, Ishizuka S, Islam MM, Kasai A, Matsubara K, Sakurai K, Yamada A, Akimoto K, Niki S. Effects of annealing under various atmospheres on electrical properties of CIGS heterostructures. *Thin Solid Films* 2008; 516:7036-7040.
- [7] Tomas SA, Vigil O, Alvarado-Gil JJ, Lozada-Morales R, Zelaya-Angel O, Vargas H, Ferreira da Silva A. Influence of thermal annealings in different atmospheres on the band-gap shift and resistivity of CdS thin films. *J Appl Phys* 1995; 78(4):2204-2207.
- [8] Mishra S, Ingale A, Roy UN, Gupta A. Study of annealing-induced changes in CdS thin films using X-ray diffraction and Raman spectroscopy. *Thin Solid Films* 2007; 516:91-98.
- [9] Haider AJ, Mousa AM, Al-Jawad SMH. Annealing effect on structural, electrical and optical properties of CdS films prepared by CBD method. *Semicond Sci Technol* 2008; 8(4):326-332.
- [10] Maticiuic N, Hiie J, Potlog T, Valdna V, Gavrilov A. Influence of annealing in H<sub>2</sub> atmosphere on the electrical properties of thin film CdS. *Mater Res Soc Symp Proc* 2012; 1324:69-74.
- [11] Lide DR, Frederikse HPR. Handbook of chemistry and physics. 78<sup>th</sup> ed. CRC Press: Boca Raton NY; 1997.
- [12] Maticiuic N, Potlog T, Hiie J, Mikli V, Poldne N, Raadik T, Valdna V, Mere A, Gavrilov A, Quinci F, Lughì V, Sergio V. Structural changes in chemically deposited CdS: effect of thermal annealing. *Moldavian Journal of the Physical Sciences* 2010; 9(3-4):275-279.
- [13] Wang J, Tang G, Wub XS, Gub M. Stable structure and effects of sulfur in CdTe/CdS heterojunctions. *Surf Interface Anal* 2012; 44:434-438.
- [14] Holloway H, McCarthy SL. *J Appl Phys* 1993; 73:103-111.
- [15] Loginova MB, Andreev JV. Melting diagrams of systems CdCl<sub>2</sub>-CdX. *Inorganic Materials* 1970; 6(10):1885-1886 (In Russian).
- [16] Kylner A. Effect of impurities in the CdS buffer layer on the performance of the CIGS thin film solar cell. *J Appl Phys* 1999; 85:533-540.
- [17] Senthil K, Mangalaraj D, Narayandass SK. Structural and optical properties of CdS thin films. *Appl Surf Sci* 2001; 169-170:476-479.
- [18] Briggs RJ, Ramdas AK. Piezospectroscopic study of the Raman spectrum of cadmium sulfide. *Phys Rev B* 1976; 13:5518-5529.
- [19] Jerominek H, Pigeon M, Patela S, Jakubczek Z, Delisle C, Tremblay R. CdS microcrystallites-doped thin-film glass waveguides. *J Appl Phys* 1988; 63:957-959.
- [20] Lee J-H. Influence of substrates on the structural and optical properties of chemically deposited CdS films. *Thin Solid Films* 2007; 515:6089-6093.
- [21] Srihari V, Sridharan V, Ravindran TR, Chandra S, Arora AK, Sastry VS, Sundar CS. Raman scattering of cadmium oxide: in B1 phase. *Proceedings of the 55th DAE Solid State Physics Symposium 2010* 2011; 1349:845-846.
- [22] Ashrafi A, Ostrikov K. Raman-active wurtzite CdO nanophase and phonon signatures in CdO/ZnO heterostructures fabricated by nonequilibrium laser plasma ablation and stress control. *Appl Phys Lett* 2011; 98:133119.
- [23] Choi J, Kim K-J, Yoo J-B, Kim D. Properties of cadmium sulfide thin films deposited by chemical bath deposition with ultrasonication. *Sol Energy* 1998; 64:41-47.
- [24] Dakhel AA. Electrical and optical properties of iron-doped CdO. *Thin Solid Films* 2010; 518:1712-1715.
- [25] Maticiuic N, Hiie J, Raadik T, Graf A, Gavrilov A. The role of Cl in the chemical bath on the properties of CdS thin films. *Thin Solid Films* 2013; 535:184-187.
- [26] Yen WM, Shionoya S, Yamamoto H. Phosphor Handbook. 2nd ed. CRC Press/Taylor: Boca Raton FL; 2007.

## **PAPER V**

**N. Maticiuc**, N. Spalatu, V. Mikli, J. Hiie, Impact of CdS annealing atmosphere on the performance of CdS–CdTe solar cell, *Appl. Surf. Sci.* 350 (2015) 14–18.





# Impact of CdS annealing atmosphere on the performance of CdS–CdTe solar cell

N. Maticiu<sup>\*</sup>, N. Spalatu, V. Mikli, J. Hiie

Tallinn University of Technology, Ehitajate tee 5, 19086 Tallinn, Estonia



## ARTICLE INFO

### Article history:

Received 31 October 2014

Accepted 22 January 2015

Available online 31 January 2015

### Keywords:

Chemical bath deposited CdS

Annealing of CdS film

Porous CdS film

CdS–CdTe solar cell

Oxychloride component

## ABSTRACT

CdS thin films obtained by chemical bath deposition and annealed in hydrogen and air ambients were combined with CdTe absorbers obtained by close spaced sublimation. CdS–CdTe solar cells in superstrate configuration were characterized by current–voltage and quantum efficiency measurements while the analysis of annealed CdS films was made by scanning electron microscopy, X-ray diffraction and UV–vis spectroscopy. It was found that in superstrate configuration, due to the big grains on CdS surface and gas emission from CdS film at high temperature deposition of the absorber, the delamination of layers take place. Annealing in H<sub>2</sub> removes the oxygen compounds from CdS grain boundaries and opens them for formation of shortcircuiting through the CdS layer. The processing in air is most advantageous due to simultaneous presence of chloride and oxygen, contributing to the recrystallization and sintering of the highly textured columnar CdS. The direct influence of the CdS annealing on the solar cell parameters is shown for CdS–CdTe solar cell.

© 2015 Elsevier B.V. All rights reserved.

## 1. Introduction

Cadmium sulfide (CdS) is a suitable n-type component for cadmium telluride (CdTe) based solar cell [1] due to its direct optical band gap ( $E_g$ ) (2.4 eV), high transparency (>80%) and the ease to prepare by different techniques [2,3]. For such application CdS film should be conductive, thin and uniform. High conductivity of CdS film increases the built-in potential in CdTe absorber which in turn improves the photovoltage of solar cell [4]. Thinning increases the transparency of CdS film and gains in short-circuit current while the uniformity of the film avoids the shorting effects between transparent conductive oxide and CdTe absorber [5].

In this context chemical bath deposition (CBD) is a proper technique to produce uniform, adherent and very thin CdS films with low cost and simplicity. Moreover, CBD CdS has high n-doping and low sheet resistance due to the high concentration of oxygen-containing impurities in the film [6]. However, the as deposited CBD CdS thin film usually forms the metastable cubic phase and has a poor crystallinity and an appropriate heat treatment is required to improve its properties. Also in a solar cell, by using the recrystallization step prior to CdCl<sub>2</sub> treatment, the diffusion of CdS into CdTe

absorber can be reduced by eliminating the diffusion pathways into absorber [7].

This annealing step of CBD CdS film was widely studied during the last years by different groups including ours in order to improve the CdS–CdTe solar cell parameters [8,9]. Beside the variation of annealing atmosphere, temperature or duration the multilayer approach for CBD CdS was studied in [9,10]. Our previous investigations showed that: (1) independent of the applied gas, the annealing results in the relaxation of CdS lattice and its transition from the metastable to stable cubic structure [11,12]; (2) CdS film annealed in oxidizing atmosphere have better crystallinity with smoother surface, but the  $E_g$  is decreased and the film contains additional phases such as CdO [8,12,13]; (3) the reducing atmosphere removes the oxides and chloride dopants from CdS film while the Cd precipitate decreases the optical parameters of the film [13]. Because each annealing atmosphere brings both positive and negative effects to CdS properties, researchers in this field have diverse opinions about the suitable annealing of CdS for application in CdTe solar cell [9,14]. Therefore, a better understanding of the influence of annealed CdS film on the properties CdS–CdTe solar cell is still needed.

In the present work we use annealed CdS films studied previously [12,13,15,16] to prepare CdTe based solar cell and illustrate the direct influence of the CdS annealing on the final parameters of CdS–CdTe solar cell in a superstrate configuration. The chemical processes responsible for the induced changes are discussed.

<sup>\*</sup> Corresponding author. Tel.: +372 620 3366; fax: +372 620 2020.  
E-mail address: [nataliamaticiu@yahoo.com](mailto:nataliamaticiu@yahoo.com) (N. Maticiu).

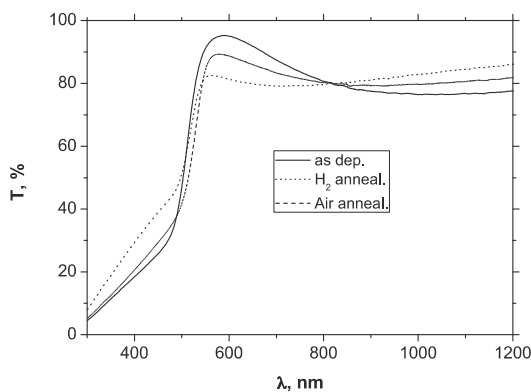


Fig. 1. Transmittance spectra of as deposited and annealed CdS films.

## 2. Experiment

Polycrystalline CdS films of 150–180 nm thickness were deposited by CBD on glass substrates coated with a 300 nm thick fluorine doped tin oxide (FTO) layer. The details of the deposition process are presented elsewhere [13]. After deposition and drying in vacuum at 120 °C CdS films were annealed for 1 h at 400 °C in two different atmospheres: hydrogen and air. With all CdS films complete CdS–CdTe solar cell devices were fabricated. A CdTe layer of 3–4 μm thickness was deposited by close space sublimation (CSS) at source and substrate temperatures of 610 °C and 500 °C respectively. This was followed by a soaking in CdCl<sub>2</sub> solution, air treatment at 420 °C, NP etching and deposition of gold back contact by evaporation. Finally the 2 cm × 2 cm samples were scribed into cells of 5 mm × 5 mm dimension.

The deposited CdS thin films were characterized by X-ray diffraction (XRD), scanning electron microscopy (SEM) and optical transmission spectra. XRD measurements were performed on a Rigaku Ultima IV diffractometer with Cu Kα radiation ( $\lambda = 1.5406 \text{ \AA}$ , 40 kV at 40 mA) using the silicon strip detector D/teX Ultra. Crystallite size and lattice constants were calculated using the software on the Rigaku's system (PDXL Version 1.4.0.3). The crystallite size was calculated using the Debye–Scherrer method and a Scherrer's constant of 0.94. The optical total transmittance and reflectance spectra of CdS films were measured in the wavelength range of 200–2500 nm on a Jasco V-670 UV–VIS–NIR spectrophotometer equipped with an integrating sphere. The  $E_g$  of the films was obtained from the absorption coefficient spectra calculated using the Bragg formula. Surface morphology of CdS films and the cross-section of CdS–CdTe solar cell were examined by high-resolution SEM apparatus (Zeiss EVO-MA15) at an operating voltage of 10 kV. The performance of CdS–CdTe solar cells were characterized by  $J$ – $V$  curves and quantum efficiency (QE) measurements under AM1.5 (100 mW/cm<sup>2</sup>) illumination.

## 3. Results and discussion

### 3.1. CBD CdS films

In the process of H<sub>2</sub> annealing the incorporated OH group decomposed with formation of CdO and Cd precipitate [12], leaving a relaxed crystalline lattice of CdS (Table 1). The metallic Cd, observed on the walls of annealing quartz tube, decreased the transparency of CdS film in the wavelength region of 500–800 nm (Fig. 1). The  $E_g$  gap was slowly decreased if compared to as deposited CdS (Table 1) and XRD spectra revealed a singular CdS phase oriented

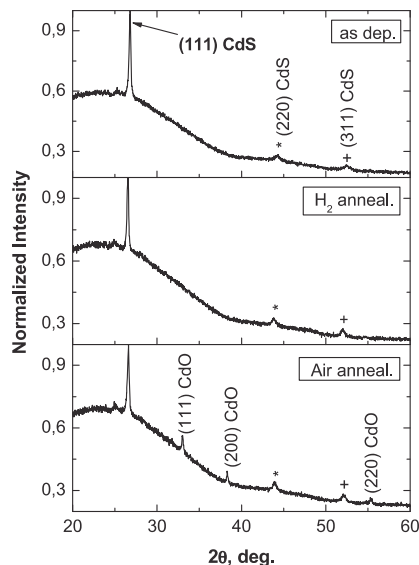


Fig. 2. XRD spectra of as deposited and annealed CdS films.

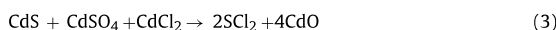
along the (1 1 1) direction (Fig. 2). It seems that H<sub>2</sub> annealing can be considered the appropriate thermal treatment for removal of impurities and for destruction of hydroxide components incorporated during the deposition of CdS film. However, because H<sub>2</sub> also removes the oxygen compounds from CdS grain boundaries leaving them opened, shortcircuiting are formed through the CdS layer.

Air annealed CdS film are described by a sharpened absorption edge and increased transmittance in the range of 500–800 nm compared to H<sub>2</sub> annealed film (Fig. 1). On the other side the  $E_g$  is decreased much more than for as deposited film (Table 1) and additional oxygen-containing phases like CdSO<sub>4</sub> [12,17] and CdO are revealed by the XRD analysis (Fig. 2). The oxide-producing reaction between chloride, oxygen and CdS was proposed by McCandless in [18]:



CdO presence may be convenient because it is expected to behave as a barrier to subsequent reaction and diffusion of Te and Cl species from the CdTe layer into the CdS window material. As an insulating oxide, CdO can also electrically passivate grain boundaries and surfaces [18].

CdSO<sub>4</sub> also is an active component as oxygen (2) and interacts with CdS and CdCl<sub>2</sub> with formation of sulfur pieces (3, 4) which will contribute to the mass transfer of CdS.



Our previous results showed that varying the annealing atmosphere and temperature up to 400 °C did not change the morphology of CdS films [12,13]. Here the surface view of CdS films was registered after CdTe deposition and CdCl<sub>2</sub> treatment (Fig. 3).

In the case of air annealing the presence of oxygen, as CdO and CdSO<sub>4</sub>, together with co-deposited chloride improved the recrystallization of CdS film, increasing the grain size. Romeo et al. [19] also observed a big change in the shape and size of the CdS grains after the recrystallization treatment of CdTe. Our CdS film became

**Table 1**  
Thickness,  $E_g$ , lattice constant, interplanar distance and grain size of CdS films after deposition and after annealing in hydrogen and air. Grain size of the films is estimated after the deposition of CdTe.

CdS film	Thickness (nm)	$E_g$ (eV)	Lattice constant (Å)	Interplanar distance (Å)	Grain size (nm)
As dep.	155.0	2.43	5.758	3.324	65.0
H <sub>2</sub> anneal.	175.0	2.37	5.824	3.354	75.0
Air anneal.	178.0	2.32	5.807	3.346	180.0

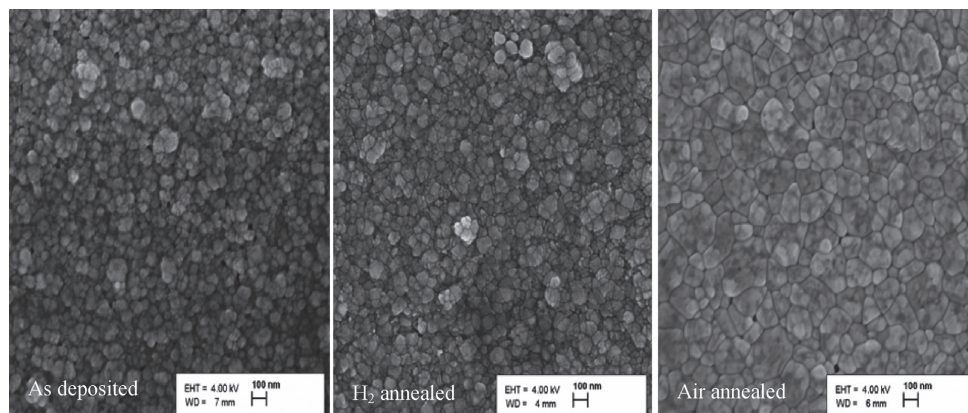


**Fig. 3.** SEM pictures of as deposited and annealed CdS films after the deposition and oxychloride treatment of CdTe.

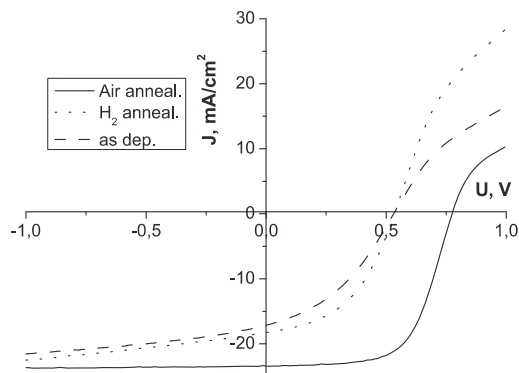


**Fig. 4.**  $J$ - $V$  characteristics of CdS-CdTe solar cells with as deposited and annealed CdS films.

porous (Fig. 3) due to the thermal shock during the preparation of absorber and short-cutting paths were formed between CdTe absorber and FTO. In order to evaluate the net influence of the annealed CdS film on the solar cell, the structures were sectioned into 5 mm<sup>2</sup> regions.

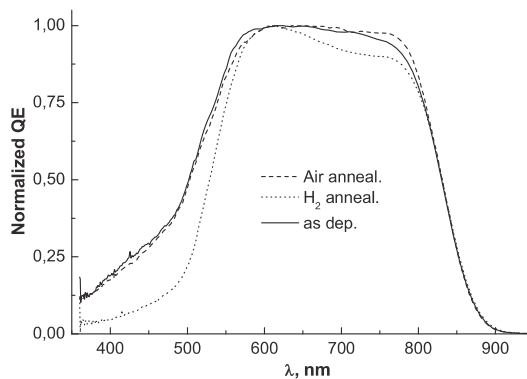
### 3.2. CdS-CdTe solar cells

Fig. 4 shows the  $J$ - $V$  characteristics of CdS-CdTe solar cells with different CdS films: as deposited CdS, H<sub>2</sub> annealed CdS and air

**Table 2**  
Performances of CdS-CdTe solar cells with as deposited and annealed CdS films.

CdS film in solar cell	$V_{oc}$ (V)	$J_{sc}$ (mA/cm <sup>2</sup> )	FF (%)	Eff. (%)
As dep.	525.7	17.7	39.1	3.6
H <sub>2</sub> anneal.	535.7	18.2	46.4	4.5
Air anneal.	777.4	23.4	62.7	11.4

annealed CdS. The photoelectric performance of these solar cells is shown in Table 2. The performance of the solar cell with CdS film annealed in air is higher than the other two. An important reason of this improvement might be attributed to the oxides which reside on grain surfaces and penetrate grain boundaries of CdS [18] making the film more stable for the following oxychloride treatment of CdS-CdTe solar cell at 420 °C (Table 2, Fig. 4). Solar cell with CdS annealed in H<sub>2</sub> show lower parameters (Table 2) due to smaller grain size of CdS film which implies a faster interdiffusion at the interface after the CdCl<sub>2</sub> treatment compared to the cell with air annealed CdS [7,11]. This interdiffusion appears to be determined by the oxygen level in the CdS. When low-oxygen-containing CdS films are used, sulfur diffusion is substantial, leading to significant consumption of the CdS layer. When these same films are annealed in oxygen, the consumption is reduced. Te diffusion into the CdS layer also appears to be reduced by oxygen present in the CdS [20]. Another reducing factor could be the metallic precipitate in CdS film after H<sub>2</sub> annealing [13] which beside lower transmittance of



**Fig. 5.** QE spectra of CdS-CdTe solar cells with as deposited and annealed CdS films.

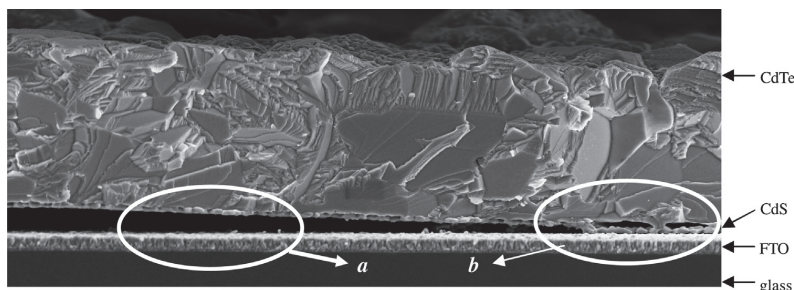


Fig. 6. Cross section of a “bad contact” region of a CdS–CdTe solar cell; the peeling *a* – between FTO and CdS, the peeling *b* – between CdS and CdTe.

the film (Fig. 1, Table 1) decreases the spectral response of the solar cell (Fig. 5).

We have obtained similar performance for CdTe solar cell [21] with CSS CdS films of a much higher quality in terms of larger grains and no porosity compared to CBD CdS. This indicates to the importance of oxygen presence namely in the place of junction formation. It seems that the oxychloride components have to be closer to the junction and the air annealing of CdS looks to be a solution as it brings the oxygen and incorporated chlorine from CdS to the place of junction formation. These components accelerate the mass transfer between the polycrystalline phases of CdS and CdTe with formation of an effective CdS–CdTe heterojunction. In other words, the CdCl<sub>2</sub> treatment in air at 420 °C applied to CdTe absorber at the back contact side does not assure a sufficient penetration of oxychloride components through CdTe layer at the place of junction formation.

The only issue of the air annealed CdS remains the uniformity of the film which after the thermal treatment becomes porous (Fig. 3). Besides the porosity of CdS films, two types of peeling were observed from the cross section view of solar cells (Fig. 6). We assume that the peeling from CdS (*b*) was caused by the undesired big grains on the surface of CdS film (Fig. 1), while the origin of the “*a*” peeling, generated only in the case of H<sub>2</sub> annealed CdS, may be caused by the penetration of the oxychloride flux through CdS porous regions.

#### 4. Conclusions

The performance of CdS–CdTe solar cell was studied for different annealing of CBD CdS films. CdS annealing in H<sub>2</sub> removes the oxygen compounds from the grain boundaries and opens them for formation of shortcircuiting through the CdS layer. The presence of CdO in the air annealed CdS showed by XRD analysis is considered benefic as it behaves as a barrier to subsequent interdiffusion between CdS and CdTe. The processing in air is most advantageous due to simultaneous presence of chloride and oxygen, contributing to the recrystallization and sintering of the highly textured columnar CBD CdS. The oxychloride components are needed at the both sides of CdTe absorber to assure the formation of an effective CdS–CdTe junction.

An issue to solve remains the porosity of annealed CBD CdS film which intensifies during the deposition of CdTe absorber and the thermal treatment in CdCl<sub>2</sub>.

#### Acknowledgements

This study was supported by European Regional Development Fund TK114 “Mesosystems: Theory and Applications”

(3.2.0101.11-0029), European Social Fund’s Doctoral Studies and Internationalization Program Dora 5 and 8, European Union through 7th FP project FLEXSOLCELL (GA-2008-230861), Estonian Science Foundation Grant ETF9142 and Estonian Ministry of Education and Research (IUT19-4).

#### References

- X. Wu, J.C. Keane, R.G. Dhere, C. DeHart, D.S. Albin, A. Duda, T.A. Gessert, S. Asher, D.H. Levi, P. Sheldon, 16.5% efficient CdS/CdTe polycrystalline thin-film solar cells, in: Proceedings of the 17th European PVSEC, 22–26 October, Munich, Germany, 2001, p. 995.
- J. Hiie, T. Dedova, V. Valdna, K. Muska, Comparative study of nano-structured CdS thin films prepared by CBD and spray pyrolysis: annealing effect, *Thin Films* 511–512 (2006) 443–447.
- C.S. Ferekides, D. Marinsky, V. Viswanathan, B. Tetali, V. Palekis, P. Selvaraj, D.L. Morel, High efficiency CSS CdTe solar cells, *Thin Solid Films* 361–362 (2000) 520–526.
- J. Fritsche, D. Kraft, A. Thißen, T. Mayer, A. Klein, W. Jaegermann, Band energy diagram of CdTe thin film solar cells, *Thin Solid Films* 403–404 (2002) 252–257.
- B.E. McCandless, K.D. Dobson, Processing options for CdTe thin film solar cells, *Sol. Energy* 77 (2004) 839–856.
- X. Wu, Y. Yan, R.G. Dhere, Y. Zhang, J. Zhou, C. Perkins, B. To, Nanostructured CdS:O film: preparation, properties, and application, *Phys. Status Solidi (c)* 1 (4) (2004) 1062–1066.
- B.E. McCandless, B.W. Birkmire, CdTe<sub>1-x</sub>S<sub>x</sub> absorber layers for thin-film CdTe/CdS solar cells, in: Proceedings of the 26th PVSEC, 30 September–3 October, Anaheim CA, USA, 1997, p. 307.
- S.A. Tomas, O. Vigil, J.J. Alvarado-Gil, R. Lozada-Morales, O. Zelaya-Angel, H. Vargas, A. Ferreira da Silva, Influence of thermal annealings in different atmospheres on the bandgap shift and resistivity of CdS thin films, *J. Appl. Phys.* 78 (4) (1995) 2204–2207.
- J. Han, C. Spanheimer, G. Haindl, G. Fu, V. Krishnakumar, J. Schaffner, C. Fan, K. Zhao, A. Klein, W. Jaegermann, Optimized chemical bath deposited CdS layers for the improvement of CdTe solar cells, *Sol. Energy Mater. Sol. Cells* 95 (2011) 816–820.
- M.E. Calixto, M. Tufiño-Velázquez, G. Contreras-Puente, O. Vigil-Galán, M. Jiménez-Escamilla, R. Mendoza-Perez, J. Sastré-Hernández, A. Morales-Acevedo, Study of chemical bath deposited CdS bi-layers and their performance in CdS/CdTe solar cell applications, *Thin Solid Films* 516 (2008) 7004–7007.
- J. Han, C. Liao, T. Jiang, G. Fu, V. Krishnakumar, C. Spanheimer, G. Haindl, K. Zhao, A. Klein, W. Jaegermann, Annealing effects on the chemical deposited CdS films and the electrical properties of CdS/CdTe solar cells, *Mater. Res. Bull.* 46 (2011) 194–198.
- N. Maticiuc, M. Kukk, N. Spalatu, T. Potlog, M. Krunks, V. Valdna, J. Hiie, Comparative study of CdS films annealed in neutral, oxidizing and reducing atmospheres, *Energy Procedia* 44 (2014) 77–84.
- N. Maticiuc, J. Hiie, V. Mikli, T. Potlog, V. Valdna, Structural and optical properties of cadmium sulfide thin films modified by hydrogen annealing, *Mater. Sci. Semicond. Process.* 26 (2014) 169–174.
- H. Kim, D. Kim, Influence of CdS heat treatment on the microstructure of CdS and the performance of CdS/CdTe solar cells, *Sol. Energy Mater. Sol. Cells* 67 (1–4) (2001) 297–304.
- N. Maticiuc, J. Hiie, T. Raadik, A. Graf, A. Gavrilo, The role of Cl in the chemical bath on the properties of CdS thin films, *Thin Solid Films* 535 (2013) 184–187.
- N. Maticiuc, J. Hiie, Annealing effect on CdS films: transition from glass to ITO, *IOP Conf. Ser.: Mater. Sci. Eng.* 49 (2013) 012061.
- W.J. Danaher, L.E. Lyons, G.C. Morris, Some properties of thin films of chemically deposited cadmium sulphide, *Sol. Energy Mater.* 12 (1985) 137–148.
- B.E. McCandless, R.W. Birkmire, Influence of window and absorber layer processing on device operation in superstrate thin film CdTe solar cells, in: Proceedings of the 28th IEEE Photovoltaic Specialists Conference, New York, USA, 2000, p. 491.

- [19] A. Romeo, D.L. Batzner, H. Zogg, C. Vignali, A.N. Tiwari, Influence of CdS growth process on structural and photovoltaic properties of CdTe/CdS solar cells, *Sol. Energy. Mater. Sol. Cells* 67 (2001) 311–321.
- [20] D.S. Albin, Y. Yan, M.M. Al-Jassim, The effect of oxygen on interface microstructure evolution in CdS/CdTe solar cells, *Prog. Photovolt.: Res. Appl.* 10 (2002) 309–322.
- [21] N. Spalatu, J. Hiie, V. Valdna, M. Krunka, M. Caraman, V. Mikli, N. Maticiuc, Effect of CdCl<sub>2</sub> vapor phase pretreatment annealing on the properties of CSS CdS and CdTe/CdS thin film solar cells, *Thin Solid Films* (2014), <http://dx.doi.org/10.1016/j.tsf.2014.11.066> (in press).



**CURRICULUM VITAE**

## 1. Personal data

Name: Natalia Maticiuc  
 Date and place of birth: 11.09.1986  
 E-mail address: [natalia.maticiuc@ttu.ee](mailto:natalia.maticiuc@ttu.ee)

## 2. Education

Educational institution	Graduation year	Education (field of study/degree)
“M. Sadoveanu” Gymnasium, Cantemir, Moldova	2004	Secondary education
Faculty of Physics and Engineering, Moldova State University, Chişinău	2008	Physics and Informatics/Bachelor degree
Faculty of Physics and Engineering, Moldova State University, Chişinău	2010	Theoretical Physics/Master degree

## 3. Language competence/skills

Language	Level
Romanian	Native
English	Fluent
Russian	Fluent
French	Average
Estonian	Basic skills

## 4. Special courses

Period	Educational or other organisation
2011–2014	Graduate school „Functional materials and technologies FMTDK“, Tallinn University of Technology, Estonia

13 May 2012	Workshop of E-MRS 2012 Spring Meeting: “Young Scientist Tutorial on Characterization Techniques for Thin-Film Solar Cells”, Strasbourg, France
9-16 September 2012	International Summer School on Photovoltaics and New Concepts of Quantum Solar Energy Conversion (Quantsol), Hirschegg, Austria
10 December 2012	FMTDK Winter School, Rakvere, Estonia
7 - 9 June 2013	Nordic Summer School on Semiconductor Physics, Nauvo, Finland
26 - 27 June 2013	FMTDK Summer School, Pühajärve, Estonia
5 - 9 August 2013	7th International Summer School “New Frontiers in Optical Technologies”, Tampere, Finland

#### 5. Professional employment

Period	Organisation	Position
2006 - 2010	“G. Calinescu” high school, Chişinău, Moldova	Teacher
2010 - 2011	Moldova State University, Chişinău, Moldova	Lector
2008 - 2010	Moldova State University, Chişinău, Moldova	Analyst
2013 - ...	Department of Material Science, Tallinn University of Technology	Engineer

#### 6. Research activity, including honors and thesis supervised

##### Projects

01.01.2008 – 31.12.2013	Thin film and nanostructured materials by chemical methods (SF 2008);
01.10.2009 – 30.09.2013	Development of flexible single and tandem II-VI based high efficiency thin film solar cells, FLEXCOLCELL (International agreement, FP7);
01.01.2012 – 31.12.2015	Absorber layers by chemical spray pyrolysis for nanostructured solar cells (ETF 2012);

01.01.2012 – 31.12.2015	Thin film solar cells on the basis of chalcogenide layers deposited from water solution (ETF 2012);
01.07.2012 – 31.12.2015	Efficient plasmonic absorbers for solar cells (National R&D program „Materials technology“);
01.01.2014 – 31.12.2019	Thin films and nanomaterials by wet-chemical methods for next-generation photovoltaics (IUT 2014).

### **Awards**

2014	Gala of the students originally from Moldova, 27.12.2014, Chisinau, Moldova, Diploma;
2011	The 15th International Conference "Inventica", 08.06-10.06.201, Iasi, Romania, Diploma of Honor (co-author);
2011	European Exhibition of Creativity and Innovation, 14.05.2011, Iasi, Romania, Gold medal (co-author);
2010	CAS Conference 2010, organized by IEEE, 13.10-15.10.2010, Sinaia, Romania, Best Student Paper;
2009	Moldova's best students contest of the 2009-2010 year, 15.12.2009, Chisinau, Moldova, The Merit Scholarship – 2nd grade.

### **Defended dissertations**

2010 Obtaining and physical properties study of CBD CdS thin films, master's thesis (Moldova State University), supervisors: Associate Professor, Dr. Tamara Potlog, Dr. Jaan Hiie;

2008 Influence of the back contact on the photovoltaic parameters of CdTe-based solar cell, bachelor's thesis (Moldova State University), supervisor: Associate Professor, Dr. Tamara Potlog.

## LIST OF PUBLICATIONS

1. **N. Maticiuc**, N. Spalatu, V. Mikli, J. Hiie, Impact of CdS annealing atmosphere on the performance of CdS–CdTe solar cell, *Appl. Surf. Sci.* 350 (2015) 14-18.
2. N. Spalatu, J. Hiie, **N. Maticiuc**, M. Krunks, A. Katerski, V. Mikli, I. Sildos, Plasmonic effect of spray-deposited Au nanoparticles on the performance of CSS CdS/CdTe solar cells, *Appl. Surf. Sci.* 350 (2015) 69-73.
3. A. Graf, **N. Maticiuc**, N. Spalatu, V. Mikli, A. Mere, A. Gavrilov, J. Hiie, Electrical characterization of annealed chemical bath-deposited CdS films and their application in superstrate configuration CdTe/CdS solar cells, *Thin Solid Films* 582 (2015) 351-355.
4. N. Spalatu, J. Hiie, V. Mikli, M. Krunks, V. Valdna, **N. Maticiuc**, et al., Effect of CdCl<sub>2</sub> annealing treatment on structural and optoelectronic properties of close spaced sublimation CdTe/CdS thin film solar cells vs deposition conditions, *Thin Solid Films* 582 (2015) 128-133.
5. **N. Maticiuc**, J. Hiie, V. Mikli, T. Potlog, V. Valdna, Structural and optical properties of cadmium sulfide thin films modified by hydrogen annealing, *Mater. Sci. Semicond. Process.* 26 (2014) 169-174.
6. **N. Maticiuc**, M. Kukk, N. Spalatu, T. Potlog, M. Krunks, V. Valdna, J. Hiie, Comparative study of CdS films annealed in neutral, oxidizing and reducing atmospheres, *Energy Procedia* 44 (2014) 77-84.
7. **N. Maticiuc**, N. Spalatu, A. Katerski, J. Hiie, V. Mikli, M. Krunks, et al., Plasmonic modification of CdTe thin films by gold nanoparticles: Methods, difficulties and solutions, *Microelectron. Eng.* 126 (2014) 173-178.
8. N. Spalatu, J. Hiie, V. Valdna, M. Caraman, **N. Maticiuc**, V. Mikli, et al., Properties of the CdCl<sub>2</sub> air-annealed CSS CdTe thin films, *Energy Procedia* 44 (2014) 85-95.
9. **N. Maticiuc**, J. Hiie, Annealing effect on CdS films: transition from glass to ITO, *IOP Conf. Ser.: Mater. Sci. Eng.* 49 (2013) 012061.
10. **N. Maticiuc**, J. Hiie, T. Raadik, A. Graf, A. Gavrilov, The role of Cl in the chemical bath on the properties of CdS thin films, *Thin Solid Films* 535 (2013) 184-187.
11. **N. Maticiuc**, J. Hiie, T. Potlog, Influence of technological conditions on the properties of CBD CdS layers. In: *Proceedings of the International semiconductor conference (CAS 2012): 2012 Oct 15-17; Sinaia, Romania*. Bucharest: I.E.E.E. Press 2012 (187-190).
12. T. Potlog, **N. Maticiuc**, A. Mirzac, P. Dumitriu, D. Scortescu, Structural and optical properties of ZnTe thin films. In: *Proceedings of the International semiconductor conference (CAS 2012): 2012 Oct 15-17; Sinaia, Romania*. Bucharest: I.E.E.E. Press 2012 (321-324).
13. T. Potlog, N. Spalatu, **N. Maticiuc**, J. Hiie, V. Valdna, V. Mikli, A. Mere, Structural reproducibility of CdTe thin films deposited on different substrates by close space sublimation method, *Phys. Status Solidi A* 209 (2012) 272-276.
14. **N. Maticiuc**, J. Hiie, T. Potlog, V. Valdna, A. Gavrilov, Influence of annealing in H<sub>2</sub> atmosphere on the electrical properties of thin film CdS, *Mater. Res. Soc. Symp. Proc.* 1324 (2012) 69-73.
15. **N. Maticiuc**, V. Nicorici, N. Spalatu, D. Scortescu, T. Potlog, J. Hiie, et al., Electrical properties of thermally annealed CdS thin films obtained by

- chemical bath deposition. In: *Proceedings of the International semiconductor conference (CAS 2011)*: 2011 Oct 11-13; Sinaia, Romania. Bucharest: I.E.E.E. Press 2011 (455-458).
16. T. Potlog, N. Spalatu, V. Fedorov, **N. Maticiuc**, C. Antoniu, J. Hiie, et al., The performance of thin film solar cells employing photovoltaic ZnSe/CdTe, CdS/CdTe and ZnTe/CdTe heterojunctions. In: *Proceedings of the 37th IEEE: Photovoltaic Specialists Conference (PVSC)*: 2011 Jun 19-24; Seattle, USA (001365-001370).
  17. **N. Maticiuc**, T. Potlog, J. Hiie, V. Mikli, N. Poldme, T. Raadik, et al., Structural changes in chemically deposited CdS: effect of thermal annealing, *Moldavian Journal of the Physical Sciences* 9 (2010) 275-279.
  18. **N. Maticiuc**, T. Potlog, N. Spalatu, Optical properties of CdS thin films deposited by close space sublimation. In: *Proceedings of International Semiconductor Conference (CAS 2010)*: 2010 Oct 11-13; Sinaia, Romania. Bucharest: I.E.E.E. Press 2010 (537-540).
  19. T. Potlog V. Botnariuc L. Gorceac N. Spalatu, **N. Maticiuc**, S. Raievschi, The characterization of the CdS-based solar cell heterojunctions. In: *Proceedings of International Semiconductor Conference (CAS 2010)*: 2010 Oct 11-13; Sinaia, Romania. Bucharest: I.E.E.E. Press 2010 (105 – 108).

## ELULOOKIRJELDUS

### 1. Isikuandmed

Ees- ja perekonnanimi: Natalia Maticiuc  
Sünniaeg ja -koht: 11.09.1986, Cantemir, Moldova  
Kodakondsus: Moldova  
E-posti aadress: [natalia.maticiuc@ttu.ee](mailto:natalia.maticiuc@ttu.ee)

### 2. Hariduskäik

Õppeasutus (nimetus lõpetamise ajal)	Lõpetamise aeg	Haridus (eriala/kraad)
“M. Sadoveanu” Gümnaasium, Cantemir, Moldova	2004	Keskharidus
Füüsika ja Tehnika Teaduskonna, Moldova Riigi Ülikool	2008	Füüsika ja informaatika / Bakalaureusekraad
Füüsika ja Tehnika Teaduskonna, Moldova Riigi Ülikool	2010	Teoreetiline füüsika /Magistrikraad

### 3. Keelteoskus

Keel	Tase
Rumeenia	Emakeel
Inglise	Kõrgtase
Vene	Kõrgtase
Prantsuse	Keskstase
Eesti	Algtase

### 4. Täiendusõpe

Õppimise aeg	Täiendusõppe korraldaja nimetus
2011–2014	TÜ ja TTÜ doktorikool „Funktsionaalsed materjalid ja tehnoloogiad” (FMTDK), Eesti
13 Mai 2012	Workshop of E-MRS 2012 Spring Meeting: “Young Scientist Tutorial on Characterization Techniques for Thin-Film Solar Cells”, Strasbourg, Prantsusmaa

9-16 September 2012	International Summer School on Photovoltaics and New Concepts of Quantum Solar Energy Conversion (Quantsol), Hirschegg, Austria
10 Detsember 2012	FMTDK Talvekool, Rakvere, Eesti
7-9 Juuni 2013	Nordic Summer School on Semiconductor Physics, Nauvo, Soome
26-27 Juuni 2013	FMTDK Suvekool, Pühajärve, Eesti
5-9 August 2013	7th Rahvusvaheline Suvekool "New Frontiers in Optical Technologies", Tampere, Soome

#### 5. Teenistuskäik

Töötamise aeg	Tööandja nimetus	Ametikoht
2006 – 2010	"G. Calinescu" Gümnaasium, Moldova	Õpetaja
2010 – 2011	Moldova Riigi Ülikool	Lektor
2008 – 2010	Moldova Riigi Ülikool	Analüütik
2013 - ...	Tallinna Tehnikaülikool, Keemia ja materjaliteaduse instituut	Insener

#### 6. Teadustegevus, sh tunnustused ja juhendatud lõputööd

##### Projektid

01.01.2008 – 31.12.2013	Õhukesekilelised ja nanostruktuursed materjalid keemilistel meetoditel (SF 2008);
01.10.2009 – 30.09.2013	Kõrge kasuteguriga õhukesekileliste elastsete mono- ja tandem-päikesepatareide arendamine II-VI pooljuhtühendite baasil, FLEXCOLCELL (Välisleping, VII raamprogramm);
01.01.2012 – 31.12.2015	Absorberkihid keemilise pihustuspürolüüsi meetodil nanostruktuursetele päikesepatareidele (ETF 2012);
01.07.2012 – 31.12.2015	Efektiivsed plasmoonilised absorberid päikesepatareidele (Riiklik T&A programm "Materjalitehnoloogia");
01.01.2014 – 31.12.2019	Õhukesed kiled ja nanomaterjalid keemilistel vedeliksadestusmeetoditel uue põlvkonna fotovoltseadistele (IUT 2014).

## Tunnustused

- 2014 Diplom, Moldovast pärit tudengite gala, Chisinau (Moldova), 27. detsember 2014;
- 2011 Austamise Diplom, XV rahvusvaheline konverents "Inventica", Iasi (Rumeenia) 8-10 juuni 2011 (kaasautor);
- 2011 Kuldmedal, Euroopa Näitus loovuse ja innovatsiooni, Iasi (Rumeenia), 14. mai 2011 (kaasautor);
- 2010 Parim õpilane raamatut CAS konverentsi 2010, korraldas IEEE, Sinaia (Rumeenia), 13-15 Oktoober 2010;
- 2009 Merit stipendium - teise klassi, kell Moldova parimad õpilased võistlus 2009-2010 aasta.

## Kaitstud lõputööd

2010 Õhukeste kaadmiumsulfiidi kilede valmistamine keemilise vannsadestuse meetodil ja füüsikaliste omaduste uurimine, magistritöö (Moldova Riiklik Ülikool), juhendajad: Dotsent Tamara Potlog, Dr. Jaan Hiie;

2008 Tagakontakti mõju CdTe päikesepatarei fotoelektrilistele parameetritele, bakalaureusetöö (Moldova Riiklik Ülikool), juhendaja: Dotsent Tamara Potlog.

**DISSERTATIONS DEFENDED AT  
TALLINN UNIVERSITY OF TECHNOLOGY ON  
NATURAL AND EXACT SCIENCES**

1. **Olav Kongas**. Nonlinear Dynamics in Modeling Cardiac Arrhythmias. 1998.
2. **Kalju Vanatalu**. Optimization of Processes of Microbial Biosynthesis of Isotopically Labeled Biomolecules and Their Complexes. 1999.
3. **Ahto Buldas**. An Algebraic Approach to the Structure of Graphs. 1999.
4. **Monika Drews**. A Metabolic Study of Insect Cells in Batch and Continuous Culture: Application of Chemostat and Turbidostat to the Production of Recombinant Proteins. 1999.
5. **Eola Valdre**. Endothelial-Specific Regulation of Vessel Formation: Role of Receptor Tyrosine Kinases. 2000.
6. **Kalju Lott**. Doping and Defect Thermodynamic Equilibrium in ZnS. 2000.
7. **Reet Koljak**. Novel Fatty Acid Dioxygenases from the Corals *Plexaura homomalla* and *Gersemia fruticosa*. 2001.
8. **Anne Paju**. Asymmetric oxidation of Prochiral and Racemic Ketones by Using Sharpless Catalyst. 2001.
9. **Marko Vendelin**. Cardiac Mechanoenergetics *in silico*. 2001.
10. **Pearu Peterson**. Multi-Soliton Interactions and the Inverse Problem of Wave Crest. 2001.
11. **Anne Menert**. Microcalorimetry of Anaerobic Digestion. 2001.
12. **Toomas Tiivel**. The Role of the Mitochondrial Outer Membrane in *in vivo* Regulation of Respiration in Normal Heart and Skeletal Muscle Cell. 2002.
13. **Olle Hints**. Ordovician Scolecodonts of Estonia and Neighbouring Areas: Taxonomy, Distribution, Palaeoecology, and Application. 2002.
14. **Jaak Nõlvak**. Chitinozoan Biostratigraphy in the Ordovician of Baltoscandia. 2002.
15. **Liivi Kluge**. On Algebraic Structure of Pre-Operad. 2002.
16. **Jaanus Lass**. Biosignal Interpretation: Study of Cardiac Arrhythmias and Electromagnetic Field Effects on Human Nervous System. 2002.
17. **Janek Peterson**. Synthesis, Structural Characterization and Modification of PAMAM Dendrimers. 2002.
18. **Merike Vaher**. Room Temperature Ionic Liquids as Background Electrolyte Additives in Capillary Electrophoresis. 2002.
19. **Valdek Mikli**. Electron Microscopy and Image Analysis Study of Powdered Hardmetal Materials and Optoelectronic Thin Films. 2003.
20. **Mart Viljus**. The Microstructure and Properties of Fine-Grained Cermets. 2003.
21. **Signe Kask**. Identification and Characterization of Dairy-Related *Lactobacillus*. 2003

22. **Tiiu-Mai Laht**. Influence of Microstructure of the Curd on Enzymatic and Microbiological Processes in Swiss-Type Cheese. 2003.
23. **Anne Kuusksalu**. 2–5A Synthetase in the Marine Sponge *Geodia cydonium*. 2003.
24. **Sergei Bereznev**. Solar Cells Based on Polycrystalline Copper-Indium Chalcogenides and Conductive Polymers. 2003.
25. **Kadri Kriis**. Asymmetric Synthesis of C<sub>2</sub>-Symmetric Bimorpholines and Their Application as Chiral Ligands in the Transfer Hydrogenation of Aromatic Ketones. 2004.
26. **Jekaterina Reut**. Polypyrrole Coatings on Conducting and Insulating Substrates. 2004.
27. **Sven Nõmm**. Realization and Identification of Discrete-Time Nonlinear Systems. 2004.
28. **Olga Kijatkina**. Deposition of Copper Indium Disulphide Films by Chemical Spray Pyrolysis. 2004.
29. **Gert Tamberg**. On Sampling Operators Defined by Rogosinski, Hann and Blackman Windows. 2004.
30. **Monika Übner**. Interaction of Humic Substances with Metal Cations. 2004.
31. **Kaarel Adamberg**. Growth Characteristics of Non-Starter Lactic Acid Bacteria from Cheese. 2004.
32. **Imre Vallikivi**. Lipase-Catalysed Reactions of Prostaglandins. 2004.
33. **Merike Peld**. Substituted Apatites as Sorbents for Heavy Metals. 2005.
34. **Vitali Syritski**. Study of Synthesis and Redox Switching of Polypyrrole and Poly(3,4-ethylenedioxythiophene) by Using *in-situ* Techniques. 2004.
35. **Lee Põllumaa**. Evaluation of Ecotoxicological Effects Related to Oil Shale Industry. 2004.
36. **Riina Aav**. Synthesis of 9,11-Secosterols Intermediates. 2005.
37. **Andres Braunbrück**. Wave Interaction in Weakly Inhomogeneous Materials. 2005.
38. **Robert Kitt**. Generalised Scale-Invariance in Financial Time Series. 2005.
39. **Juss Pavelson**. Mesoscale Physical Processes and the Related Impact on the Summer Nutrient Fields and Phytoplankton Blooms in the Western Gulf of Finland. 2005.
40. **Olari Ilison**. Solitons and Solitary Waves in Media with Higher Order Dispersive and Nonlinear Effects. 2005.
41. **Maksim Säkki**. Intermittency and Long-Range Structurization of Heart Rate. 2005.
42. **Enli Kiipli**. Modelling Seawater Chemistry of the East Baltic Basin in the Late Ordovician–Early Silurian. 2005.
43. **Igor Golovtsov**. Modification of Conductive Properties and Processability of Polyparaphenylene, Polypyrrole and polyaniline. 2005.
44. **Katrin Laos**. Interaction Between Furcellaran and the Globular Proteins (Bovine Serum Albumin  $\beta$ -Lactoglobulin). 2005.

45. **Arvo Mere.** Structural and Electrical Properties of Spray Deposited Copper Indium Disulphide Films for Solar Cells. 2006.
46. **Sille Ehala.** Development and Application of Various On- and Off-Line Analytical Methods for the Analysis of Bioactive Compounds. 2006.
47. **Maria Kulp.** Capillary Electrophoretic Monitoring of Biochemical Reaction Kinetics. 2006.
48. **Anu Aaspõllu.** Proteinases from *Vipera lebetina* Snake Venom Affecting Hemostasis. 2006.
49. **Lyudmila Chekulayeva.** Photosensitized Inactivation of Tumor Cells by Porphyrins and Chlorins. 2006.
50. **Merle Uudsemaa.** Quantum-Chemical Modeling of Solvated First Row Transition Metal Ions. 2006.
51. **Tagli Pitsi.** Nutrition Situation of Pre-School Children in Estonia from 1995 to 2004. 2006.
52. **Angela Ivask.** Luminescent Recombinant Sensor Bacteria for the Analysis of Bioavailable Heavy Metals. 2006.
53. **Tiina Lõugas.** Study on Physico-Chemical Properties and Some Bioactive Compounds of Sea Buckthorn (*Hippophae rhamnoides* L.). 2006.
54. **Kaja Kasemets.** Effect of Changing Environmental Conditions on the Fermentative Growth of *Saccharomyces cerevisiae* S288C: Auxo-accelerostat Study. 2006.
55. **Ildar Nisamedtinov.** Application of <sup>13</sup>C and Fluorescence Labeling in Metabolic Studies of *Saccharomyces* spp. 2006.
56. **Alar Leibak.** On Additive Generalisation of Voronoï's Theory of Perfect Forms over Algebraic Number Fields. 2006.
57. **Andri Jagomägi.** Photoluminescence of Chalcopyrite Tellurides. 2006.
58. **Tõnu Martma.** Application of Carbon Isotopes to the Study of the Ordovician and Silurian of the Baltic. 2006.
59. **Marit Kauk.** Chemical Composition of CuInSe<sub>2</sub> Monograin Powders for Solar Cell Application. 2006.
60. **Julia Kois.** Electrochemical Deposition of CuInSe<sub>2</sub> Thin Films for Photovoltaic Applications. 2006.
61. **Iiona Oja Açıık.** Sol-Gel Deposition of Titanium Dioxide Films. 2007.
62. **Tiia Anmann.** Integrated and Organized Cellular Bioenergetic Systems in Heart and Brain. 2007.
63. **Katrin Trummal.** Purification, Characterization and Specificity Studies of Metalloproteinases from *Vipera lebetina* Snake Venom. 2007.
64. **Gennadi Lessin.** Biochemical Definition of Coastal Zone Using Numerical Modeling and Measurement Data. 2007.
65. **Enno Pais.** Inverse problems to determine non-homogeneous degenerate memory kernels in heat flow. 2007.
66. **Maria Borissova.** Capillary Electrophoresis on Alkylimidazolium Salts. 2007.

67. **Karin Valmsen**. Prostaglandin Synthesis in the Coral *Plexaura homomalla*: Control of Prostaglandin Stereochemistry at Carbon 15 by Cyclooxygenases. 2007.
68. **Kristjan Piirimäe**. Long-Term Changes of Nutrient Fluxes in the Drainage Basin of the Gulf of Finland – Application of the PolFlow Model. 2007.
69. **Tatjana Dedova**. Chemical Spray Pyrolysis Deposition of Zinc Sulfide Thin Films and Zinc Oxide Nanostructured Layers. 2007.
70. **Katrin Tomson**. Production of Labelled Recombinant Proteins in Fed-Batch Systems in *Escherichia coli*. 2007.
71. **Cecilia Sarmiento**. Suppressors of RNA Silencing in Plants. 2008.
72. **Vilja Mardla**. Inhibition of Platelet Aggregation with Combination of Antiplatelet Agents. 2008.
73. **Maie Bachmann**. Effect of Modulated Microwave Radiation on Human Resting Electroencephalographic Signal. 2008.
74. **Dan Hüvonen**. Terahertz Spectroscopy of Low-Dimensional Spin Systems. 2008.
75. **Ly Villo**. Stereoselective Chemoenzymatic Synthesis of Deoxy Sugar Esters Involving *Candida antarctica* Lipase B. 2008.
76. **Johan Anton**. Technology of Integrated Photoelasticity for Residual Stress Measurement in Glass Articles of Axisymmetric Shape. 2008.
77. **Olga Volobujeva**. SEM Study of Selenization of Different Thin Metallic Films. 2008.
78. **Artur Jõgi**. Synthesis of 4'-Substituted 2,3'-dideoxynucleoside Analogues. 2008.
79. **Mario Kadastik**. Doubly Charged Higgs Boson Decays and Implications on Neutrino Physics. 2008.
80. **Fernando Pérez-Caballero**. Carbon Aerogels from 5-Methylresorcinol-Formaldehyde Gels. 2008.
81. **Sirje Vaask**. The Comparability, Reproducibility and Validity of Estonian Food Consumption Surveys. 2008.
82. **Anna Menaker**. Electrosynthesized Conducting Polymers, Polypyrrole and Poly(3,4-ethylenedioxythiophene), for Molecular Imprinting. 2009.
83. **Lauri Ilison**. Solitons and Solitary Waves in Hierarchical Korteweg-de Vries Type Systems. 2009.
84. **Kaia Ernits**. Study of In<sub>2</sub>S<sub>3</sub> and ZnS Thin Films Deposited by Ultrasonic Spray Pyrolysis and Chemical Deposition. 2009.
85. **Veljo Sinivee**. Portable Spectrometer for Ionizing Radiation “Gammamapper”. 2009.
86. **Jüri Virkepu**. On Lagrange Formalism for Lie Theory and Operadic Harmonic Oscillator in Low Dimensions. 2009.
87. **Marko Piirsoo**. Deciphering Molecular Basis of Schwann Cell Development. 2009.
88. **Kati Helmja**. Determination of Phenolic Compounds and Their Antioxidative Capability in Plant Extracts. 2010.
89. **Merike Sõmera**. Sobemoviruses: Genomic Organization, Potential for Recombination and Necessity of P1 in Systemic Infection. 2010.

90. **Kristjan Laes.** Preparation and Impedance Spectroscopy of Hybrid Structures Based on CuIn<sub>3</sub>Se<sub>5</sub> Photoabsorber. 2010.
91. **Kristin Lippur.** Asymmetric Synthesis of 2,2'-Bimorpholine and its 5,5'-Substituted Derivatives. 2010.
92. **Merike Luman.** Dialysis Dose and Nutrition Assessment by an Optical Method. 2010.
93. **Mihhail Berezovski.** Numerical Simulation of Wave Propagation in Heterogeneous and Microstructured Materials. 2010.
94. **Tamara Aid-Pavlidis.** Structure and Regulation of BDNF Gene. 2010.
95. **Olga Bragina.** The Role of Sonic Hedgehog Pathway in Neuro- and Tumorigenesis. 2010.
96. **Merle Randrüüt.** Wave Propagation in Microstructured Solids: Solitary and Periodic Waves. 2010.
97. **Marju Laars.** Asymmetric Organocatalytic Michael and Aldol Reactions Mediated by Cyclic Amines. 2010.
98. **Maarja Grossberg.** Optical Properties of Multinary Semiconductor Compounds for Photovoltaic Applications. 2010.
99. **Alla Maloverjan.** Vertebrate Homologues of Drosophila Fused Kinase and Their Role in Sonic Hedgehog Signalling Pathway. 2010.
100. **Priit Pruunsild.** Neuronal Activity-Dependent Transcription Factors and Regulation of Human *BDNF* Gene. 2010.
101. **Tatjana Knjazeva.** New Approaches in Capillary Electrophoresis for Separation and Study of Proteins. 2011.
102. **Atanas Katerski.** Chemical Composition of Sprayed Copper Indium Disulfide Films for Nanostructured Solar Cells. 2011.
103. **Kristi Timmo.** Formation of Properties of CuInSe<sub>2</sub> and Cu<sub>2</sub>ZnSn(S,Se)<sub>4</sub> Monograin Powders Synthesized in Molten KI. 2011.
104. **Kert Tamm.** Wave Propagation and Interaction in Mindlin-Type Microstructured Solids: Numerical Simulation. 2011.
105. **Adrian Popp.** Ordovician Proetid Trilobites in Baltoscandia and Germany. 2011.
106. **Ove Pärn.** Sea Ice Deformation Events in the Gulf of Finland and This Impact on Shipping. 2011.
107. **Germo Väli.** Numerical Experiments on Matter Transport in the Baltic Sea. 2011.
108. **Andrus Seiman.** Point-of-Care Analyser Based on Capillary Electrophoresis. 2011.
109. **Olga Katargina.** Tick-Borne Pathogens Circulating in Estonia (Tick-Borne Encephalitis Virus, *Anaplasma phagocytophilum*, *Babesia* Species): Their Prevalence and Genetic Characterization. 2011.
110. **Ingrid Sumeri.** The Study of Probiotic Bacteria in Human Gastrointestinal Tract Simulator. 2011.
111. **Kairit Zovo.** Functional Characterization of Cellular Copper Proteome. 2011.

112. **Natalja Makarytsheva**. Analysis of Organic Species in Sediments and Soil by High Performance Separation Methods. 2011.
113. **Monika Mortimer**. Evaluation of the Biological Effects of Engineered Nanoparticles on Unicellular Pro- and Eukaryotic Organisms. 2011.
114. **Kersti Tepp**. Molecular System Bioenergetics of Cardiac Cells: Quantitative Analysis of Structure-Function Relationship. 2011.
115. **Anna-Liisa Peikolainen**. Organic Aerogels Based on 5-Methylresorcinol. 2011.
116. **Leeli Amon**. Palaeoecological Reconstruction of Late-Glacial Vegetation Dynamics in Eastern Baltic Area: A View Based on Plant Macrofossil Analysis. 2011.
117. **Tanel Peets**. Dispersion Analysis of Wave Motion in Microstructured Solids. 2011.
118. **Liina Kaupmees**. Selenization of Molybdenum as Contact Material in Solar Cells. 2011.
119. **Allan Olsper**. Properties of VPg and Coat Protein of Sobemoviruses. 2011.
120. **Kadri Koppel**. Food Category Appraisal Using Sensory Methods. 2011.
121. **Jelena Gorbatšova**. Development of Methods for CE Analysis of Plant Phenolics and Vitamins. 2011.
122. **Karin Viipsi**. Impact of EDTA and Humic Substances on the Removal of Cd and Zn from Aqueous Solutions by Apatite. 2012.
123. **David Schryer**. Metabolic Flux Analysis of Compartmentalized Systems Using Dynamic Isotopologue Modeling. 2012.
124. **Ardo Illaste**. Analysis of Molecular Movements in Cardiac Myocytes. 2012.
125. **Indrek Reile**. 3-Alkylcyclopentane-1,2-Diones in Asymmetric Oxidation and Alkylation Reactions. 2012.
126. **Tatjana Tamberg**. Some Classes of Finite 2-Groups and Their Endomorphism Semigroups. 2012.
127. **Taavi Liblik**. Variability of Thermohaline Structure in the Gulf of Finland in Summer. 2012.
128. **Priidik Lagemaa**. Operational Forecasting in Estonian Marine Waters. 2012.
129. **Andrei Errapart**. Photoelastic Tomography in Linear and Non-linear Approximation. 2012.
130. **Külliki Krabbi**. Biochemical Diagnosis of Classical Galactosemia and Mucopolysaccharidoses in Estonia. 2012.
131. **Kristel Kaseleht**. Identification of Aroma Compounds in Food using SPME-GC/MS and GC-Olfactometry. 2012.
132. **Kristel Kodar**. Immunoglobulin G Glycosylation Profiling in Patients with Gastric Cancer. 2012.
133. **Kai Rosin**. Solar Radiation and Wind as Agents of the Formation of the Radiation Regime in Water Bodies. 2012.
134. **Ann Tiiman**. Interactions of Alzheimer's Amyloid-Beta Peptides with Zn(II) and Cu(II) Ions. 2012.
135. **Olga Gavrilova**. Application and Elaboration of Accounting Approaches for Sustainable Development. 2012.

136. **Olesja Bondarenko**. Development of Bacterial Biosensors and Human Stem Cell-Based *In Vitro* Assays for the Toxicological Profiling of Synthetic Nanoparticles. 2012.
137. **Katri Muska**. Study of Composition and Thermal Treatments of Quaternary Compounds for Monograin Layer Solar Cells. 2012.
138. **Ranno Nahku**. Validation of Critical Factors for the Quantitative Characterization of Bacterial Physiology in Accelerostat Cultures. 2012.
139. **Petri-Jaan Lahtvee**. Quantitative Omics-level Analysis of Growth Rate Dependent Energy Metabolism in *Lactococcus lactis*. 2012.
140. **Kerti Orumets**. Molecular Mechanisms Controlling Intracellular Glutathione Levels in Baker's Yeast *Saccharomyces cerevisiae* and its Random Mutagenized Glutathione Over-Accumulating Isolate. 2012.
141. **Loreida Timberg**. Spice-Cured Sprats Ripening, Sensory Parameters Development, and Quality Indicators. 2012.
142. **Anna Mihhalevski**. Rye Sourdough Fermentation and Bread Stability. 2012.
143. **Liisa Arike**. Quantitative Proteomics of *Escherichia coli*: From Relative to Absolute Scale. 2012.
144. **Kairi Otto**. Deposition of In<sub>2</sub>S<sub>3</sub> Thin Films by Chemical Spray Pyrolysis. 2012.
145. **Mari Sepp**. Functions of the Basic Helix-Loop-Helix Transcription Factor TCF4 in Health and Disease. 2012.
146. **Anna Suhhova**. Detection of the Effect of Weak Stressors on Human Resting Electroencephalographic Signal. 2012.
147. **Aram Kazarjan**. Development and Production of Extruded Food and Feed Products Containing Probiotic Microorganisms. 2012.
148. **Rivo Uiboupin**. Application of Remote Sensing Methods for the Investigation of Spatio-Temporal Variability of Sea Surface Temperature and Chlorophyll Fields in the Gulf of Finland. 2013.
149. **Tiina Kriščiunaite**. A Study of Milk Coagulability. 2013.
150. **Tuuli Levandi**. Comparative Study of Cereal Varieties by Analytical Separation Methods and Chemometrics. 2013.
151. **Natalja Kabanova**. Development of a Microcalorimetric Method for the Study of Fermentation Processes. 2013.
152. **Himani Khanduri**. Magnetic Properties of Functional Oxides. 2013.
153. **Julia Smirnova**. Investigation of Properties and Reaction Mechanisms of Redox-Active Proteins by ESI MS. 2013.
154. **Mervi Sepp**. Estimation of Diffusion Restrictions in Cardiomyocytes Using Kinetic Measurements. 2013.
155. **Kersti Jääger**. Differentiation and Heterogeneity of Mesenchymal Stem Cells. 2013.
156. **Victor Alari**. Multi-Scale Wind Wave Modeling in the Baltic Sea. 2013.
157. **Taavi Päll**. Studies of CD44 Hyaluronan Binding Domain as Novel Angiogenesis Inhibitor. 2013.
158. **Allan Niidu**. Synthesis of Cyclopentane and Tetrahydrofuran Derivatives. 2013.

159. **Julia Geller**. Detection and Genetic Characterization of *Borrelia* Species Circulating in Tick Population in Estonia. 2013.
160. **Irina Stulova**. The Effects of Milk Composition and Treatment on the Growth of Lactic Acid Bacteria. 2013.
161. **Jana Holmar**. Optical Method for Uric Acid Removal Assessment During Dialysis. 2013.
162. **Kerti Ausmees**. Synthesis of Heterobicyclo[3.2.0]heptane Derivatives *via* Multicomponent Cascade Reaction. 2013.
163. **Minna Varikmaa**. Structural and Functional Studies of Mitochondrial Respiration Regulation in Muscle Cells. 2013.
164. **Indrek Koppel**. Transcriptional Mechanisms of BDNF Gene Regulation. 2014.
165. **Kristjan Pilt**. Optical Pulse Wave Signal Analysis for Determination of Early Arterial Ageing in Diabetic Patients. 2014.
166. **Andres Anier**. Estimation of the Complexity of the Electroencephalogram for Brain Monitoring in Intensive Care. 2014.
167. **Toivo Kallaste**. Pyroclastic Sanidine in the Lower Palaeozoic Bentonites – A Tool for Regional Geological Correlations. 2014.
168. **Erki Kärber**. Properties of ZnO-nanorod/In<sub>2</sub>S<sub>3</sub>/CuInS<sub>2</sub> Solar Cell and the Constituent Layers Deposited by Chemical Spray Method. 2014.
169. **Julia Lehner**. Formation of Cu<sub>2</sub>ZnSnS<sub>4</sub> and Cu<sub>2</sub>ZnSnSe<sub>4</sub> by Chalcogenisation of Electrochemically Deposited Precursor Layers. 2014.
170. **Peep Pitk**. Protein- and Lipid-rich Solid Slaughterhouse Waste Anaerobic Co-digestion: Resource Analysis and Process Optimization. 2014.
171. **Kaspar Valgepea**. Absolute Quantitative Multi-omics Characterization of Specific Growth Rate-dependent Metabolism of *Escherichia coli*. 2014.
172. **Artur Noole**. Asymmetric Organocatalytic Synthesis of 3,3'-Disubstituted Oxindoles. 2014.
173. **Robert Tsanev**. Identification and Structure-Functional Characterisation of the Gene Transcriptional Repressor Domain of Human Gli Proteins. 2014.
174. **Dmitri Kartofelev**. Nonlinear Sound Generation Mechanisms in Musical Acoustic. 2014.
175. **Sigrid Hade**. GIS Applications in the Studies of the Palaeozoic Graptolite Argillite and Landscape Change. 2014.
176. **Agne Velthut-Meikas**. Ovarian Follicle as the Environment of Oocyte Maturation: The Role of Granulosa Cells and Follicular Fluid at Pre-Ovulatory Development. 2014.
177. **Kristel Hälvin**. Determination of B-group Vitamins in Food Using an LC-MS Stable Isotope Dilution Assay. 2014.
178. **Mailis Päri**. Characterization of the Oligoadenylylate Synthetase Subgroup from Phylum Porifera. 2014.
179. **Jekaterina Kazantseva**. Alternative Splicing of *TAF4*: A Dynamic Switch between Distinct Cell Functions. 2014.

180. **Jaanus Suurväli**. Regulator of G Protein Signalling 16 (RGS16): Functions in Immunity and Genomic Location in an Ancient MHC-Related Evolutionarily Conserved Synteny Group. 2014.
181. **Ene Viiard**. Diversity and Stability of Lactic Acid Bacteria During Rye Sourdough Propagation. 2014.
182. **Kristella Hansen**. Prostaglandin Synthesis in Marine Arthropods and Red Algae. 2014.
183. **Helike Lõhelaid**. Allene Oxide Synthase-lipoxygenase Pathway in Coral Stress Response. 2015.
184. **Normunds Stivriņš**. Postglacial Environmental Conditions, Vegetation Succession and Human Impact in Latvia. 2015.
185. **Mary-Liis Kütt**. Identification and Characterization of Bioactive Peptides with Antimicrobial and Immunoregulating Properties Derived from Bovine Colostrum and Milk. 2015.
186. **Kazbulat Šogenov**. Petrophysical Models of the CO<sub>2</sub> Plume at Prospective Storage Sites in the Baltic Basin. 2015.
187. **Taavi Raadik**. Application of Modulation Spectroscopy Methods in Photovoltaic Materials Research. 2015.
188. **Reio Pöder**. Study of Oxygen Vacancy Dynamics in Sc-doped Ceria with NMR Techniques. 2015.
189. **Sven Siir**. Internal Geochemical Stratification of Bentonites (Altered Volcanic Ash Beds) and its Interpretation. 2015.
190. **Kaur Jaanson**. Novel Transgenic Models Based on Bacterial Artificial Chromosomes for Studying BDNF Gene Regulation. 2015.
191. **Niina Karro**. Analysis of ADP Compartmentation in Cardiomyocytes and Its Role in Protection Against Mitochondrial Permeability Transition Pore Opening. 2015.
192. **Piret Laht**. B-plexins Regulate the Maturation of Neurons Through Microtubule Dynamics. 2015.
193. **Sergei Žari**. Organocatalytic Asymmetric Addition to Unsaturated 1,4-Dicarbonyl Compounds. 2015.
194. **Natalja Buhhalko**. Processes Influencing the Spatio-temporal Dynamics of Nutrients and Phytoplankton in Summer in the Gulf of Finland, Baltic Sea. 2015.